Università degli Studi “G. d'Annunzio”

Chieti-Pescara

Scuola Superiore “G. d'Annunzio”

PhD Course in Geosciences

XXXVIII Cycle

Impacts of Climate Change on Water Resources: Hydroclimatic Variability and Drought Assessment of the Arno River Basin Tuscany, Italy

Disciplinary Scientific Area PHYS-05/B

PhD Candidate

Hafeez Ahmed Talpur

Supervisor

Prof. Piero Di Carlo

PhD Coordinator

Prof. Nicola Sciarra

Final Exam Year 2026

Dedication

To the loving memory of my father, taken too soon in 1999, yet his strength, values, and silent prayers still echo in every step I take.

To my mother, whose resilience and love carried us through shadows into light.

To my brothers, a guiding hand and steady heart, who stood in the storm and became our pillar when we needed one most, whose loyalty and strength have always been by my side.

& to my wife, whose love is both my refuge and my flame, lighting the path through every challenge and triumph.

TABLE OF CONTENT

LIST OF TABLES

LIST OF FIGURES

Abstract

Climate change is altering the global water cycle through rising temperatures, shifting precipitation patterns, and increasing evapotranspiration, with direct consequences for water availability in regions that depend on surface water resources. The Mediterranean basin has been consistently identified as a climate change hotspot, where warming rates exceed the global mean by approximately 60% and where robust summer drying signals are projected to intensify throughout the twenty-first century. In Italy, these trends are of particular concern for river basins that support large populations and sustain critical agricultural, urban, and ecological functions. The Arno River basin in Tuscany (8,228 km^2), which supports approximately 2.2 million inhabitants including the cities of Florence and Pisa, has historically experienced both devastating floods and severe droughts, yet prior to this work it lacked an integrated assessment that jointly examined observed hydroclimatic variability over recent decades and projected future changes under state-of-the-art emission scenarios. Understanding the trajectory of hydroclimatic change in this basin is essential for proactive water resources planning and climate adaptation.

This PhD thesis presents a comprehensive assessment of historical hydroclimatic variability and future climate change impacts on water resources and drought in the Arno River basin, combining observational analysis with hydrological modelling and climate projections. The study employed two complementary approaches: a detailed observational analysis of temperature, precipitation, and streamflow variability and trends over the period 1994–2023, and a model-based projection of twenty-first-century changes using the SWAT+ hydrological model forced by Quantile Delta Mapping (QDM) bias-corrected CMIP6 outputs under SSP2-4.5 and SSP5-8.5 scenarios.

The first approach (Chapter 3) used data from 18 precipitation stations, 7 temperature stations, and the S. Giovanni alla Vena gauging station, analysed through non-parametric methods including the Modified Mann-Kendall test, Sen's slope estimator, the Standardized Anomaly Index, and Spearman's rank correlation analysis. The analysis revealed a statistically significant warming trend of +0.052 °C yr^{-1} at the annual scale, with the strongest seasonal warming in autumn (+0.072 °C yr^{-1}) and summer (+0.064 °C yr^{-1}), and an acceleration of positive anomalies since 2014. In contrast, no statistically significant trends were detected in annual or seasonal precipitation or streamflow over the same period, with the dominant feature being pronounced interannual variability (precipitation CV = 18.2%; streamflow CV up to 65.8%). Correlation analysis confirmed a predominantly precipitation-controlled streamflow

regime (ρ = 0.51–0.93 across seasons), while a significant negative summer temperature–streamflow correlation (ρ = −0.57, $p < 0.001$) identified warming-driven evapotranspiration as an already active influence on warm-season hydrology.

The second approach (Chapter 4) employed SWAT+, calibrated and validated against observed monthly streamflow (NSE = 0.74/0.93; KGE = 0.72/0.85), driven by QDM bias-corrected outputs from five CMIP6 GCMs across three future periods (2015–2040, 2041–2070, 2071–2100). All five models projected unequivocal warming reaching approximately 3 °C under SSP2-4.5 and 5 °C under SSP5-8.5 by late century, with increasing model convergence toward declining precipitation (−15.1% median under SSP5-8.5 far-future, with all models agreeing) and corresponding streamflow reductions of 18.4–32.0%. Drought characterization using SPI-12 and SRI-12 revealed marked intensification: total drought duration increased from historical baselines of 41 months (SPI-12) and 32 months (SRI-12) to up to 99 and 106 months, respectively, under SSP5-8.5 far-future. Hydrological drought severity exceeded meteorological drought severity under the most extreme projections, indicating that the catchment's storage capacity may become insufficient to buffer drought stress under enhanced evapotranspiration. Persistent high correlations between SPI-12 and SRI-12 (r = 0.80–0.95) across all scenarios supported the use of meteorological indicators for hydrological drought early warning.

The methodological framework adopted in this thesis, together with the results, provides a quantitative and integrated understanding of the relationship between climate drivers and the hydrological response of the Arno River basin. The high degree of consistency between the observed warming trajectory and the CMIP6-projected signal strengthens confidence in both the empirical baseline and the projection framework, and identifies the basin as being in a transitional phase where significant warming is underway but its full hydrological impact remains partially masked by high natural precipitation variability. These findings provide an actionable evidence base for climate adaptation planning and water resources management in one of the Mediterranean's most significant river basins, and the framework is readily transferable to other catchments facing similar challenges.

Chapter 1 General Introduction

1.1 Background and context

Climate change represents one of the most pressing global challenges of the twenty-first century, fundamentally altering the Earth's hydrological cycle and reshaping the distribution, timing, and availability of freshwater resources across the planet (IPCC, 2021, 2023). The Sixth Assessment Report (AR6) of the Intergovernmental Panel on Climate Change confirms that human-induced warming has already reached approximately 1.1 °C above pre-industrial levels, with profound consequences for precipitation regimes, evapotranspiration rates, snow and ice dynamics, and river discharge patterns worldwide (IPCC, 2021). Global greenhouse gas emissions implied by nationally determined contributions are projected to make it likely that warming will exceed 1.5 °C during the twenty-first century, intensifying the hydrological perturbations already observed and creating cascading risks for ecosystems, food security, energy production, and human well-being (IPCC, 2023).

In this context, understanding how climate change translates into tangible impacts on water resources at the regional and basin scales has become a scientific and societal imperative.

The hydrological consequences of climate change are not uniformly distributed across the globe. Semi-arid and Mediterranean-type climatic regions are among the most vulnerable, as they are characterized by a combination of high seasonal and interannual variability in precipitation, strong dependence on cool-season rainfall for water supply, and increasing competition for limited water resources among agricultural, urban, industrial, and environmental uses (García-Ruiz et al., 2011; Iglesias et al., 2007). In these regions, even modest changes in mean climate conditions can amplify existing water stress, trigger more frequent and severe drought episodes, and reduce the reliability of surface water and groundwater supplies upon which millions of people depend (Cosgrove & Loucks, 2015; Cramer et al., 2018).

The Mediterranean Basin has been consistently identified as a primary climate change hotspot, where warming rates exceed the global mean by approximately 20% and where drying tendencies are amplified by the complex interaction of large-scale atmospheric circulation patterns, intricate topography, and strong land–sea thermal contrasts (Giorgi, 2006; Giorgi & Lionello, 2008; Lionello & Scarascia, 2018). Observational records and climate model projections converge in indicating that the Mediterranean region is experiencing, and will continue to experience, significant increases in mean and extreme temperatures, coupled with reductions in annual precipitation particularly during the warm season and a general intensification of the hydrological cycle that manifests through more prolonged dry spells interspersed with more intense rainfall events (Cos et al., 2022; Lionello et al., 2006; Noto et al., 2023). These changes have far-reaching implications for water resources, agriculture, biodiversity, and the cultural heritage of the region, which hosts some of the world's oldest and most densely populated river basins (Cramer et al., 2018).

Italy, situated in the central Mediterranean, epitomizes these climate-related challenges. The Italian Peninsula spans a wide range of climatic and topographic conditions, from the Alpine and Apennine mountain ranges to the coastal lowlands and islands, resulting in considerable spatial heterogeneity in hydroclimatic responses to climate change (Brunetti et al., 2006; Spano et al., 2020). Long instrumental records reveal a coherent warming signal across the peninsula, with mean air temperature increases of approximately 1 °C over the period 1865–2003 (Brunetti et al., 2006), and continued warming projected for the coming decades under various emission scenarios (D'Oria et al., 2017; Spano et al., 2020).

Precipitation trends, in contrast, exhibit marked spatial heterogeneity and are often weak or non-significant at regional scales, although increasing variability and changes in the frequency of extreme events both heavy precipitation and prolonged droughts have been documented (Caloiero et al., 2018; Longobardi & Villani, 2010; Philandras et al., 2011). Streamflow trends across Italian catchments have yielded mixed results, with some basins exhibiting declining trends attributed to reduced precipitation and enhanced evapotranspiration, while others show no statistically significant change (Masseroni et al., 2021; Stahl et al., 2010). These findings underscore the critical importance of basin-scale assessments that capture local hydroclimatic dynamics and their sensitivity to regional climate forcing.

Within this broader context, the Arno River basin in Tuscany, central Italy, stands out as a catchment of particular scientific significance and societal relevance. Covering approximately 8,228 km^2, the Arno River basin drains a large portion of central Tuscany from the Apennine headwaters to the Ligurian Sea, encompassing major urban centers including Florence and Pisa cities of immense historical, cultural, and economic importance (Caporali et al., 2005; Diodato et al., 2021; Ghinassi et al., 2023). The Arno River has a long and well-documented history of hydrological extremes, including devastating floods most notably the catastrophic 1966 Florence flood and recurrent low-flow episodes that have periodically impacted water supply, infrastructure, economic activity, and the preservation of irreplaceable cultural heritage

(Caporali et al., 2005). The basin's hydrological regime is strongly seasonal, with high flows occurring from late autumn to early spring under cyclonic precipitation and saturated catchment conditions, and markedly reduced discharges during summer under limited rainfall and elevated evapotranspiration (Castelli et al., 2009; Diodato et al., 2021). This combination of seasonal extremes, cultural significance, and vulnerability to climate change makes the Arno River basin an ideal case study for investigating the impacts of hydroclimatic variability and change on Mediterranean water resources.

1.2 Thesis outline

This thesis is organized into five chapters, structured as follows:

Chapter 1 (General Introduction) provides the background and context for the research, and outlines the structure of the thesis.

Chapter 2 (Literature Review) reviews the relevant literature, identifies the research gaps, and states the aims and objectives.

Chapter 3 (Hydroclimatic variability and trend analysis of the Arno River basin, Tuscany, Italy) presents a comprehensive observational assessment of temperature, precipitation, and streamflow variability and trends in the Arno River basin over the period 1994–2023. The chapter employs non-parametric statistical methods including the Modified Mann-Kendall test, Sen's slope estimator, coefficient of variation analysis, and Spearman's rank correlation to characterize the basin's hydroclimatic regime and identify the dominant controls on its hydrological response. This chapter is based on a manuscript submitted to *Sustainable Water Resources Management* and is currently under review.

Chapter 4 (Investigating future hydroclimatic trends and drought characterization using CMIP6 and SWAT+ in the Arno River basin, Tuscany, Italy) quantifies future climate change impacts on streamflow and drought in the Arno River basin using the SWAT+ hydrological model forced by Quantile Delta Mapping bias-corrected CMIP6 projections under SSP2-4.5 and SSP5-8.5 scenarios. The chapter analyzes projected changes in temperature, precipitation, and streamflow across three future periods and characterizes future meteorological and hydrological drought using SPI-12 and SRI-12, including drought propagation analysis. This chapter is based on a manuscript submitted to *Water Cycle* and is currently under review.

Chapter 5 (General conclusions and perspective) summarizes the principal findings of the thesis in relation to the stated research objectives and highlights the overall contribution and significance of the work, examines the broader implications for water resources management and climate adaptation, and outlines recommendations for future research directions.

Chapter 2 Literature Review

2.1 Observed hydroclimatic variability and trends in the Mediterranean region

A substantial body of literature has documented the observed hydroclimatic changes in the Mediterranean region over the past several decades. Temperature increases have been particularly pronounced, with the Mediterranean warming at rates that consistently exceed the global average. (Lionello & Scarascia, 2018) demonstrated that the relationship between Mediterranean and global warming is approximately linear but amplified, with Mediterranean surface temperatures rising approximately 20% faster than the global mean. This amplified warming has been attributed to the combined effects of increased greenhouse gas concentrations, land-atmosphere feedback mechanisms involving soil moisture depletion, and changes in large-scale atmospheric circulation patterns (Barcikowska et al., 2020; Giorgi & Lionello, 2008). In Italy specifically, (Brunetti et al., 2006) analyzed homogenized temperature series spanning nearly 140 years (1865–2003) and documented a long-term warming of approximately 1 °C per century, with an acceleration of warming in recent decades. More recent national assessments confirm the continuation and intensification of this warming trend (Aruffo & Carlo, 2019; Spano et al., 2020).

Precipitation trends in the Mediterranean region present a more complex picture. Unlike the spatially coherent warming signal, precipitation changes are characterized by substantial spatial heterogeneity, strong interannual and interdecadal variability, and often weak or non-significant trends at basin and regional scales (Caloiero et al., 2018; Longobardi & Villani, 2010; Philandras et al., 2011). This complexity arises from the multiple controls on Mediterranean precipitation, including the interplay of large-scale atmospheric modes such as the North Atlantic Oscillation (NAO), local topographic effects, and land–sea thermal contrasts (Hurrell & Van Loon, 1997; Xoplaki et al., 2004). In Tuscany, (Bartolini et al., 2018) analyzed precipitation records from 1955 to 2013 found changes in the temporal distribution of precipitation, including a tendency toward more concentrated rainfall events, rather than a clear monotonic trend in annual totals. At the broader Italian scale, (Longobardi & Villani, 2010) reported predominantly non-significant trends in annual rainfall across numerous stations, while (Caloiero et al., 2018) confirmed similar patterns across the wider European Mediterranean. However, some studies have detected localized or seasonal precipitation trends, particularly in southern Italy and during the transitional seasons (Caloiero et al., 2019).

Streamflow trends across Mediterranean catchments have been examined by several large-scale and regional studies. (Stahl et al., 2010) analyzed streamflow trends across Europe using a dataset of near-natural catchments and found evidence of declining streamflow in Mediterranean and southern European regions, consistent with reduced precipitation and increased evapotranspiration. (Masseroni et al., 2021) investigated 63 years of streamflow volume changes across Europe with a particular focus on the Mediterranean basin, reporting a general tendency toward reduced annual streamflow volumes in southern European catchments, although with considerable inter-basin variability. In Italy, basin-scale studies have produced mixed results, with some catchments showing significant declines and others exhibiting stable or even increasing flows depending on the period analyzed, the degree of anthropogenic modification, and the relative influence of temperature and precipitation changes (Masseroni et al., 2021). (Estrada et al., 2024) further documented the spatio-temporal patterns and trends of streamflow in water-scarce Mediterranean basins, highlighting the vulnerability of these systems to ongoing climate change. These findings highlight the need for detailed basin-specific assessments to understand local hydrological responses to regional climate forcing.

The variability of Mediterranean hydroclimatic systems extends beyond long-term trends to encompass substantial interannual and interdecadal fluctuations. Mediterranean-climate rivers are inherently characterized by high variability, which constitutes a defining component of their hydrological and ecological identity (Cid et al., 2017). This variability is driven by the episodic nature of Mediterranean precipitation, which is strongly modulated by large-scale atmospheric circulation patterns. The NAO, in particular, exerts a dominant influence on wet-season precipitation across the western and central Mediterranean, with positive NAO phases generally associated with reduced precipitation and negative phases with enhanced rainfall (Hurrell & Van Loon, 1997; Xoplaki et al., 2004).). In Tuscany, (Luppichini et al., 2021) confirmed the statistical relationships between large-scale circulation patterns and local precipitation regimes. This pronounced variability has important implications for water resources management, as it means that Mediterranean basins are subject to substantial year-to-year fluctuations in water availability that can be as consequential as long-term trends for planning and operations.

2.2 Hydrological modelling in Mediterranean basins using SWAT and SWAT+

Hydrological models serve as essential tools for translating climate projections into quantitative assessments of water resource impacts at the watershed scale. Among the numerous models available, the Soil and Water Assessment Tool (SWAT), developed by the United States Department of Agriculture (Arnold et al., 1998), has emerged as one of the most widely applied physically-based, semi-distributed watershed models worldwide. SWAT simulates the major hydrological processes at the basin scale, including surface runoff, lateral flow, groundwater recharge and baseflow, evapotranspiration, and channel routing, using daily or sub-daily time steps (Arnold et al., 1998). Its ability to integrate spatially distributed data on topography, land use, soils, and climate has made it a popular choice for climate change impact assessments in diverse geographical settings, including Mediterranean basins (Aloui et al., 2023; Keller et al., 2023).

A comprehensive review of 260 SWAT studies conducted in Mediterranean catchments between 2002 and 2022 found that while 62% were carried out in Greece, Italy, or Spain, the majority of Italian applications were concentrated in southern regions, leaving central Italian basins comparatively understudied (Aloui et al., 2023). Furthermore, most of these applications employed the original SWAT model rather than its successor, SWAT+, which was introduced by (Bieger et al., 2017), as a completely restructured version offering enhanced flexibility in landscape representation, improved connectivity between landscape units, and a more modular architecture that facilitates the incorporation of management practices and conservation measures (Arnold et al., 2018; Bieger et al., 2017). SWAT+ addresses several limitations of the original SWAT, including more flexible spatial representation of hydrological response units and improved routing of water between landscape elements. Despite these advantages, SWAT+ applications in Italian watersheds remain limited (Pulighe et al., 2021; Tariq et al., 2024) and its application to the Arno River basin with CMIP6 climate projections represents a novel contribution.

In the Arno River basin specifically, previous hydrological modelling studies have provided important insights. (Burlando & Rosso, 2002) investigated the effects of transient climate change on runoff variability in the Arno basin, establishing it as representative of southern European climatic environments and documenting expected changes in water balance seasonality. (Campo et al., 2006) applied distributed hydrological modelling with multi-platform remote sensing for model calibration in the Arno basin. (El Jeitany, Pacetti, et al., 2024a) evaluated climate change effects on hydrological functionality and water-related ecosystem services in the upper Arno basin using SWAT, reporting declining streamflow trends under future scenarios. (El Jeitany, Nussbaum, et al., 2024) further demonstrated that landscape metrics significantly influence runoff and groundwater recharge predictions across the basin. However, none of these studies employed the SWAT+ framework with CMIP6 projections and advanced bias correction techniques, leaving a significant methodological gap.

2.3 Climate change projections for the Mediterranean: From CMIP5 to CMIP6

General Circulation Models (GCMs) constitute the primary tools for projecting future climate change and its impacts on hydrological systems. The evolution from the Coupled Model Intercomparison Project Phase 5 (CMIP5) to Phase 6 (CMIP6) has brought significant advances in model physics, resolution, and scenario design (Eyring et al., 2016). CMIP6 introduced the Scenario Model Intercomparison Project (ScenarioMIP), a novel framework grounded in the Shared Socioeconomic Pathways (SSPs), which integrates socioeconomic development trajectories with radiative forcing levels to produce a richer and more policy-relevant set of future scenarios (O'Neill et al., 2016; Tebaldi et al., 2021). The SSP framework represents a notable advance over the Representative Concentration Pathways (RCPs) used in CMIP5, as it explicitly accounts for the socioeconomic conditions that shape both emissions trajectories and adaptive capacities. Key scenarios widely employed in impact assessments include SSP2-4.5 (a middle-of-the-road pathway with moderate forcing of +4.5 W m^{-2}) and SSP5-8.5 (a high-end forcing pathway of +8.5 W m^{-2} under fossil-fuel-intensive development) (O'Neill et al., 2016).

For the Mediterranean region, CMIP6 projections consistently indicate amplified warming and a general drying tendency relative to the global average. (Cos et al., 2022) compared the Mediterranean climate change signal in CMIP5 and CMIP6 projections and confirmed that the Mediterranean remains a pronounced climate change hotspot in the newer generation of models, with warming amplification of 20–50% above the global mean depending on the season and scenario. Precipitation projections indicate widespread reductions in annual and summer rainfall across most of the Mediterranean basin, with the largest decreases projected for the western and central Mediterranean under high-emission scenarios (Cos et al., 2022; Zittis et al., 2021). (Tarín-Carrasco et al., 2024) assessed future precipitation changes across Mediterranean climate regions using the CMIP6 ensemble and confirmed the dominance of drying trends, particularly during the warm season, while highlighting the substantial inter-model spread that characterizes precipitation projections.

In Italy, regional climate projections based on CMIP5 and CMIP6 have consistently indicated continued warming and general reductions in water availability. (D'Oria et al., 2017, 2019) developed high-resolution future climate projections for northern Tuscany and quantified the impacts on water resources, reporting expected increases in temperature and reductions in annual runoff by the 2050s under RCP4.5 and RCP8.5 scenarios. More recently, CMIP6-based studies in Italian watersheds have demonstrated substantial inter-model uncertainty; for example, (Abdelwahab et al., 2025) reported mean annual flow reductions ranging from −7% to −67% in the Carapelle basin (Apulia) depending on GCM selection, underscoring the importance of multi-model ensemble approaches for robust impact assessment. Similarly, (Senatore et al., 2022) evaluated the uncertainty of climate model structure and bias correction on hydrological impacts in a Mediterranean catchment in southern Italy, highlighting the need for careful methodological choices in climate impact studies.

2.4 Bias correction of climate model outputs

A critical challenge in using GCM outputs for hydrological impact assessment is the systematic biases inherent in climate model simulations of precipitation and temperature, particularly at the watershed scale. Raw GCM outputs typically exhibit biases in the mean, variance, and distributional properties of climate variables that, if left uncorrected, can lead to unreliable and misleading hydrological simulations (H. Li et al., 2010; Tong et al., 2021). Consequently, statistical bias-correction techniques are widely employed as a preprocessing step before driving hydrological models with climate projections.

Among bias-correction methods, quantile mapping (QM) has been one of the most frequently applied approaches, as it adjusts the entire distribution of a simulated variable to match the observed distribution (H. Li et al., 2010). However, standard QM approaches can distort the climate change signal embedded in GCM projections, particularly for precipitation extremes, because they apply a static correction derived from the historical period without accounting for the changes in the distribution that the model projects for the future (Cannon et al., 2015; Switanek et al., 2017). This limitation has motivated the development of more advanced techniques, such as Quantile Delta Mapping (QDM), which explicitly preserves the relative changes in quantiles projected by the climate model while adjusting the baseline distribution to match observations (Cannon et al., 2015). QDM has been shown to better preserve the climate change signal, particularly in the tails of the distribution that correspond to extreme events, making it particularly suitable for impact studies focused on droughts and extremes (Padulano et al., 2025; Song & Chung, 2025). Despite these advantages, QDM remains underutilized in Mediterranean catchments compared to simpler methods, representing an opportunity for methodological advancement in regional climate impact studies (Padulano et al., 2025).

2.5 Drought assessment frameworks: concepts, indices, and propagation

Drought is a complex, multi-faceted natural hazard that manifests across different components of the hydrological cycle, from precipitation deficits (meteorological drought) to soil moisture depletion (agricultural drought), reduced streamflow (hydrological drought), and inadequate water supply to meet demands (socioeconomic drought) (Mishra & Singh, 2010; Van Loon, 2015). Understanding the characteristics, severity, duration, and spatial extent of drought events is essential for effective water resources management and climate adaptation planning.

Standardized drought indices have become widely adopted tools for drought monitoring and characterization due to their ability to facilitate comparison across different climatic regions and time scales. The Standardized Precipitation Index (SPI), proposed by (McKee et al., 1993), quantifies precipitation anomalies relative to a fitted probability distribution at specified accumulation periods, providing a standardized measure of wetness or dryness. The World Meteorological Organization has recommended the SPI as a primary meteorological drought index and suggested that SPI values at 12 months or longer accumulation periods are appropriate for assessing hydrological impacts, as groundwater, streamflow, and reservoir storage reflect longer-term precipitation anomalies (Svoboda et al., 2012). The SPI has been applied across diverse global settings, including Mediterranean regions, where its utility for capturing the variable precipitation regimes has been well established (Edwards, 1997; Spinoni et al., 2014).

To complement the SPI, the Standardized Runoff Index (SRI) was developed to quantify hydrological drought using streamflow data in an analogous framework (Shukla & Wood, 2008). The SRI applies the same standardization approach to runoff data, allowing direct comparison between meteorological and hydrological drought conditions. This paired use of SPI and SRI enables the analysis of drought propagation the process by which a precipitation deficit cascades through the hydrological system to produce reduced streamflow, groundwater depletion, and water supply shortages (Barker et al., 2016; Huang et al., 2017; Van Loon, 2015). Additionally, the Standardized Precipitation Evapotranspiration Index (SPEI) incorporates both precipitation and potential evapotranspiration, making it sensitive to warming-induced increases in atmospheric evaporative demand (Beguería et al., 2014). The SPEI has proven particularly relevant in warming-dominated drought contexts, where temperature-driven increases in evaporative demand contribute to drought severity even in the absence of significant precipitation declines.

The propagation of meteorological drought to hydrological drought is a critical process for water resources management, as it determines the lag and transformation between atmospheric forcing and the hydrological response experienced by water users and ecosystems. Recent studies have demonstrated that climate change accelerates this propagation process, while anthropogenic factors such as reservoir operations can modulate propagation timescales (Ullah et al., 2025; Wang et al., 2019; Wu et al., 2022). (Odongo et al., 2023) showed that propagation thresholds vary substantially across timescales and methodological choices, emphasizing the need for systematic propagation analysis in climate impact assessments. (Muthuvel & Qin, 2025) further demonstrated the importance of probabilistic approaches to future drought propagation analysis under climate change.

Recent global drought analysis has revealed that atmospheric evaporative demand has increased drought severity by an average of 40% globally, with areas experiencing drought expanding by 74% during 2018–2022 compared to 1981–2017 (Gebrechorkos et al., 2025). For the Mediterranean region specifically, drought projections under CMIP6 scenarios indicate intensification of both meteorological and hydrological drought frequency, duration, and severity, with the most pronounced changes expected under high-emission pathways (Baronetti et al., 2022; Cammalleri et al., 2020; Spinoni et al., 2018, 2020). (Ullah et al., 2022) projected that the frequency of historically rare drought events may double across large continental areas under 1.5 °C warming, with Mediterranean regions facing exacerbated drought severity under warming scenarios of 1.5–3.0 °C.

2.6 Previous studies on the Arno River basin

The Arno River basin has been the subject of several hydroclimatic and hydrological investigations across different temporal scales and thematic foci. A millennium-long storm erosivity reconstruction by (Diodato et al., 2021) provided insights into the interplay between long-term climate variability and erosive events in the basin, revealing oscillatory patterns linked to Mediterranean climate dynamics. This long-term perspective complements more recent observational studies that focus on instrumental-period variability and trends.

From a hydrological modelling perspective, (Burlando & Rosso, 2002) conducted one of the earliest assessments of climate change impacts on runoff in the Arno basin, establishing its representativeness for southern European climatic environments. (Campo et al., 2006) advanced the application of distributed hydrological modelling in the basin through multi-platform remote sensing calibration. (Castelli et al., 2009) developed a distributed modelling package for sustainable water management in the Arno basin. More recently, (D'Oria et al., 2019) used high-resolution regional projections to quantify the impacts of climate change on water resources in northern Tuscany, projecting increasing temperatures and reductions in annual runoff by the 2050s under RCP4.5 and RCP8.5 scenarios.

Studies specifically focused on ecosystem services and landscape interactions in the Arno basin have further enriched the understanding of climate-hydrology-landscape interactions. (Pacetti et al., 2021) assessed water ecosystem services footprints of agricultural production in central Italy, including the Arno basin. (El Jeitany, Pacetti, et al., 2024a) evaluated climate change effects on hydrological functionality and water-related ecosystem services in the upper Arno basin using SWAT modelling, indicating declining streamflow trends and negative impacts on provisioning and supporting services under future scenarios. (El Jeitany, Nussbaum, et al., 2024) demonstrated that landscape metrics significantly influence runoff and groundwater recharge predictions across the Arno basin, highlighting the importance of landscape configuration for hydrological modelling.

Despite these valuable contributions, several important gaps remain in the hydroclimatic understanding of the Arno River basin. Most existing studies have focused on specific thematic aspects storm erosivity, future projections under earlier-generation climate models, or ecosystem services without providing an integrated observational analysis of the basin's recent hydroclimatic behavior that jointly considers temperature, precipitation, and streamflow variability and trends over a consistent multi-decadal period. Furthermore, applications of the advanced SWAT+ framework with CMIP6 projections and QDM bias correction technique have not been conducted for the Arno basin, and systematic drought propagation analysis under future climate scenarios remains lacking.

2.7 Research Gap

Based on the review of existing literature, several critical knowledge gaps can be identified that motivate the present thesis:

First, there is a notable absence of integrated, up-to-date observational assessments of the hydroclimatic behavior of the Arno River basin. While individual studies have addressed specific aspects such as storm erosivity (Diodato et al., 2021), future projections (D'Oria et al., 2019), and ecosystem services (El Jeitany, Pacetti, et al., 2024a), relatively few observational studies have focused specifically on jointly analyzing temperature, precipitation, and streamflow variability and trends over a consistent multi-decadal period that includes the most recent decades. This gap is significant because the period since approximately 2014 has been characterized by an acceleration of warming in the Mediterranean region and the occurrence of several notable hydrological anomalies in central Italy (IPCC, 2022a; Spano et al., 2020). An integrated assessment covering this recent period is essential for establishing the baseline conditions against which future changes should be evaluated and for identifying the dominant climatic controls on the basin's hydrological regime.

Second, applications of the advanced SWAT+ framework remain limited in Italian watersheds, despite its enhanced flexibility for representing landscape connectivity and management practices (Bieger et al., 2017; Pulighe et al., 2021; Tariq et al., 2024). The majority of hydrological modelling studies in Italian Mediterranean basins have employed the original SWAT model, and the application of SWAT+ coupled with CMIP6 projections has not been conducted for the Arno River basin. Given that SWAT+ offers improved capabilities for representing the complex landscape heterogeneity of the Arno basin and that CMIP6 represents the current state-of-the-art in climate projections with the more comprehensive SSP scenario framework, this represents a significant methodological gap. Furthermore, while bias-correction techniques are routinely applied to GCM outputs, advanced methods such as Quantile Delta Mapping (QDM) which better preserve the climate change signal in precipitation extremes remain underutilized in Mediterranean catchments (Cannon et al., 2015; Padulano et al., 2025).

Third, relatively few studies have explicitly examined the propagation of meteorological drought into hydrological drought using standardized indices under future climate scenarios for the Arno River basin and central Italian catchments more broadly. While drought indices such as SPI and SRI are well-established tools, their systematic application to quantify future drought characteristics including duration, severity, frequency, and the temporal relationships between meteorological and hydrological drought remains limited for this basin. Recent advances in multivariate drought propagation frameworks have demonstrated that propagation thresholds vary substantially across timescales and methods (Odongo et al., 2023; Ullah et al., 2022, 2025), emphasizing the need for basin-specific drought propagation analysis to support drought preparedness and early warning systems. The absence of such analysis for the Arno basin represents a critical gap for regional water resources management and climate adaptation planning.

2.8 Aims and objectives

The overarching aim of this thesis is to assess historical hydroclimatic variability and project future changes in climate, streamflow, and drought in the Arno River basin, Tuscany, Italy, in order to provide an integrated scientific evidence base for water resources management and climate adaptation planning.

To achieve this aim, the thesis addresses two complementary sets of specific objectives, organized across two core research chapters:

2.8.1 Objectives addressed in Chapter 3 (Historical Hydroclimatic Variability and Trend Analysis)

(1) To characterize the recent climatological patterns of temperature and precipitation across the Arno River basin over the period 1994–2023; (2) to quantify the interannual and seasonal variability of temperature, precipitation, and streamflow; (3) to detect and quantify long-term trends in these hydroclimatic variables at annual and seasonal scales using non-parametric statistical methods; and (4) to assess the co-variability among temperature, precipitation, and streamflow to identify the dominant climatic controls on the basin's hydrological regime.

2.8.2 Objectives addressed in Chapter 4 (Future Hydroclimatic Projections and Drought Characterization)

(1) To calibrate and validate a SWAT+ hydrological model for the Arno River basin using observed hydrometeorological data; (2) to apply Quantile Delta Mapping bias correction to CMIP6 GCM outputs under SSP2-4.5 and SSP5-8.5 scenarios; (3) to project future changes in temperature, precipitation, and streamflow across near-future (2015–2040), mid-future (2041–2070), and far-future (2071–2100) periods relative to the historical baseline (1994–2014); and (4) to characterize future meteorological and hydrological drought using Standardized Precipitation Index (SPI) and Standardized Runoff Index (SRI) at the 12-month accumulation scale, including analysis of drought propagation, duration, severity, and frequency.

Together, these objectives provide a comprehensive assessment that bridges the gap between historical observations and future projections, linking the observed hydroclimatic baseline to model-based scenarios of change and thereby informing evidence-based adaptation strategies for the Arno River basin.

Chapter 3 Hydroclimatic variability and trend analysis of the Arno River basin, Tuscany, Italy

This Chapter based on a manuscript submitted to the Sustainable Water Resources Management (under review)

3.1 Introduction

Climate change is increasingly altering the global water cycle, with observable shifts in temperature, precipitation regimes, and hydrological responses documented across many regions of the world (Ahmed et al., 2026; IPCC, 2021). The Mediterranean region has been identified as a primary climate change hotspot, where warming rates exceed the global mean and hydroclimatic variability is amplified by the interaction of large-scale atmospheric circulation, complex topography, and land–sea contrasts (Giorgi, 2006; Giorgi & Lionello, 2008; Lionello & Scarascia, 2018). In such regions, relatively modest changes in mean climate can translate into substantial impacts on water resources, ecosystems, and socio-economic systems, especially where dense populations and intensive water use converge in climatically sensitive catchments (Ahmed et al., 2026; Cramer et al., 2018; IPCC, 2022a; Talpur et al., 2024).

The Mediterranean climate is characterized by mild, wet winters and warm to hot, dry summers, with precipitation largely concentrated in the cool and transitional seasons and strong year-to-year variability superimposed on this pronounced seasonality (Lionello et al., 2006; Xoplaki et al., 2004). In many Mediterranean basins, a large fraction of annual runoff is generated during a relatively short wet season, while prolonged summer dry spells lead to low flows and recurrent hydrological droughts (Cid et al., 2017; Merheb et al., 2016). This combination of strong seasonality and high interannual variability makes Mediterranean river systems particularly sensitive to shifts in atmospheric circulation, changes in storm tracks, and warming-induced increases in evaporative demand (Barcikowska et al., 2020; García-Ruiz et al., 2011; Vicente-Serrano, Lopez-Moreno, et al., 2014). Understanding how temperature, precipitation, and streamflow have co-evolved in recent decades at the basin scale is therefore essential for assessing ongoing climate impacts and informing adaptation strategies.

Italy, located in the central Mediterranean, exemplifies these climate-related challenges. Long instrumental records show coherent warming across the peninsula, with mean air temperature increases of approximately 1°C over the period 1865–2003 (Brunetti et al., 2006), and continued warming projected for the coming decades under various emission scenarios (Spano et al., 2020). Precipitation trends, in contrast, are spatially heterogeneous and often weak or non-significant at regional scales, although tendencies toward increased variability and changes in the frequency of droughts and heavy precipitation events have been reported (Caloiero et al., 2018; Longobardi & Villani, 2010; Philandras et al., 2011). Streamflow trends across Italian and broader Mediterranean catchments have yielded mixed results, with some basins exhibiting declining trends attributed to reduced precipitation and increased evapotranspiration, while others show no significant change (Masseroni et al., 2021; Stahl et al., 2010). These findings underscore the importance of basin-scale assessments that capture local responses to regional climate forcing.

Within this context, the Arno River basin in Tuscany is of particular scientific and societal interest. Covering approximately 8,228 km², the basin drains a large portion of central Tuscany from the Apennine headwaters to the Ligurian Sea and encompasses major urban centers including Florence and Pisa (Diodato et al., 2021; Ghinassi et al., 2023). The Arno River has a long history of hydrological extremes, including devastating floods, most notably the catastrophic 1966 Florence flood, and severe low-flow episodes that have periodically impacted infrastructure, economic activity, and cultural heritage (Caporali et al., 2005). The basin's hydrological regime is strongly seasonal, with high flows typically occurring from late autumn to early spring under cyclonic precipitation and saturated catchment conditions, and reduced discharges in summer under scarce rainfall and high evapotranspiration (Caporali et al., 2005; Castelli et al., 2009; Diodato et al., 2021). This makes the Arno River basin a representative case study for assessing hydroclimatic variability and change in Italian river systems.

Previous studies have addressed various aspects of Arno's hydroclimate across different temporal scales. A millennium-long storm erosivity reconstruction revealed the interplay between climate variability and erosive events (Diodato et al., 2021). Climate change effects on hydrological functionality and water-related ecosystem services have been evaluated in the upper Arno River basin using Soil and Water Assessment Tool (SWAT) modelling, indicating declining streamflow trends and negative impacts on provisioning and supporting services under future scenarios (El Jeitany, Pacetti, et al., 2024b), while landscape metrics have been shown to significantly influence runoff and groundwater recharge predictions across the basin (El Jeitany, Nussbaum, et al., 2024). Earlier work established the Arno River basin as representative of southern European climatic environments and documented expected changes in water balance seasonality and extremes (Burlando & Rosso, 2002), with more recent projections indicating increasing temperatures and reductions in annual runoff by the 2050s under RCP4.5 and RCP8.5 scenarios (D'Oria et al., 2019). At broader scales, studies have examined precipitation and streamflow trends across Italian and Mediterranean catchments (Caloiero et al., 2018; Longobardi & Villani, 2010; Masseroni et al., 2021; Merheb et al., 2016). However, relatively rare observational studies have focused specifically on the recent hydroclimatic behavior of the Arno River basin, jointly analyzing temperature, precipitation, and streamflow variability and trends over a consistent multi-decadal period.

Despite advances in regional climate and hydrological research, several knowledge gaps remain for the Arno River basin. First, most existing studies either focus on specific aspects such as storm erosivity, future projections, and drought indices or address broader Mediterranean or national scales without resolving basin-specific behavior (Brunetti et al., 2006; Diodato et al., 2021; Hertig & Tramblay, 2017). Second, there is a need for updated observational analyses that explicitly include the most recent decades, during which warming has accelerated and several notable hydrological anomalies have occurred in central Italy (IPCC, 2022a; Spano et al., 2020). Third, integrated assessments that jointly consider temperature, precipitation, and streamflow variability, trends, and interrelationships at both annual and seasonal scales remain scarce for the Arno, limiting the capacity to link atmospheric forcing to hydrological response in a quantitative and management-relevant framework.

The objectives of this study are to (1) characterize the recent climatological patterns of temperature and precipitation across the Arno River basin; (2) quantify the interannual and seasonal variability of temperature, precipitation, and streamflow; (3) detect and quantify long-term trends in these hydroclimatic variables at annual and seasonal scales; and (4) assess the co-variability among temperature, precipitation, and streamflow to identify the dominant climatic controls on the basin's hydrological regime. The findings provide insights for water resources management and climate adaptation planning in the basin.

3.2 Materials and methods

3.2.1 Study area

The Arno River basin is located in the Tuscany region of central Italy and drains westwards into the Ligurian Sea. The basin extends nearly between 42°40′–44°10′ N and 10°00′–12°00′ E and covers an area of about 8,230 km², with elevations ranging from near sea level at the outlet to ~1,625 m a.s.l. along the Apennines (Figure. 3.1a–c). The climate is Mediterranean, characterized by mild, wet winters and warm to hot, dry summers, modulated by Atlantic synoptic forcing and strong orographic effects (Diodato et al., 2021; Lionello et al., 2006). The hydrological regime of the Arno River is strongly seasonal with high flows usually occurring from late autumn to early spring in response to cyclonic precipitation and saturated catchment conditions, whereas low flows prevail during summer when precipitation is scarce and evapotranspiration demand is high. Land use is dominated by mixed agricultural and urban areas in the lowlands and forested and shrub-covered slopes in the upper basin (Diodato et al., 2021; El Jeitany, Pacetti, et al., 2024b).

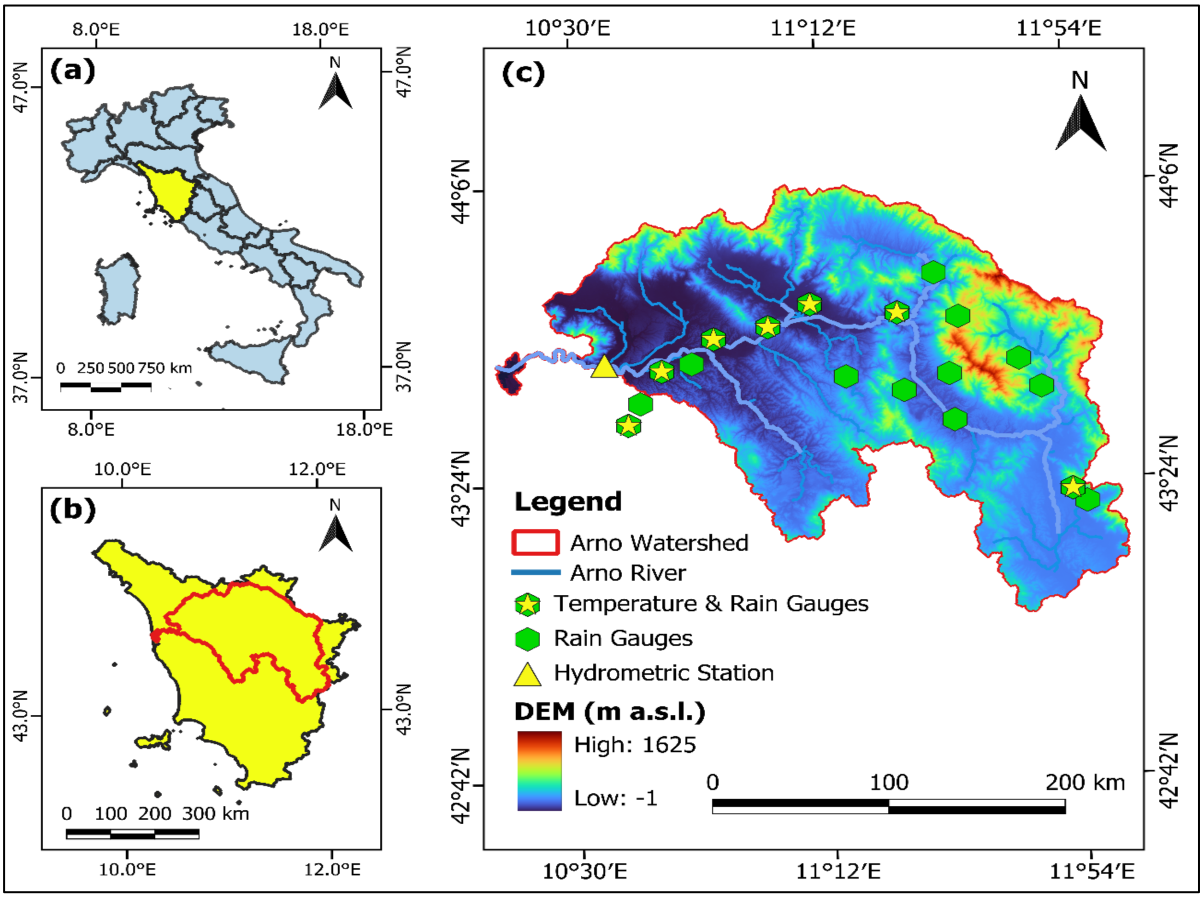

Figure 3.1 Location of the study area: (a) Italy with the Tuscany region highlighted, (b) Tuscany region with the Arno River Basin boundary, and (c) (DEM) of the Arno watershed, rain-gauge and temperature stations, and the hydrometric station

3.3 Hydro-meteorological data and preprocessing

Daily precipitation and air temperature records (1994–2023) were obtained from the regional hydrological service of Tuscany (Servizio Idrologico Regionale della Toscana, SIR). The station network comprises 18 precipitation stations and 7 temperature stations distributed across the basin; the stations were selected based on data completeness and spatial representativeness. For this study, streamflow was analyzed at the S. Giovanni alla Vena hydrometric station, which is located in the lower part of the basin and integrates runoff from most of the upstream catchment. The digital elevation model (DEM) was obtained from Copernicus DEM GLO-30 dataset via CREODIAS platform at 30-meter resolution; the DEM was used to delineate the study area (Table 3.1).

S.No	Station number	Station name	Data type	Data Frequency	Latitude (°N)	Longitude (°E)	Elevation
1	TOS01000601	Ortignano	(Precip)	1994−2023	43.682	11.752	346
2	TOS01000651	Salutio	(Precip)	1994−2023	43.615	11.813	315
3	TOS01000761	Castiglion Fiorentino	(Precip)	1994−2023	43.343	11.929	270
4	TOS01000881	Pian di Scò	(Precip)	1994−2023	43.65	11.555	395
5	TOS01000891	Il Palagio	(Precip)	1994−2023	43.613	11.427	315
6	TOS01001029	Dicomano	(Precip)	1994−2023	43.888	11.52	148
7	TOS01001041	Consuma	(Precip)	1994−2023	43.784	11.585	955
8	TOS01001129	Ferrone	(Precip)	1994−2023	43.648	11.264	150
9	TOS01001225	Case Passerini	(Precip), Temp)	1994−2023	43.82	11.168	33
10	TOS01001491	S. Miniato (Cimitero)	(Precip)	1994−2023	43.684	10.831	102
11	TOS01004571	Montevarchi	(Precip)	1994−2023	43.541	11.566	133.8
12	TOS01005131	Capannoli	(Precip)	1994−2023	43.592	10.684	28.61
13	TOS11000016	Terricciola	(Precip), Temp)	1994−2023	43.542	10.649	127
14	TOS11000024	Remole	(Precip , Temp)	1994−2023	43.796	11.413	230
15	TOS11000038	Ottavo	(Precip , Temp)	1994−2023	43.373	11.89	313
16	TOS11000046	Montopoli	(Precip , Temp)	1994−2023	43.668	10.746	29
17	TOS11000071	Cerreto Guidi	(Precip , Temp)	1994−2023	43.742	10.894	70
18	TOS11000076	Artimino	(Precip , Temp)	1994−2023	43.768	11.048	107
19	TOS01005191	S.Giovanni alla VV	River Discharge	1994−2023	43.685	10.585	7.63

Table 3.1 List of stations precipitation (Precip), temperature (Temp) and streamflow in the study area

Daily precipitation totals were aggregated to monthly, seasonal, and annual totals; daily temperatures were aggregated to monthly, seasonal, and annual means. Seasons were defined according to standard climatological practice for the Mediterranean region: spring (MAM), summer (JJA), autumn (SON), and winter (DJF). To ensure temporal representativeness, monthly values were retained only when a sufficient number of daily observations was available (≥25 days per month), annual values when coverage was near-complete (≥350 days per year), and seasonal values when at least 80 daily observations were available within the season. Streamflow values ($m^3 s^{-1}$) were converted to equivalent water depth (mm) by dividing discharge volumes by the contributing catchment area to facilitate comparison with precipitation totals.

3.4 Basin averaging and spatial interpolation

To characterize the behavior of hydroclimatic variables, basin-averaged time series of temperature and precipitation were derived following the arithmetic-mean approach used in similar basin-scale studies (Asfaw et al., 2018; Orke & Li, 2021). The spatial distribution of mean annual and seasonal precipitation was mapped using inverse distance weighting (IDW) interpolation in QGIS (v3.34). IDW is a deterministic interpolation method in which the value at an unsampled location is estimated as a weighted average of values at surrounding stations, with weights decreasing with distance (Lu & Wong, 2008; Shepard, 1968). The accuracy of the interpolation was assessed using leave-one-out cross-validation (LOOCV) was executed in R using the *gstat* package on projected station coordinates (UTM 32N; EPSG: 32632), whereby each station was sequentially withheld, the remaining stations were used to predict the value at the withheld location, and prediction errors were summarized as root mean square error (RMSE). The resulting gridded fields were clipped to the basin boundary and used to produce the precipitation maps shown in (Figure. 3.3).

3.5 Variability analysis

Hydroclimatic variability was quantified using the coefficient of variation (CV) and the standardized anomaly index (SAI), following common practice in regional climate studies (Asfaw et al., 2018; Orke & Li, 2021).

Coefficient of variation (CV). The CV provides a dimensionless measure of relative variability and is defined as:

$$CV = \left(\frac{\sigma}{\mu}\right) \times 100 \quad (1)$$

where σ is the standard deviation and μ is the long-term mean of the series, CV values were classified as indicating low (CV < 20%), moderate (20–30%), or high (> 30%) variability (Orke & Li, 2021).

Standardized anomaly index (SAI). To characterize relatively wet/dry years and seasons for precipitation and streamflow, standardized anomalies were calculated using the SAI (Asfaw et al., 2018; McKee et al., 1993).

$$SAI_t = \frac{X_t - \mu}{\sigma} \quad (2)$$

where X_t is the annual or seasonal value in year t and μ and σ are the corresponding long-term mean and standard deviation over 1994–2023. SAI values were classified using the categories in Table 3.2.

SAI Value	Category
2.00 and above	Extremely Wet
1.50 to 1.99	Very Wet
1.00 to 1.49	Moderately Wet
−0.99 to 0.99	Near Normal
−1.49 to -1.00	Moderately Dry
−1.99 to -1.50	Severely Dry
−2.00 and less	Extremely Dry

Table 3.2 Classification of Standardized Anomaly Index (SAI) values

3.6 Trend analysis

Long-term monotonic trends in annual and seasonal basin-averaged temperature, precipitation and streamflow were assessed using a modified Mann–Kendall (MK) test that corrects for serial correlation in the data, combined with Sen's slope estimator to quantify trend magnitude (Hamed & Ramachandra Rao, 1998; Kendall, M. G, 1975; Mann, 1945; Sen, 1968; Yue & Wang, 2004). The classical MK test is a rank-based nonparametric method widely used in hydro-climatology because it does not require normally distributed residuals and is relatively robust to outliers (Helsel & Hirsch, 2002; Yue et al., 2002). The MK test statistic S is defined as:

$$S = \sum_{i=1}^{n-1} \sum_{j=i+1}^{n} sgn\,(X_j - X_i) \tag{3}$$

where n is the length of the series, X_i and X_j are observations at times i and j , and sgn ( ) is the sign function. Under the null hypothesis of no trend, S has mean zero and variance $Var(S)$ that depends on n and ties. The standardized test statistic Z is given by:

$$Z = \begin{cases} \frac{S-1}{\sqrt{Var(S)}}\ if\ S > 0 \\ 0\ if\ S = 0 \\ \frac{S+1}{\sqrt{Var(S)}}\ if\ S < 0 \end{cases} \tag{4}$$

and is approximately standard normal for $n \gtrsim 10$ (Helsel & Hirsch, 2002). Because hydroclimatic time series often exhibit positive autocorrelation, which inflates the variance of S and may lead to over-estimation of trend significance, we applied the variance-corrected modified MK test proposed by (Hamed & Ramachandra Rao, 1998; Yue & Wang, 2004). In this approach, the effective sample size is reduced as a function of statistically significant positive autocorrelation in the ranks, and Var(S) is adjusted accordingly, for estimating the effective sample size and corrected test statistics. Trend magnitudes were estimated using Sen's slope estimator (Sen, 1968), which calculates the median of all pairwise slopes between data points by:

$$\beta = \text{median}\left(\frac{X_j - X_k}{j-k}\right),\ j > k \tag{5}$$

The resulting slopes β are expressed per year °C yr^{-1} for temperature, mm yr^{-1} for precipitation and streamflow. Positive (negative) values of β indicate increasing (decreasing) trends. For each series, we report Kendall's tau (τ), the modified MK Z statistic, the corresponding two-sided p-value and Sen's slope. Statistical significance was evaluated at $p < 0.05$, 0.01, and 0.001.

3.7 Correlation analysis

To examine the co-variability between basin-averaged temperature, precipitation, and streamflow, non-parametric Spearman rank correlation coefficients (ρ) were computed at both annual and seasonal scales (Helsel & Hirsch, 2002; Spearman, 1904). Spearman's ρ measures the strength and direction of a monotonic association between two variables based on the ranks of the data, and is less sensitive to outliers and non-normal distributions than the Pearson correlation. The coefficient is defined as:

$$\rho = 1 - \frac{6 \sum d_i^2}{n(n^2-1)} \quad (6)$$

where d_i is the difference between the ranks of corresponding values of the two variables and n is the number of paired observations.

3.8 Results

3.8.1 Climate characteristics of the study area

Over the period 1994–2023, the Arno River basin exhibits a pronounced seasonal cycle in both temperature and precipitation (Figure. 3.2). Mean monthly air temperature shows a typical Mediterranean pattern, increasing from a minimum basin-averaged value of 6.4 °C in January to a maximum of 24.4 °C in August, and then declining towards early winter. Mean monthly maximum temperature T_{max} rises from 10.31 °C in January to 31.18 °C in July and August, while minimum temperature T_{min} increases from 2.54 °C in January to 17.45 and 17.58 °C in July and August, respectively. Seasonally, mean average temperature T_{avg} is lowest in winter 7.00 °C, increases through spring 13.66 °C, peaks in summer 23.46 °C, and remains relatively mild in autumn 15.69 °C. Basin-averaged precipitation also displays a strong intra-annual variability, with a pronounced autumn–winter maximum and a dry summer (Figure. 3.2). The wettest month is November, with a mean total of 132.5 mm, followed by December 98.7 mm, whereas July is the driest month with only 32 mm. The long-term mean annual precipitation is approximately 895.8 mm, of which about 34.7 % falls in autumn, 28 % in winter, 23.4 % in spring, and only 14.0 % in summer. This distribution highlights the concentration of precipitation in the cool and transitional seasons and the relative dryness of the summer months in the Arno River basin.

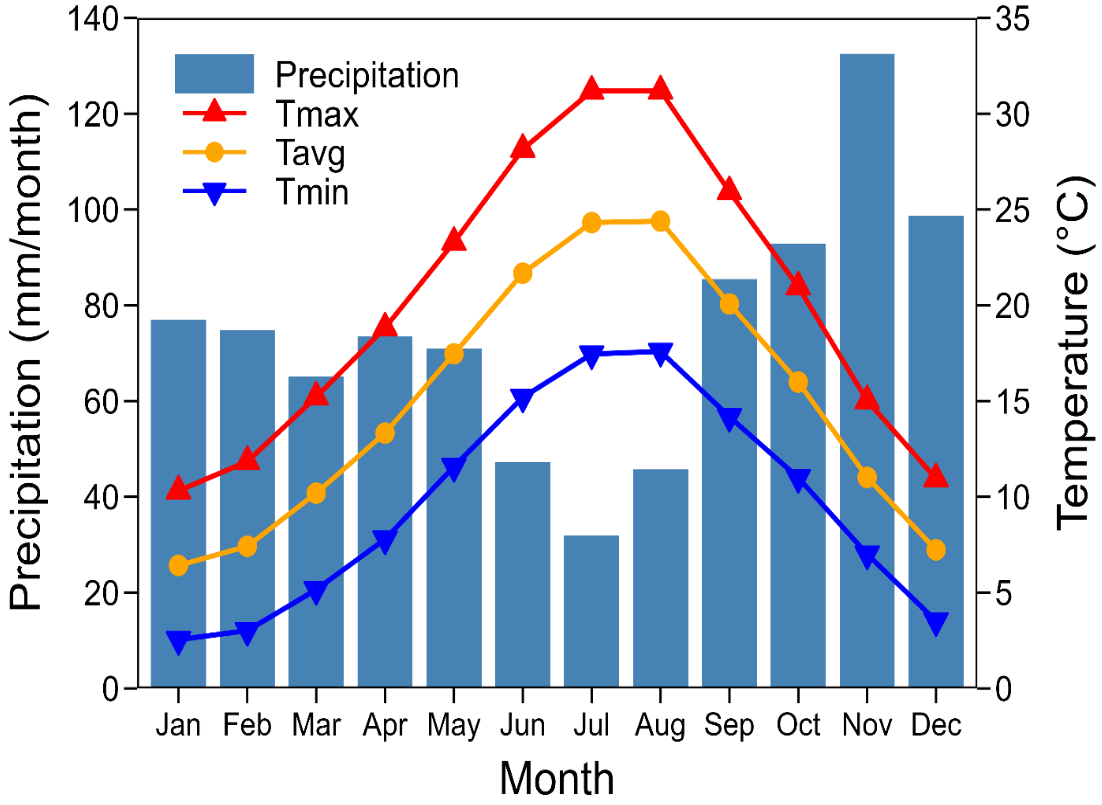

Figure 3.2 Monthly climatology of basin-averaged precipitation and temperature for the period 1994–2023. Bars (left axis) show mean monthly rainfall totals, and lines (right axis) indicate temperature as maximum (Tmax), mean (Tavg), and minimum (Tmin).

3.8.2 Spatial distribution of annual and seasonal precipitation

The spatial distribution of precipitation across the Arno River basin on annual and seasonal scales is presented in Figure 3. Annual precipitation (Figure. 3.3a) exhibits considerable spatial variability, ranging from approximately 720–830 mm in the central and southwestern lowlands to more than 1,160 mm in the northeastern headwater areas along the Apennine ridge. This pattern indicates a pronounced orographic gradient, with precipitation increasing progressively from the lower Arno valley towards the elevated mountainous sectors. Seasonal maps (Figure. 3.3b–e) demonstrate that this orographic influence persists throughout the year, though with varying intensity across seasons. In spring (Figure. 3.3b), precipitation totals range between 175 and 315 mm, with maximum values concentrated in the northeastern uplands and minimum values over the central plains. Summer (Figure. 3.3c) represents the driest season, with precipitation totals predominantly between 90 and 170 mm; even the orographic enhancement over the mountainous areas remains modest during this period. Autumn (Figure. 3.3d) exhibits a marked increase in precipitation, with totals ranging from 240 to 410 mm. The highest values are again concentrated along the Apennine crest, while lower amounts characterize the central and western lowlands. Winter (Figure. 3.3e) displays relatively high totals between 180 and 370 mm, with a spatial pattern broadly similar to autumn, though slightly weaker in magnitude.

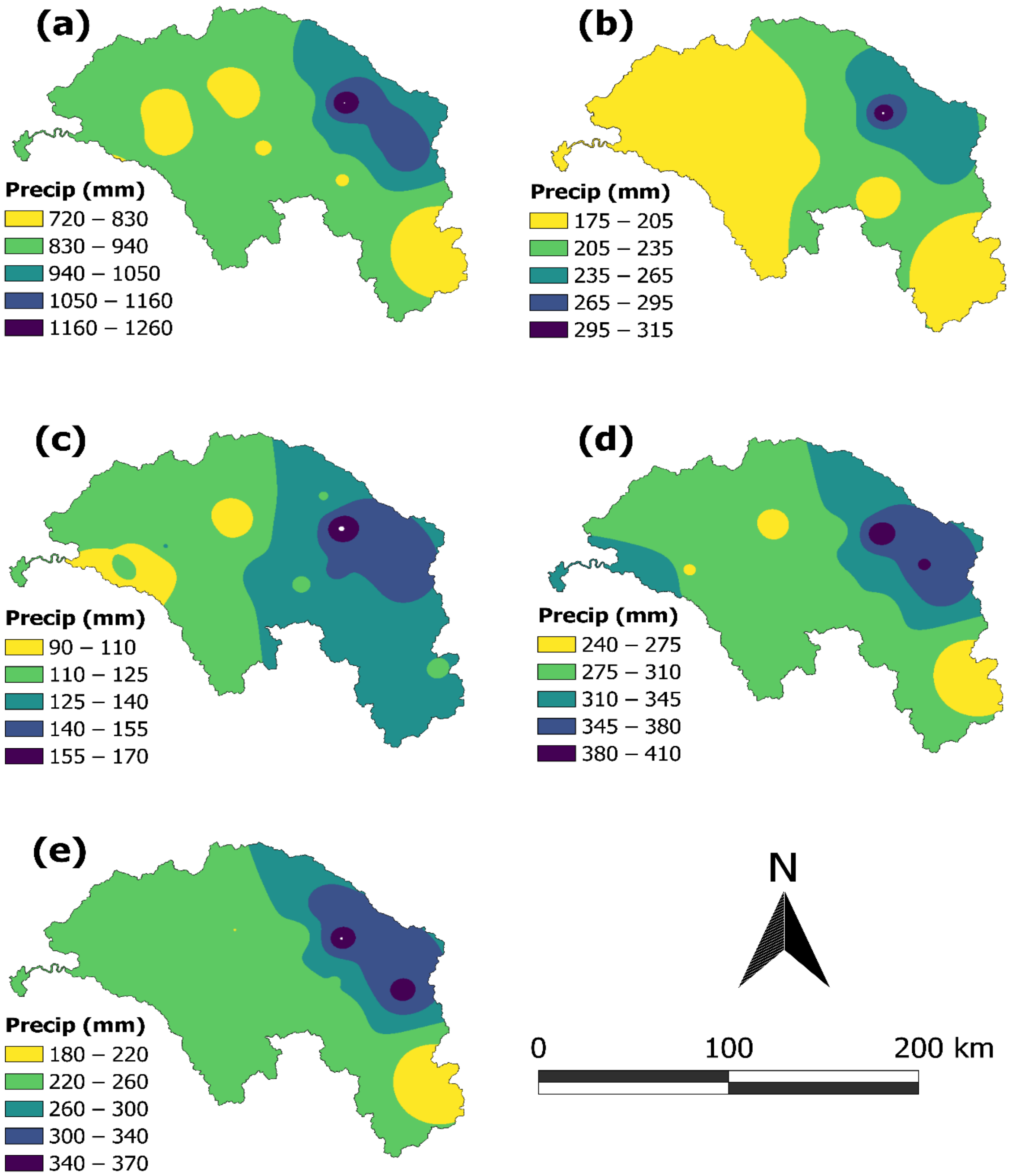

Figure 3.3 Spatial distribution of mean precipitation (mm) across the Arno River Basin for the period 1994–2023: (a) Annual, (b) Spring (MAM), (c) Summer (JJA), (d) Autumn (SON), and (e) Winter (DJF)

This spatial variation in precipitation distribution across the watershed is mainly attributed to the orographic effect of the Apennine Mountains, which enhance precipitation on their windward slopes. The pattern reveals a consistent northeast-to-southwest gradient, with higher precipitation in elevated areas and lower values in the coastal and valley lowlands throughout all seasons. The LOOCV validation of IDW interpolation indicated satisfactory performance, with relative RMSE ranging from 10.9% in autumn to 14.1% in winter.

3.8.3 Seasonal contribution to annual precipitation and streamflow

Seasonal contributions of precipitation and streamflow to the annual water balance exhibit marked differences in the Arno River watershed Table 3.3. On average, autumn accounts for the largest share of annual precipitation 34.76%, followed by winter 30.09%, spring 23.4%, and summer with only 14.08%. The interannual variability of these seasonal fractions is moderate for spring and summer SD ≈ 5%, but considerably larger in autumn SD = 8.44% and particularly in winter SD = 15.16%. In contrast, streamflow is strongly concentrated in the cold season. Winter contributes on average 45.35% of the annual runoff, followed by spring 31.77%, whereas autumn and summer account for only 18.17% and 6.53%, respectively. The standard deviation of seasonal runoff fractions is highest in winter SD = 16.37% and autumn SD = 11.49% and substantially lower in spring SD = 7.9% and summer SD = 2.73%. These patterns indicate substantial year-to-year variability in the seasonal distribution of discharge, particularly during the wettest months.

Season	Mean Precipitation (%)	SD (%)	Mean Streamflow (%)	SD (%)
Spring	23.41	5.01	31.77	7.9
Summer	14.08	4.94	6.53	2.73
Autumn	34.76	8.44	18.17	11.49
Winter	30.09	15.16	45.35	16.37

Table 3.3 Seasonal contribution to annual totals of precipitation and streamflow

3.9 Variability analysis

3.9.1 Temperature variability

Annual temperature variability in the Arno River basin was assessed using (CV) and (SAI) for the period 1994–2023. The annual CV of T_{min} 6.6% was higher than those of T_{avg} 4.5% and T_{max} 3.9%, indicating that interannual variability is modest for mean and maximum temperature but substantially higher for minimum temperature. Seasonally, winter exhibited the strongest variability, with CV values of 16.2%, 10.3%, and 40.2% for T_{avg}, T_{max}, and T_{min}, respectively, whereas summer displayed the lowest variability CV of 4.8%, 4.7%, and 5.4% for T_{avg}, T_{max}, and T_{min}. Spring and autumn showed intermediate CVs, with T_{min} systematically more variable than T_{max} and T_{avg} in all seasons Table 3.4.

Season	CV T_{avg} (%)	CV T_{max} (%)	CV T_{min} (%)	CV Precipitation (%)	CV Streamflow (%)
Spring	5.7	5.2	9.3	29.5	46.2
Summer	4.8	4.7	5.4	36	37.7
Autumn	6.2	5.3	9.5	29.8	65.8
Winter	16.2	10.3	40.2	36.9	50.3
Annual	4.5	3.9	6.6	18.2	33.4

Table 3.4 Interannual coefficients of variation (CV, %) of seasonal and annual basin-averaged temperature (Tavg), maximum temperature (Tmax), minimum temperature (Tmin), precipitation, and streamflow for the period 1994–2023

Figure 4 shows that annual temperature anomalies for all three temperatures were predominantly negative or near zero from 1994 to about 2013, followed by a sequence of mostly positive anomalies from 2014 onward, with markedly warm years concentrated toward the end of the record. The strongest negative anomalies varied: T_{max} in 2010 −1.56 °C, T_{avg} in 2005 −1.32 °C and T_{min} in 1995 −1.33 °C. In contrast, 2022 and 2023 recorded the strongest positive anomalies, reaching up to +1.94 °C for T_{max}, +1.54 °C for T_{avg}, and +1.37 °C for T_{min}. Linear regression fitted to the anomaly series indicates coherent warming across all temperatures, with trends of 0.056 °C yr^{-1} for T_{max} and 0.054 °C yr^{-1} for both T_{avg} and T_{min} (Figure. 3.4a–c). Taken together, the relatively low annual CV, the strong seasonal contrast in variability especially the high winter and T_{min} variability and the persistent positive anomalies since the mid-2010s point to a robust basin-wide warming signal over the past three decades.

3.9.2 Precipitation variability

Annual precipitation in the basin shows moderate interannual variability, with a CV of 18.2%. Seasonally, winter and summer exhibited the highest CV of 36.9% and 36.0%, respectively, while spring and autumn showed slightly lower CV values of 29.5% and 29.8%, respectively

Table 3.4. This pattern reflects the sensitivity of cold-season and convective summer precipitation to synoptic-scale circulation anomalies over the central Mediterranean.

The annual SAI series (Figure. 3.5a) reveals alternating wet and dry years with no pronounced long-term trend of the 30 years analyzed, with 16 years exhibiting negative and 14 positive SAI values, indicating a slight predominance of drier years. The strongest positive anomaly occurred in 2010: SAI = +2.55, followed by 2013 and 2014: SAI = +1.48, +1.43. Conversely, the most pronounced negative anomalies were recorded in 2011: SAI = −1.76. Seasonal patterns exhibit distinct characteristics across seasons. Spring recorded its driest conditions in 2011 and 2017: SAI ≈ −1.42, while the wettest springs occurred in 2013 and 2018: SAI ≈ +2.61 (Figure. 3.5b). Summer showed the strongest negative anomalies in 2017: SAI = −1.85, with the wettest summers in 2002: SAI = +2.40 (Figure. 3.5c). Autumn displayed its most pronounced dry anomaly in 2011: SAI = −1.94, whereas 2019: SAI = +1.87 was the wettest autumn (Figure. 3.5d). Winter experienced its driest conditions in 2012: SAI = −1.53, and the wettest winters in 2021: SAI = +2.33 (Figure. 3.5e).

Notably, 2011 emerged as a consistently dry year across multiple seasons, with the strongest negative annual and the most pronounced autumn deficit. Similarly, 2017 recorded severe dry anomalies in spring, summer, and winter. In contrast, 2010 stands out as an exceptionally wet year, with the highest annual SAI driven primarily by abundant winter precipitation. The absence of a systematic trend in the SAI series, combined with moderate to high seasonal CVs, suggests that precipitation variability in the Arno River basin is characterized by substantial year-to-year fluctuations rather than a progressive shift toward wetter or drier conditions.

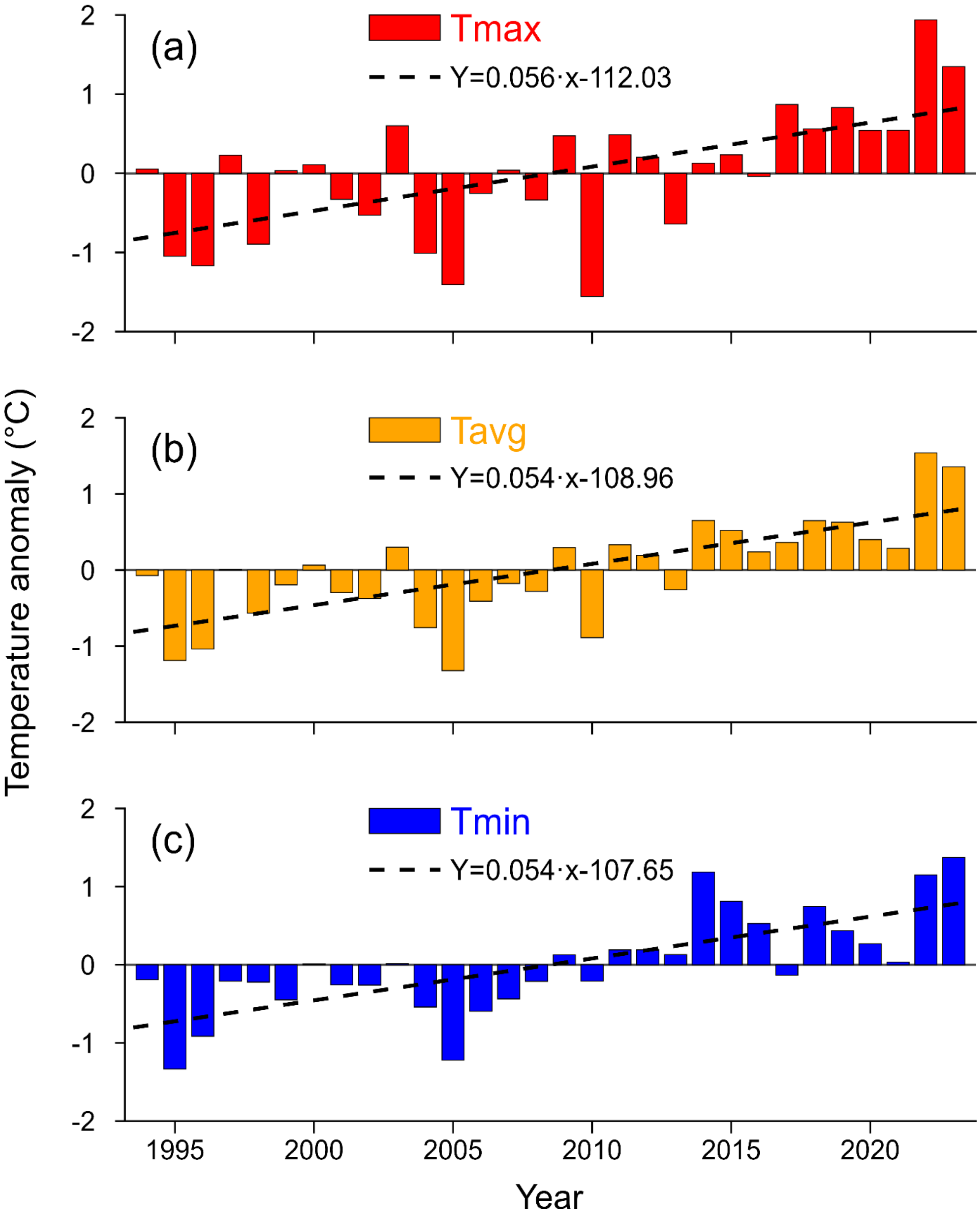

Figure 3.4 Annual temperature anomalies (a) maximum temperature (Tmax), (b) mean temperature (Tavg), and (c) minimum temperature (Tmin). Bars show standardized anomalies relative to the 1994–2023 mean, and dashed lines represent linear regression trends

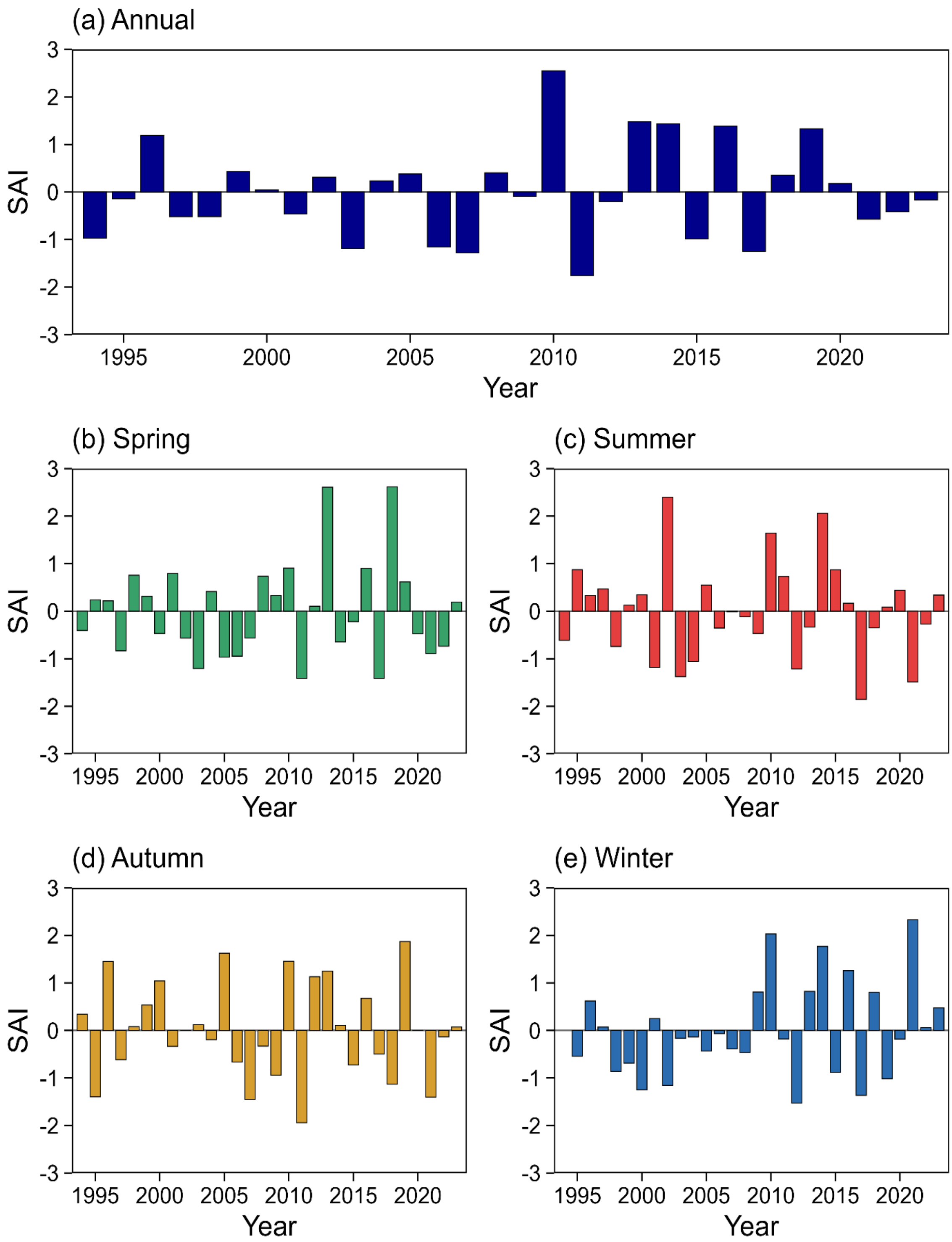

Figure 3.5 Standardized anomaly index (SAI) of basin-averaged precipitation for the period 1994–2023: (a) Annual scale and (b–e) seasonal scales for (b) Spring (MAM), (c) Summer (JJA), (d) Autumn (SON) and (e) Winter (DJF)

3.9.3 Streamflow variability

Annual and seasonal streamflow variability at the S. Giovanni alla Vena gauging station was assessed using CV and the SAI of streamflow (Table 3.4; Figure. 3.6). The annual CV of streamflow is 33.4%, indicating pronounced interannual variability, considerably higher than that of precipitation 18.2%. Seasonal CVs are even larger, ranging from 37.7% in summer to 65.8% in autumn, with spring and winter also highly variable 46.2% and 50.3%, respectively. These values reflect the strong concentration of runoff in a limited number of high-flow events and the sensitivity of river discharge to year-to-year changes in cool-season precipitation and soil-moisture conditions.

The annual streamflow SAI series (Figure. 3.6) shows alternating high and low flow years without a clear long-term trend. Of the 30 years analyzed, 19 exhibit negative SAI values and 11 positive values, indicating a predominance of below-average runoff conditions. The largest positive anomaly occurs in 2010 SAI = +2.69, followed by 2013 and 2014 SAI = +1.95 and +1.88, corresponding to very wet years for the basin. The most pronounced negative anomaly is recorded in 2007 SAI = −1.36, with additional strongly negative years in 2015 SAI = −1.06, 2017 SAI = −1.04, and 2022 SAI = −1.01. Overall, the combination of high seasonal CVs and frequent positive and negative annual SAI values indicates a highly variable streamflow regime dominated by episodic high-flow years interspersed with numerous low-flow years, rather than a monotonic shift toward either wetter or drier hydrological conditions.

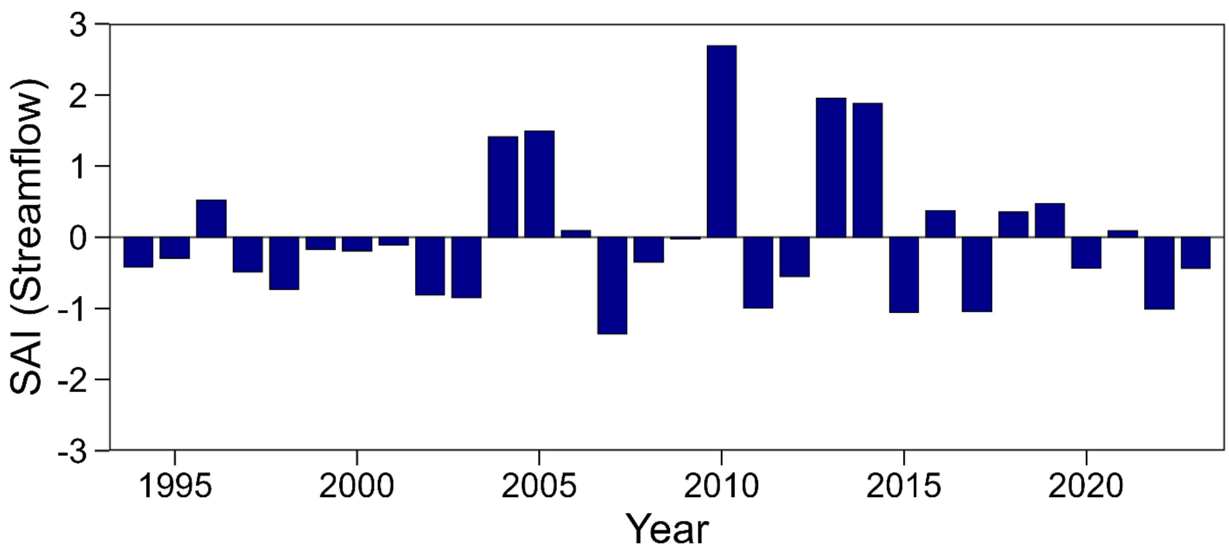

Figure 3.6 Annual standardized anomaly index (SAI) of streamflow at the S. Giovanni alla Vena gauging station for the period 1994–2023

3.10 Trend analysis

3.10.1 Temperature trends

Trends in mean temperature were analyzed using the modified Mann–Kendall test and Sen's slope for the period 1994–2023 (Figure. 3.7; Table 3.5). The annual mean temperature shows a statistically significant warming trend, with a Sen's slope of 0.052°C yr^{-1} ($\tau = 0.531$, $p = 0.021$), corresponding to an increase of 1.56°C over the study period (Figure. 3.7a; Table 3.5). Seasonally, positive trends are detected in all four seasons, but with differing magnitudes and significance levels. Spring exhibits the weakest trend, with a Sen's slope of 0.026°C yr^{-1} ($\tau = 0.182$, $p = 0.159$), which is not statistically significant (Figure. 3.7b; Table 3.5). In contrast, summer, autumn, and winter all show significant warming. Summer mean temperature increases at 0.064°C yr^{-1} ($\tau = 0.416$, $p = 0.001$), autumn at 0.072°C yr^{-1} ($\tau = 0.485$, $p < 0.001$), and winter at 0.053°C yr^{-1} ($\tau = 0.260$, $p = 0.040$) (Figure. 3.7c–e; Table 3.5). Autumn thus displays the strongest seasonal trend, equivalent to roughly 2.2°C over the 30-year period, followed by summer and winter. The consistently positive Kendall's τ values and significant Sen's slopes for annual, summer, autumn, and winter temperatures indicate a robust and seasonally pervasive warming signal in the Arno River basin, with particularly pronounced increases during the warm and cool seasons, while spring warming remains weaker and statistically non-significant.

Season	**Temp Kendall's τ**	**Temp p-value**	**Temp Sen's Slope (°C yr^{-1})**	**Precip Kendall's τ**	**Precip p-value**	**Precip Sen's Slope (mm yr^{-1})**	**Streamflow Kendall's τ**	**Stream flow p-value**	**Streamflow Sen's Slope (mm yr^{-1})**
Spring	0.182	0.159	0.026	−0.007	0.957	−0.017	−0.076	0.626	−0.463
Summer	0.416	0.001 **	0.064	−0.039	0.762	−0.329	−0.113	0.382	−0.146
Autumn	0.485	<0.001 ***	0.072	−0.071	0.598	−1.092	−0.076	0.556	−0.349
Winter	0.260	0.040 *	0.053	0.140	0.269	2.537	0.037	0.773	0.421
Annual	0.531	0.021 *	0.052	0.044	0.735	1.113	−0.007	0.957	−0.071

Table 3.5 Seasonal and annual modified Mann–Kendall statistics Kendall's τ, p-value and Sen's slope for mean temperature (Temp), precipitation (Precip), and streamflow, with corresponding p-values; significance (* $p < 0.05$; ** $p < 0.01$; *** $p < 0.001$)

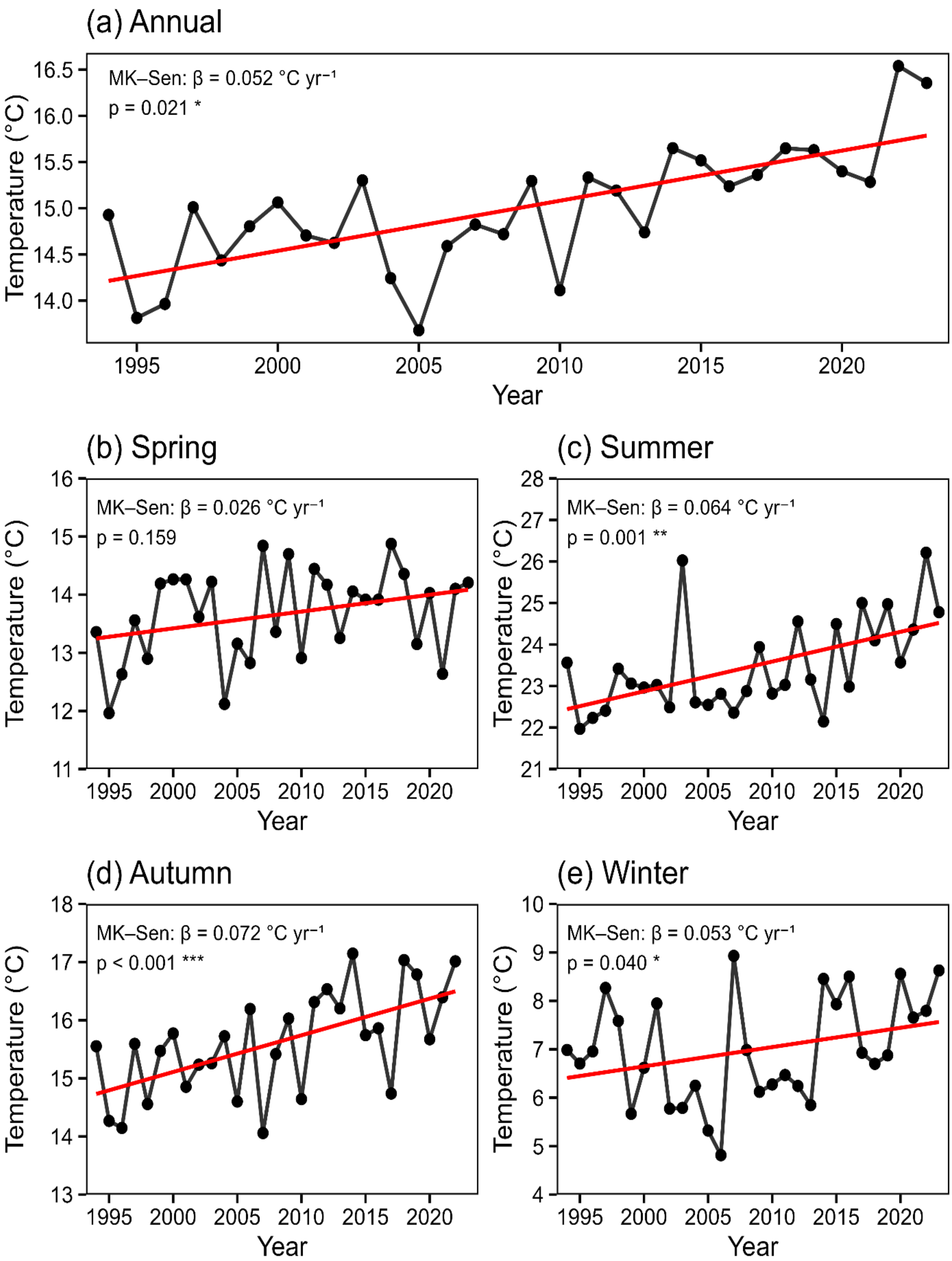

Figure 3.7 Annual and seasonal trends (a) Annual (b) Spring (MAM) (c) Summer (JJA) (d) Autumn (SON) and (e) Winter (DJF). Red line are Sen's slope estimates. M–K Sen's slope (β, °C yr^{-1}) and p-values. Significance levels: * $p < 0.05$; ** $p < 0.01$; *** $p < 0.001$

3.10.2 Precipitation trends

Trends in mean precipitation over 1994–2023 were assessed using the modified Mann–Kendall test and Sen's slope estimator (Figure. 3.8; Table 3.5). At the annual scale, precipitation shows a very weak and statistically non-significant upward tendency, with Kendall's ($\tau = 0.044$, $p = 0.735$) and a Sen's slope of 1.113 mm yr^{-1}, corresponding to an increase of roughly 30–35 mm over the study period. The annual series is characterized by large year-to-year fluctuations, with several markedly wet and dry years, but the regression line (Figure. 3.8a; Table 3.5) indicates no persistent monotonic trend. Seasonally, precipitation trends are small in magnitude and non-significant in all seasons. Spring exhibits an almost negligible negative slope (Sen's slope = −0.017 mm yr^{-1}; $\tau = -0.007$, $p = 0.957$) (Figure. 3.8b; Table 3.5). While summer and autumn show slightly stronger but still weak decreasing tendencies (−0.329 and −1.092 mm yr^{-1}; $\tau = -0.039$ and -0.071, $p = 0.762$ and 0.598, respectively) (Figure. 3.8c and d; Table 3.5). Winter is the only season with a positive Sen's slope (2.537 mm yr^{-1}; $\tau = 0.140$, $p = 0.269$), but this increase is likewise not statistically significant (Figure. 3.8e; Table 3.5). Overall, these trends indicate that, unlike temperature, annual and seasonal precipitation in the Arno River basin has not experienced a significant long-term trend over 1994–2023 and is instead dominated by pronounced interannual variability.

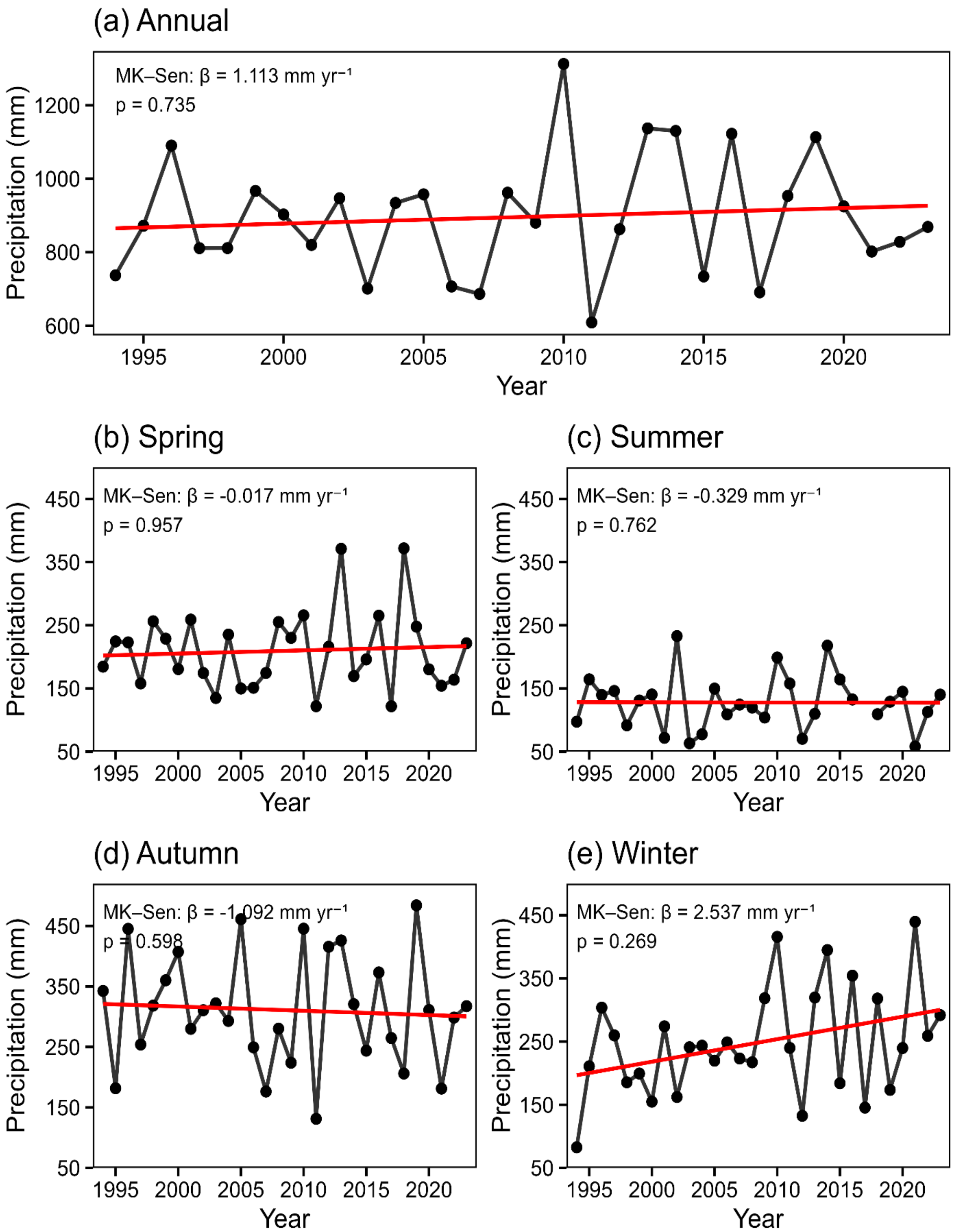

Figure 3.8 Annual and seasonal trends (a) Annual (b) Spring (MAM) (c) Summer (JJA) (d) Autumn (SON) and (e) Winter (DJF). Red lines show Sen's slope estimates of the modified M–K trend. The M–K Sen's slope (β, mm yr^{-1}) and p-values are reported in each panel

3.10.3 Streamflow trends

Trends in annual and seasonal streamflow at the S. Giovanni alla Vena gauging station were evaluated using the modified Mann–Kendall test and Sen's slope for the period 1994–2023 (Figure. 3.9; Table 3.5). The annual series exhibits pronounced year-to-year variability, with several high-flow years (e.g., around 2004–2005 and 2010, 2013, and 2014 and marked low-flow years e.g., 2003, 2007, 2011, 2015, 2017, 2022, but no clear monotonic tendency is apparent in the regression line (Figure. 3.9a; Table 3.5). Statistically, the annual trend is negligible and non-significant, with Kendall's ($\tau = -0.007$, $p = 0.957$) and a Sen's slope of -0.071 mm yr^{-1}, corresponding to an overall change of only about -2 mm over the 30-year period. At the seasonal scale, all trends are likewise weak and non-significant. Spring streamflow shows a small negative tendency (Sen's slope = -0.463 mm yr^{-1}; $\tau = -0.076$, $p = 0.626$), while summer and autumn also exhibit modest declines (-0.146 and -0.349 mm yr^{-1}; $\tau = -0.113$ and -0.076, $p = 0.382$ and 0.556, respectively) (Figure. 3.9b–d; Table 3.5). Winter is the only season with a positive Sen's slope (0.421 mm yr^{-1}; $\tau = 0.037$, $p = 0.773$), but this trend is far from statistically significant (Figure. 3.9e; Table 3.5). Overall, the Mann–Kendall results indicate that, despite substantial interannual and seasonal variability, there is no evidence of a significant long-term change in streamflow over 1994–2023, in line with the absence of significant trends in basin precipitation.

3.11 Spearman's rank correlation analysis

Seasonal and annual relationships among basin-averaged temperature, precipitation, and streamflow were evaluated using Spearman's rank correlation coefficient (ρ) Table 3.6. Precipitation and streamflow are strongly and positively correlated in all seasons, with coefficients ranging from 0.51 in spring ($p < 0.01$) to 0.93 in autumn ($p < 0.001$). Winter ($\rho = 0.83$, $p < 0.001$) and summer ($\rho = 0.59$, $p < 0.001$) demonstrate high and highly significant precipitation–streamflow correlations, and the annual correlation remains strong ($\rho = 0.77$, $p < 0.001$), confirming that interannual discharge variability is largely driven by precipitation.

However, correlations involving temperature are generally weaker and often non-significant. Temperature and precipitation show only modest negative associations in spring ($\rho = -0.20$) and autumn ($\rho = -0.04$), and a weak positive, non-significant relationship in winter ($\rho = 0.07$). A notable exception occurs in summer, where temperature is significantly and negatively correlated with both precipitation ($\rho = -0.53$, $p < 0.01$) and streamflow ($\rho = -0.57$, $p < 0.001$), indicating that hotter summers tend to coincide with drier conditions and reduced runoff. At the annual scale, temperature exhibits a weak negative correlation with precipitation ($\rho = -0.18$) and a moderate negative correlation with streamflow ($\rho = -0.33$), though neither is statistically significant at the 5% level. Together, these correlations highlight a predominantly precipitation-controlled streamflow regime, with temperature exerting a stronger influence during summer through enhanced evaporative demand and associated low-flow conditions.

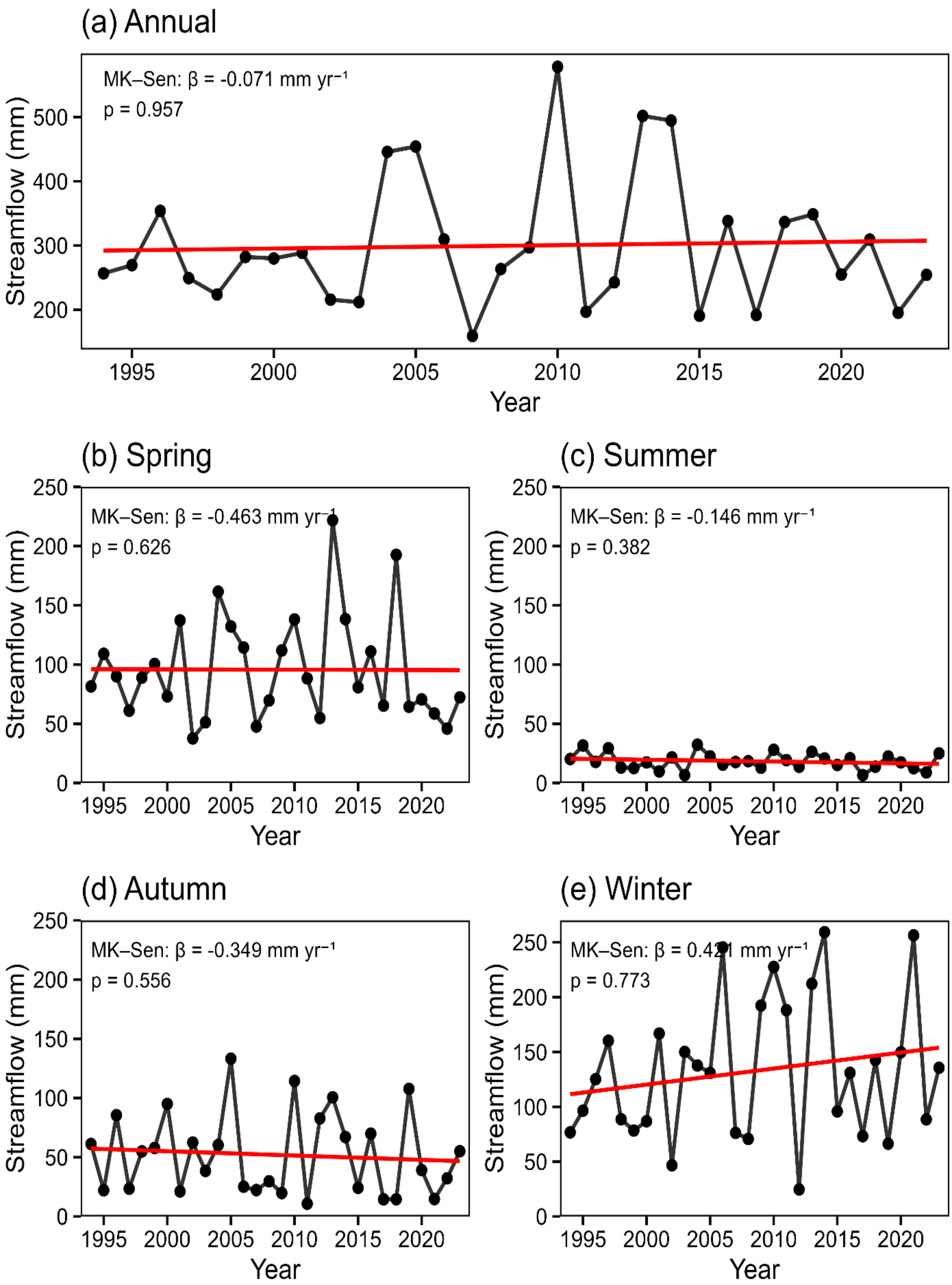

Figure 3.9 Annual and seasonal trends of streamflow (a) Annual (b) Spring (MAM) (c) Summer (JJA) (d) Autumn (SON) and (e) Winter (DJF) Red lines show Sen's slope estimates. Modified M–K Sen's slope (β, mm yr^{-1}) and p-values are reported in each panel

Season	Temp & Precip correlation	Temp & Precip p-value	Temp & Streamflow correlation	Temp & Streamflow p-value	Precip & Streamflow correlation	Precip & Streamflow p-value
Spring	−0.20	0.2926	−0.22	0.2417	0.51	0.0041 **
Summer	−0.53	0.0027 **	−0.57	<0.001 ***	0.59	<0.001 ***
Autumn	−0.04	0.8309	−0.03	0.8951	0.93	<0.001 ***
Winter	0.07	0.698	−0.08	0.6506	0.83	<0.001 ***
Annual	−0.18	0.3292	−0.33	0.0767	0.77	<0.001 ***

Table 3.6 Seasonal and annual Spearman correlations between temperature (Temp), precipitation (Precip), and streamflow for 1994–2023, with corresponding p-values; asterisks indicate significance (* $p < 0.05$; ** $p < 0.01$; *** $p < 0.001$)

3.12 Discussion

3.12.1 Regional hydroclimatic characteristics

The hydroclimatic characteristics of the Arno River basin documented in this study are consistent with the broader Mediterranean climate regime, characterized by warm, dry summers and mild, wet winters (Lionello et al., 2006). The observed seasonal precipitation distribution, with autumn contributing 34.76% and winter 30.09% of annual totals while summer accounts for only 14.08%, Table 3.3, indicates a strong cool-season concentration and a pronounced summer minimum, consistent with Mediterranean precipitation seasonality (Lionello et al., 2006; Xoplaki et al., 2004). This pronounced seasonality reflects the influence of large-scale circulation during the wet season, with variability linked to synoptic dynamics and broader circulation modes affecting Mediterranean precipitation (Xoplaki et al., 2004).

The spatial distribution of precipitation across the Arno River basin reveals a strong orographic gradient, with annual totals ranging from approximately 720 mm in the central lowlands to over 1,160 mm along the Apennine ridge (Figure. 3.3a). Such topographic modulation of precipitation is a well-established feature of mountainous terrain and is documented for central Italy, where Apennine orography contributes to the spatial variability of rainfall (Daly et al., 1994; Silvestri et al., 2022). The persistence of this gradient across all seasons, though with reduced intensity during summer, underscores the fundamental role of orography in shaping the basin's water resources.

3.12.2 Temperature trends

The significant warming trend of +0.052 °C yr^{-1} detected in the Arno River basin corresponds to an increase of approximately 1.56 °C over the 30-year study period (Figure. 3.7a). This magnitude is consistent with assessments for the Mediterranean Basins, where surface temperature is reported to be ~1.5 °C above the pre-industrial level, and regional warming has exceeded the global average since the 1980s (Aruffo & Carlo, 2019; IPCC, 2022a). Projections further indicate that future annual warming rates in the Mediterranean are expected to be about 20% higher than the global annual average (IPCC, 2022a). In Italy, long instrumental records similarly reported a sustained warming signal: an increase of about 1 °C per century in mean temperature over Italy for 1865–2003 (Brunetti et al., 2006). Consistent with this broader context, national scenario syntheses also highlight continued warming for Italy, with climate-model ensembles indicating increases up to ~2 °C for 2021–2050 relative to 1981–2010 (Aruffo & Carlo, 2019; Spano et al., 2020). The seasonal pattern of warming observed in this study, with autumn exhibiting the strongest trend +0.072 °C yr^{-1}, followed by summer +0.064 °C yr^{-1} and winter +0.053 °C yr^{-1}, while spring warming remains non-significant (Figure. 3.7b–e), is broadly consistent with evidence of amplified warm-season warming in Mediterranean Europe. Such seasonal amplification has been linked to land–atmosphere coupling and soil-moisture limitations that enhance near-surface temperature increases under drier conditions (Barcikowska et al., 2020; Giorgi & Lionello, 2008).

3.12.3 Precipitation variability and absence of significant trends

Despite the robust warming signal, annual and seasonal precipitation in the Arno River basin showed no statistically significant trends over 1994–2023, exhibiting instead high interannual variability CV = 18.2% annually, up to 36.9% in winter Table 3.4. This outcome is consistent with Mediterranean-scale evidence that trends are spatially heterogeneous and often weak or non-significant at basin/regional scales, even where temperature trends are robust (Caloiero et al., 2019; Longobardi & Villani, 2010; Philandras et al., 2011). At a sub-regional scale, similarly, no trend in annual precipitation was reported for a western French Mediterranean study area over 1970–2006, despite clear increases in temperature and potential evapotranspiration (Chaouche et al., 2010).

The alternating sequence of wet and dry years, with 2010 emerging as very wet SAI = +2.55 and 2011 as severely dry SAI = −1.76 (Figure. 3.5a), illustrates the episodic nature of Mediterranean precipitation variability. Such year-to-year swings are strongly influenced by large-scale atmospheric circulation, including variability associated with the North Atlantic Oscillation (NAO), which modulates precipitation over large parts of Europe and the Mediterranean basin (Hurrell & Van Loon, 1997; Philandras et al., 2011). The absence of a systematic trend, combined with high seasonal variability, suggests that future water resource planning in the Arno River basin should prioritize adaptation to interannual variability rather than monotonic change.

3.12.4 Streamflow dynamics and precipitation–runoff relationships

The streamflow regime of the Arno River exhibits pronounced seasonality, with winter and spring together contributing 77% of annual runoff despite receiving only 53.5% of annual precipitation Table 3.3. This seasonal redistribution is consistent with Mediterranean catchment behavior, where cool-season runoff is supported by lower evaporative demand and catchment wetting, while summer drought conditions promote soil moisture depletion and reduced discharge (Gallart et al., 2002; Merheb et al., 2016). During summer, high evaporative losses and limited rainfall typically translate into strongly reduced flows, a characteristic of Mediterranean-climate river regimes (Cid et al., 2017; Lupon et al., 2018).

The strong positive correlation between precipitation and streamflow ($\rho = 0.77$ annually, reaching $\rho = 0.93$ in autumn) Table 3.6, indicates that interannual discharge variability in the Arno River basin is primarily driven by precipitation variability, consistent with the dominant role of precipitation seasonality and year-to-year rainfall fluctuations in Mediterranean flow dynamics (Cid et al., 2017; Merheb et al., 2016). The absence of significant streamflow trends is therefore coherent with the lack of precipitation trends over the study period. This contrasts with evidence from broader Mediterranean regions where long-term decreases in streamflow have been linked to warming-driven increases in evapotranspiration, compounded by declining precipitation (Masseroni et al., 2021).

3.12.5 Temperature–streamflow coupling and evapotranspiration effects

The significant negative correlation between temperature and streamflow during summer ($\rho = -0.57$, $p < 0.001$) highlights the role of atmospheric evaporative demand in modulating warm-season hydrology Table 3.6. Evapotranspiration is a dominant component of Mediterranean water balances, and a very large fraction of annual rainfall can be returned to the atmosphere through evapotranspiration in Mediterranean climates (Dakhlaoui et al., 2020). Moreover, process-based evidence from Mediterranean catchments shows that evapotranspiration (including riparian evapotranspiration) can substantially influence seasonal streamflow dynamics, with the strongest effects during the vegetative/summer period (Lupon et al., 2018). The concurrent negative correlation between temperature and precipitation in summer ($\rho = -0.53$, $p < 0.01$) Table 3.6, indicates that warm anomalies tend to co-occur with dry conditions, compounding streamflow reductions through both reduced inputs and enhanced losses. These results are consistent with climate-impact modelling evidence that increases in evaporative demand can reduce water yield and baseflow under future warming. For example, SWAT+ simulations for a Mediterranean watershed in Sardinia project decreases in water yield, surface runoff, and baseflow driven primarily by enhanced evapotranspiration (Pulighe et al., 2021).

3.13 Implications for water resources management

The results of this study carry significant implications for water resources management in the Arno basin. First, the combination of robust warming trends with stable but highly variable precipitation creates conditions conducive to increased drought severity and frequency, even without systematic precipitation declines (Hertig & Tramblay, 2017; IPCC, 2022a; Tariq et al., 2024). The high coefficient of variation in seasonal streamflow, particularly in autumn 65.8% and winter 50.3% Table 3.4, indicates substantial year-to-year uncertainty in water availability that must be incorporated into reservoir operation and allocation strategies.

Second, the seasonal redistribution of runoff, with summer flows comprising only 6.53% of the annual total while experiencing the strongest temperature–streamflow coupling, identifies the warm season as the period of greatest vulnerability. As warming continues, competition among agricultural irrigation, urban supply, and environmental flows during summer low-flow periods is likely to intensify. Ecosystem services provided by the Arno River, including water supply, flood regulation, and biodiversity support, face heightened vulnerability under scenarios of continued warming (IPCC, 2022a; Tariq et al., 2024).

Finally, the strong precipitation–streamflow correlation across all seasons suggests that improvements in seasonal precipitation forecasting could substantially enhance water management capabilities Table 3.6. Given the influence of large-scale climate modes such as the North Atlantic Oscillation on Mediterranean precipitation (Hurrell & Van Loon, 1997;

Luppichini et al., 2021), integration of climate teleconnection indices into operational forecasting systems represents a promising avenue for adaptation (Giuliani et al., 2019).

3.14 Study limitations and future research directions

Several limitations of this study are acknowledged. First, the 30-year study period (1994–2023), while sufficient for detecting climate signals, may not capture longer-term cycles or trends that operate on multi-decadal timescales. Second, streamflow analysis was based on a single gauging station (S. Giovanni alla Vena), which, while representative of the lower basin, may not fully reflect spatial variability in hydrological response across the sub-basins. Third, the study did not explicitly account for anthropogenic influences such as water abstractions, land use changes, or reservoir operations, which may modulate the climate–hydrology relationships. Future work should extend the analysis to include longer observational or reconstructed datasets where available, incorporate multiple streamflow gauging stations to assess spatial patterns, and employ hydrological modelling to separate climatic from anthropogenic influences on streamflow. Additionally, analysis of extreme events (floods and droughts) and their changing frequency and intensity would complement the mean-state analysis presented here.

3.15 Conclusions

This study analyzed hydroclimatic variability and trends in the Arno River basin, Tuscany Italy, focusing on annual and seasonal patterns of temperature, precipitation, and streamflow from 1994 to 2023. The analysis reveals a statistically significant annual warming rate of 0.052 °C yr^{-1} corresponding to approximately 1.56 °C over the study period, with the strongest seasonal increases in autumn +0.072 °C yr^{-1} and summer +0.064 °C yr^{-1}, while spring warming remains non-significant. The concentration of positive temperature anomalies since 2014 indicates an acceleration of warming, consistent with broader Mediterranean patterns. In contrast, precipitation and streamflow exhibit no significant monotonic trends at annual or seasonal scales, but instead display pronounced interannual variability, with CV up to 36.9% for winter precipitation and 65.8% for autumn streamflow. The spatial distribution of precipitation reveals a strong orographic gradient, with annual totals ranging from approximately 720–830 mm in the central lowlands to over 1,160 mm along the Apennine ridge. The alternating occurrence of wet and dry years reflects the episodic nature of the Mediterranean hydroclimate, likely modulated by large-scale atmospheric circulation. Correlation analysis confirms a precipitation-dominated streamflow regime ($\rho = 0.51–0.93$ across seasons), with winter and spring together contributing approximately 77% of annual runoff. The significant negative temperature–streamflow correlation in summer ($\rho = -0.57$) indicates that increasing evaporative demand is already influencing warm-season hydrology. This coupling, combined with ongoing warming, suggests that summer low-flow conditions may intensify even in the absence of declining precipitation.

These findings carry important implications for water-resources management. The high hydroclimatic variability underscores the need for adaptive management strategies that can accommodate strong year-to-year fluctuations. Summer emerges as the season of greatest vulnerability, characterized by minimal runoff contribution ~ 6.5%, strong temperature–streamflow coupling, and continued warming. The robust precipitation–streamflow relationship suggests that improved seasonal forecasting could enhance operational water resource management. Overall, the combination of robust warming, high hydroclimatic variability, and emerging summer water stress highlights the importance of integrated hydroclimatic monitoring and proactive climate-adaptation planning in the Arno River basin.

Chapter 4 Investigating future hydroclimatic trends and drought characterization using CMIP6 and SWAT+ in the Arno River basin, Tuscany, Italy

This Chapter is based on a research paper published in Water Cycle
https://doi.org/10.1016/j.watcyc.2026.03.006

4.1 Introduction

Climate change is intensifying Earth's hydrological cycle, reshaping water resources, ecosystem services, and socioeconomic systems worldwide (Ahmed et al., 2026; IPCC, 2022b). The intergovernmental Panel on Climate Change (IPCC) Sixth Assessment Report (AR6) emphasizes that global GHG emissions in 2030 implied by nationally determined contributions make it likely that warming will exceed 1.5 °C during the 21st century and make it harder to limit warming below 2°C (IPCC, 2023). Recent global drought analysis reveals that atmospheric evaporative demand has increased drought severity by an average of 40% globally, with areas experiencing drought expanding by 74% during 2018–2022 compared to 1981–2017 (Gebrechorkos et al., 2025). Temperature and precipitation extremes are cascading into runoff deficits and hydrological drought through increased evapotranspiration and altered precipitation patterns (IPCC, 2022b). Understanding how meteorological droughts propagate into hydrological droughts has become increasingly important, as recent studies demonstrate that climate change accelerates this propagation while human activities such as reservoir operations can delay it by several months (Ullah et al., 2025; Wang et al., 2019; Wu et al., 2022).

These global patterns highlight the critical importance of regional assessments to understand local vulnerabilities and adaptation requirements under accelerating climate change. However, effective water resource management requires climate projections at watershed scales that can capture the local topographic, hydrological, and land-use heterogeneity that controls how global climate signals translate into local impacts, watershed boundaries represent the natural hydrologic units where precipitation is converted to streamflow, making them the appropriate scale for assessing climate impacts on water resources and developing targeted adaptation strategies (Cosgrove & Loucks, 2015; Keller et al., 2023).

General circulation models (GCMs) serve as important tools for quantifying hydroclimatic extreme impacts projected under future scenarios (Nakhaei et al., 2024; O'Neill et al., 2016).

In principle, GCMs simulate detailed processes of the land, atmosphere, and oceans (Tebaldi et al., 2021). The newest edition of the Coupled Model Intercomparison Project Phase 6 (CMIP6) incorporates a series of updates (O'Neill et al., 2016). In particular, it launches the Scenario Model Intercomparison Project, a novel framework grounded in the Shared Socioeconomic Pathways (SSPs) (Eyring et al., 2016). This represents a notable milestone in the IPCC's international initiative, through the incorporation and assessment of socioeconomic factors as pointed out in the AR6 report (IPCC, 2023). SSP shapes particular greenhouse gas (GHG) emission trajectories for instance, SSP2-4.5 (+4.5 W m^{-2}; medium forcing middle-of-the-road pathway), and SSP5-8.5 (+8.5 W m^{-2}; high-end forcing pathway) under reference scenarios (O'Neill et al., 2016). Recent CMIP6-based projections indicate that the frequency of 50-year historical droughts may double across large continental areas under 1.5°C warming, with Mediterranean regions projected to experience exacerbated drought severity under warming scenarios of 1.5–3.0°C (Ullah et al., 2022). Integrating such emission scenarios into hydrological models facilitates a more comprehensive understanding of how climatic and socioeconomic drivers physically affect hydrological processes (O'Neill et al., 2016).

The Mediterranean region has emerged as a pronounced climate change hotspot, exhibiting amplified warming and drying trends that exceed global averages (Cos et al., 2022; Noto et al., 2023). Regional assessments consistently indicate reductions in precipitation, declining streamflow, and rising evapotranspiration, confirming the region's acute vulnerability to hydroclimatic extremes (Eekhout et al., 2025; Estrada et al., 2024; IPCC, 2022b). In Italy, basin-scale studies likewise project significant reductions in water availability and more severe drought conditions (Abdelwahab et al., 2025; Senatore et al., 2022; Tariq et al., 2024). Recent applications of hydrological models with CMIP6 projections in Italian watersheds have demonstrated substantial inter-model uncertainty; for example, studies in the Carapelle basin (Apulia) reported mean annual flow reductions ranging from -7% to -67% depending on GCM selection (Abdelwahab et al., 2025), while investigations in the Aterno-Pescara watershed found strong correlations between 12-month meteorological and hydrological drought indices ($r = 0.63$–0.93) (Tariq et al., 2024). Collectively, these findings underscore the exposure of Mediterranean catchments to water scarcity.

Despite these advances, important knowledge gaps remain. First, while the Soil and Water Assessment Tool (SWAT) has been widely used to assess climate hydrology interactions (Arnold et al., 1998; Bhatta et al., 2019; C. Li & Fang, 2021). Applications of the advanced SWAT+ framework remain limited in Italian watersheds despite its enhanced flexibility for representing landscape connectivity and management practices (Bieger et al., 2017; Leone et al., 2023; Pulighe et al., 2021). A comprehensive review of 260 SWAT studies in Mediterranean catchments (2002–2022) found that while 62% were conducted in Greece, Italy, or Spain (Aloui et al., 2023), most Italian applications concentrated in southern regions (Abdelwahab et al., 2025; Pulighe et al., 2021), leaving central Italian basins comparatively understudied. Second, although CMIP6 scenarios are increasingly employed, their raw outputs contain substantial biases in precipitation and temperature that, if uncorrected, lead to unreliable hydrological simulations. While statistical bias-correction techniques such as quantile mapping are commonly applied, these approaches can distort climate signals; advanced methods like quantile delta mapping (QDM) better preserve distributional changes but remain underutilized in Mediterranean catchments (Cannon et al., 2015; Padulano et al., 2025; Song & Chung, 2025). QDM explicitly preserves relative changes in precipitation quantiles, addressing a critical limitation of standard quantile mapping that can artificially alter future model-projected trends, especially for precipitation extremes (Cannon et al., 2015). Third, relatively few studies explicitly examine the propagation of meteorological drought into hydrological drought using standardized indices, despite its importance for water management and drought adaptation planning. Recent multivariate frameworks have demonstrated that propagation thresholds vary substantially across timescales and methods, emphasizing the need for systematic propagation analysis in climate impact assessments (Odongo et al., 2023; Ullah et al., 2025). Regarding drought index selection, the World Meteorological Organization recommends SPI values at 12 months or longer for hydrological impact assessment, as groundwater, streamflow, and reservoir storage reflect longer-term precipitation anomalies (Svoboda et al., 2012). This guidance is supported by comparative studies demonstrating that 12-month accumulation periods effectively capture hydrological memory in Mediterranean-type catchments with distinct seasonal variability (Baez-Villanueva et al., 2024; Tariq et al., 2024). While shorter accumulation periods (1–6 months) are valuable for agricultural drought monitoring, the 12-month timescale is most appropriate for assessing long-term water resource availability and basin-scale hydrological responses that are the focus of this study.

The Arno River basin is critical for climate change drought analysis because it sustains more than 2.2 million people, supports key urban and agricultural economies, and is already exposed to marked seasonal water stress (Bartolini et al., 2018; Venturi et al., 2014). These factors create high competition among domestic, agricultural, industrial, and ecological water uses, making the basin particularly vulnerable to projected climate-driven reductions in water availability.

Assessing drought dynamics in this context not only advances scientific understanding of Mediterranean hydroclimatic changes but also provides evidence directly relevant for basin-scale water management and for regional policy. Building on recent SWAT+ and CMIP6 applications in Aterno-Pescara watershed (Tariq et al., 2024). This study extends the integrated modeling framework to the Arno River basin, implementing QDM bias correction and comprehensive drought propagation analysis using standardized indices (SPI/SRI). This methodological approach advances Mediterranean climate-hydrology assessment by combining process-based hydrological modeling with systematic quantification of meteorological-to-hydrological drought transmission under future climate scenarios. This study addresses three research questions: (1) How well can the SWAT+ model simulate the hydrological processes of the Arno River basin, and which parameters most strongly control streamflow response (2) How will precipitation, temperature, and streamflow change across near-future (2015–2040), mid-future (2041–2070), and far-future (2071–2100), periods under moderate SSP2-4.5 and high SSP5-8.5 emission scenarios, and what is the uncertainty range across the five GCMs ensemble and (3) How will meteorological drought propagate into hydrological drought under future climate conditions, and what are the projected changes in drought duration, severity, and frequency.

To address these questions, we calibrate and validate SWAT+ using observed data, apply QDM bias correction to five CMIP6 models under both SSP scenarios, and characterize drought evolution using 12-month SPI and SRI indices with run-sum event identification method. The findings aim to provide both methodological contributions through the integration of SWAT+ with bias-corrected CMIP6 projections and transferable insights for adaptive water management in the Arno River basin and other Mediterranean watersheds.

4.2 Materials and methods

4.2.1 Study area

The Arno River basin, located in central Italy, represents one of the major watersheds in the Mediterranean region with a drainage area of approximately 8,230 km^2 and extending approximately 240 km (Figure. 4.1). The catchment is characterized by complex topography with elevations ranging from -1 to 1,625 m above sea level (average 342 m), creating distinct physiographic zones from mountainous headwaters in the Tuscan Apennines to alluvial plains near the Tyrrhenian Sea outlet (Figure. 4.2a). The basin includes major urban centers such as Florence and Pisa, which serve as important socioeconomic hubs (Campo et al., 2006; Diodato et al., 2021). The climate is Mediterranean, with annual precipitation ranging from 700 to 1,700 mm and mean temperatures between 12 and 22°C (Burlando & Rosso, 2002). Land-use distribution comprises forest cover (51%), agricultural land (26.7%), urban areas (15.6%), and rangeland (6.6%) (Figure. 4.2b). Soil distribution is characterized by five main types including loam soils covering 69.6% of the basin (Bd68-2bc: 60.9%, Re85-2b: 8.7%), clay loam soils accounting for 28.5% (Be130-2-3: 20.5%, Be133-2-3: 8.0%), and sandy loam soils representing 2.0% (Po28-1bc) of the total area, where codes indicate FAO-HWSD soil classification units (Figure. 4.2c).

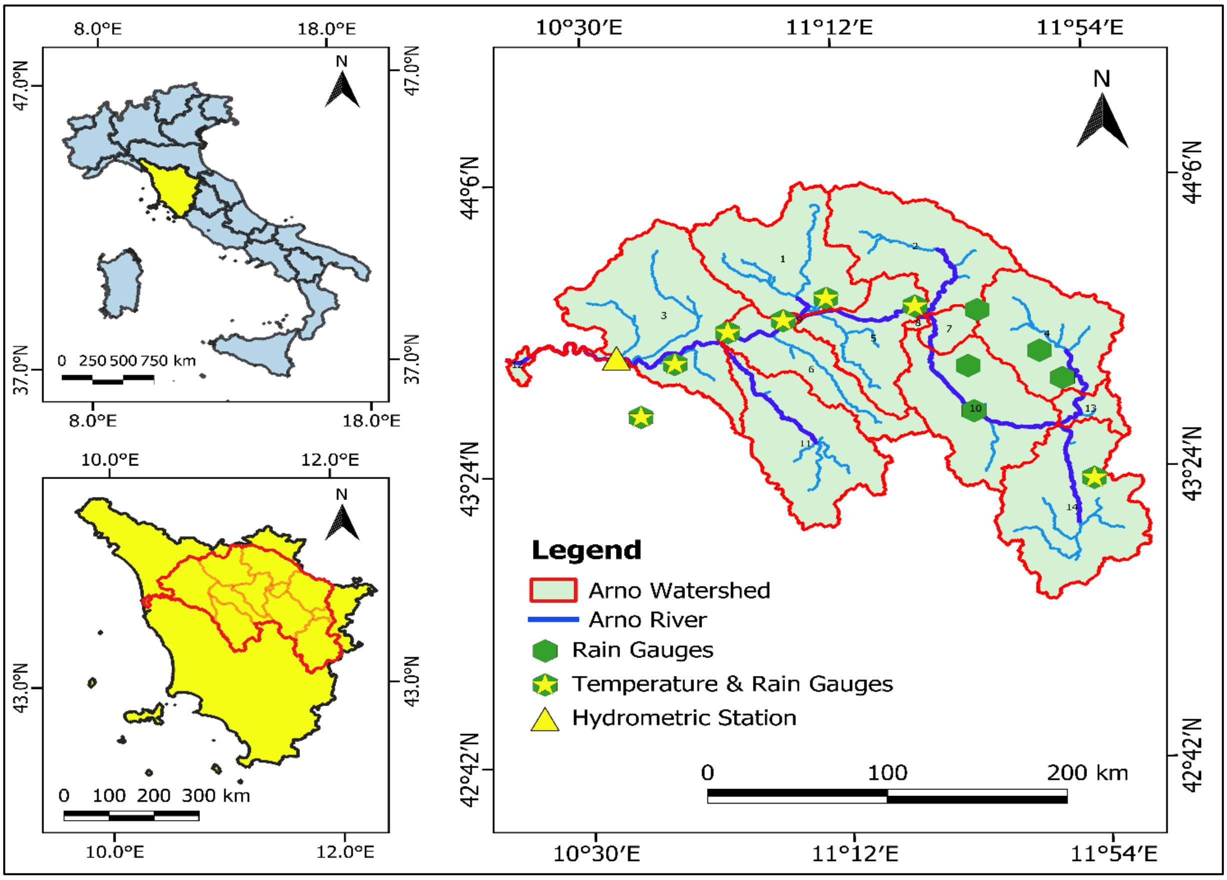

Figure 4.1 Study area map of the Arno river watershed with temperature, rain gauge and hydrometric stations

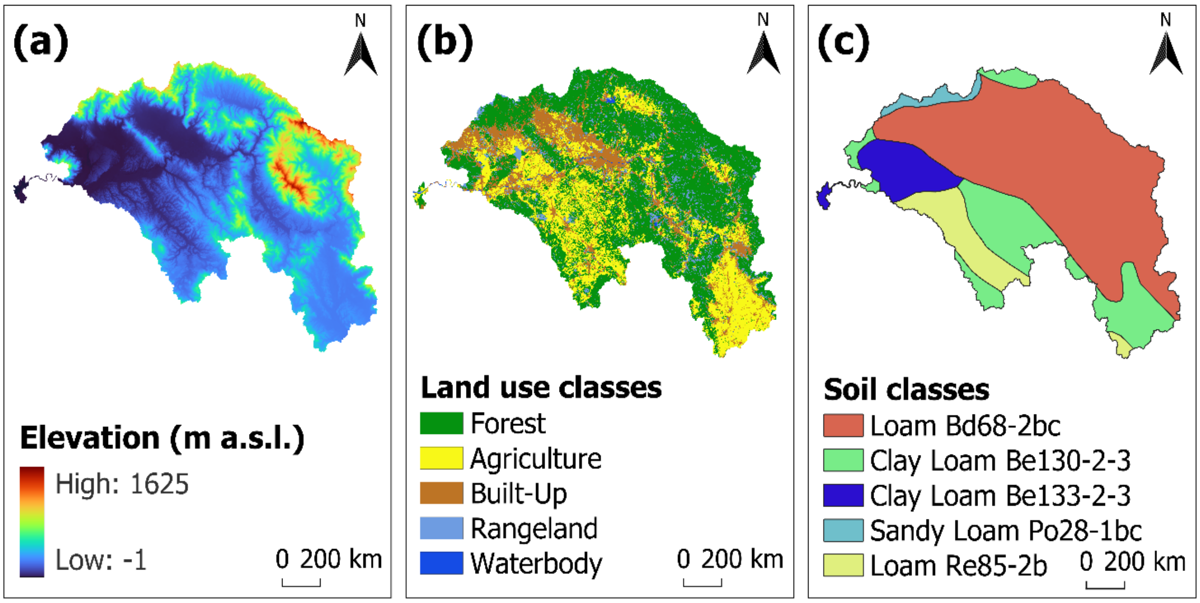

Figure 4.2 Spatial input details used in SWAT+ (a) DEM (b) land use and (c) soil classification

4.2.2 Data Collection

4.2.3 Hydrometeorological data

Daily hydrometeorological data (1994-2014) were obtained from the Regional Hydrological Service of Tuscany (SIR), including maximum and minimum temperatures from seven stations and precipitation from twelve stations distributed across the basin. These datasets served as baseline observations for bias-correcting raw CMIP6 model outputs. River discharge data (2005-2014) from the S. Giovanni alla Vena valle gauging station were acquired from the same source for SWAT+ model calibration and validation (Figure. 4.1; Table 4.1 and 4.2).

Data Type	Source	Spatial resolution	Temporal resolution
DEM	CREODIAS (https://explore.creodias.eu/)	30 m	–
LULC	Esri Living Atlas (https://livingatlas.arcgis.com/landcover/)	10 m	2023
Soil Map	FAO Harmonized World Soil Database v1.2 (http://www.fao.org)	1:5,000,000	–
Precipitation	Regional Hydrological Service	12 Stations	Daily (1994–2014)
Temperature	Regional Hydrological Service	07 Stations	Daily (1994–2014)
River Runoff	Regional Hydrological Service	01 Station	Daily (2005–2014)

Table 4.1 Input data used in SWAT+ and corresponding sources

S. No	Station number	Station name	Data type	Data frequency
1.	TOS01000601	Ortignano	(Prcip)	Daily (1994-2014)
2.	TOS01000651	Salutio	(Prcip)	Daily (1994-2014)
3.	TOS01000881	Pian di Scò	(Prcip)	Daily (1994-2014)
4.	TOS01001041	Consuma	(Prcip)	Daily (1994-2014)
5.	TOS01001225	Case Passerini	(Prcip, Temp)	Daily (1994-2014)
6.	TOS01004571	Montevarchi	(Prcip)	Daily (1994-2014)
7.	TOS11000016	Terricciola	(Prcip, Temp)	Daily (1994-2014)
8.	TOS11000024	Remole	(Prcip, Temp)	Daily (1994-2014)
9.	TOS11000038	Ottavo	(Prcip, Temp)	Daily (1994-2014)
10.	TOS11000046	Montopoli	(Prcip, Temp)	Daily (1994-2014)
11.	TOS11000071	Cerreto Guidi	(Prcp, Temp)	Daily (1994-2014)
12.	TOS11000076	Artimino	(Prcip, Temp)	Daily (1994-2014)
13.	TOS01005191	S.Giovanni alla VV	River Discharge	Daily (2005-2014)

Table 4.2 List of meteorological and hydrological stations in study area

4.2.4 Topography, land-use, and soil data

The digital elevation model (DEM) was obtained from Copernicus DEM GLO-30 dataset via CREODIAS platform at 30-meter resolution. Land-use/land cover (LULC) was derived from ESRI 2023 Global Land Cover product at 10-meter resolution. To isolate climate change effects on hydrological processes and to ensure projected streamflow changes are driven exclusively by climate variables, land cover remained constant at 2023 levels for all historical and future simulations, following established climate-impact modeling methodology (C. Li & Fang, 2021). This fixed-LULC configuration represents a climate-only experiment designed to attribute projected hydrological and drought changes primarily to climatic forcing. It does not represent possible future land-use trajectories (e.g., urban expansion, agricultural shifts, or vegetation changes), which are therefore treated as an additional source of uncertainty and discussed in Section 4.4. The Soil data were acquired from the Harmonized World Soil Database (HWSD) Version 1.2, developed by the Food and Agriculture Organization of the United Nations (FAO-UN) (Figure. 4.2; Table 4.1).

4.2.5 SWAT+ model set-up

The SWAT+ hydrological model (rev.61.0.1) was employed using the QGIS interface (QSWAT+3.0.3) and SWAT+ Editor (3.0.8), following the workflow illustrated in (Figure. 4.3) (Arnold et al., 2018; López-Ballesteros et al., 2024). Watershed delineation was carried out using the Copernicus DEM (30 m) in QSWAT+3.0.3, with a channel threshold of 80,329 cells approximately (53.5 km²) and a stream threshold of 803,296 cells approximately (534.7 km²). The outlet was defined at the S. Giovanni alla Vena valle gauging station. This threshold-based delineation resulted in 14 sub-basins, further subdivided into 1,176 HRUs defined by unique combinations of land-use, soil type, and slope. The selected thresholds balance the representation of spatial heterogeneity in topography, land cover, and soils with computational efficiency required for multi-GCM ensemble climate simulations. Model calibration (2007–2011) and validation (2012–2014) were performed at monthly time steps following a 2-year warm-up period (2005–2006) to stabilize initial conditions. Model calibration and validation were conducted at the S. Giovanni alla Vena Valle gauging station, located near the basin outlet. This outlet-based calibration approach is commonly adopted in SWAT/SWAT+ climate impact studies, as the downstream station integrates hydrological responses from the entire contributing area, providing a comprehensive measure of basin-scale water balance (Leone et al., 2023; C. Li & Fang, 2021; Pulighe et al., 2021; Tariq et al., 2024). The observed record both wet dry hydrological years, ensuring representation of contrasting flow regimes relevant for model parameterization. The Penman-Monteith method was applied for potential evapotranspiration (PET) estimation due to its physical basis and consistent performance across diverse climatic conditions (Allen et al., 1998; Yimer et al., 2023). Monthly time steps were chosen to capture seasonal and long-term hydrological patterns relevant to drought analysis while reducing computational demands associated with multi-model ensemble simulations.

Sobol's global sensitivity analysis was conducted using SWAT+ Toolbox (v 2.4.1) to identify parameters most influential on basin hydrology. This approach quantifies individual parameter contributions and their interactions to output variance, providing a robust ranking of parameter importance (Sobol', 1990). Previous SWAT+ applications in Mediterranean catchments far-future have demonstrated that parameters controlling surface runoff (cn2, cn3_swf), groundwater processes (alpha_bf, lat_ttime), and soil characteristics (bd) exert the strongest influence on hydrological dynamics (Leone et al., 2023; Pulighe et al., 2021; Tariq et al., 2024). Guided by these insights from similar climatic environments, our sensitivity analysis identified nine parameters with the highest sensitivity to streamflow simulation in the study catchment. Model calibration was conducted at the S. Giovanni alla Vena valle station using 500 autocalibration iterations with a consistent parameter set, emphasizing the soil and groundwater parameters identified as critical in Mediterranean hydrological modeling. The parameter adjustment range of −15% to +15% was applied using the "percent change" type to optimize autocalibration performance Table 4.3. This parameterization ensured the model configuration reflected both the hydro-climatic characteristics of the Arno River basin and established practices from prior SWAT+ applications in Mediterranean watersheds.

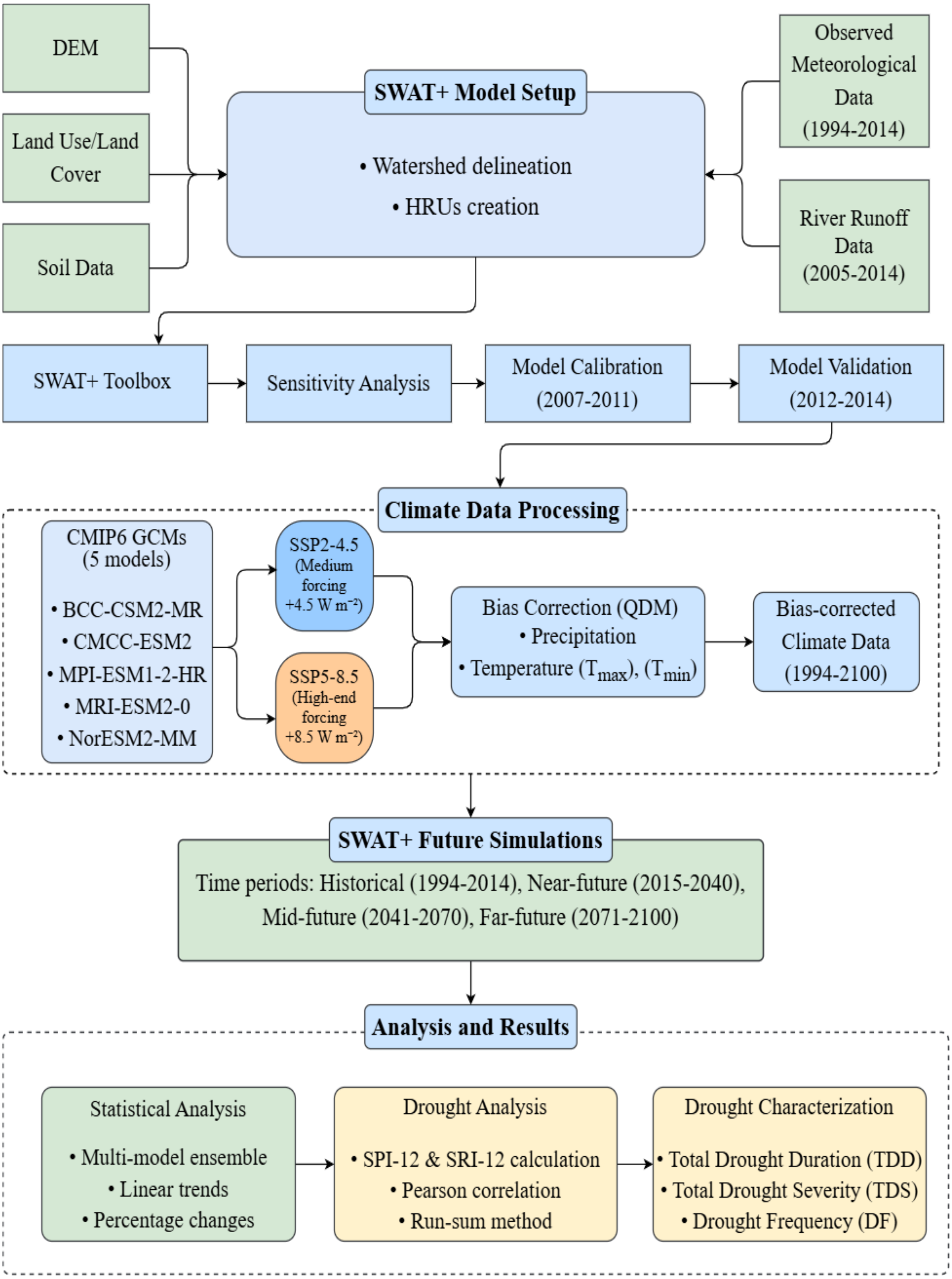

Figure 4.3 Detailed flowchart of hydrologic modelling and climate data processing methodology applied in this study

Parameter	Description	Group	Adj. Min (%)	Adj. Max (%)	Abs.min	Abs.max	Calibrated adj. (%)	Units
cn2	Curve number	hru	-15	15	35	95	12.241	—
cn3_swf	Evaporation coefficient	hru	-15	15	0	1	-13.661	—
lat_ttime	Lateral flow travel time	hru	-15	15	0.5	180	5.790	days
snomelt_lag	Snowmelt lag factor	hru	-15	15	0	1	1.230	—
bd	Soil bulk density	sol	-15	15	0.9	2.5	14.617	Mg m^{-3}
awc	Available water capacity of the soil layer	sol	-15	15	0.01	1	0.070	mm H_2O/mm
k	Saturated hydraulic conductivity	sol	-15	15	0.0001	2000	-0.009	mm/hr
surlag	Surface runoff lag coefficient	bsn	-15	15	0.05	24	-1.535	days
alpha	Base-Flow alpha factor	aqu	-15	15	0	1	6.934	days

Table 4.3 SWAT+ Toolbox autocalibration parameters used for monthly streamflow calibration, showing adjustment bounds (Adj. Min/Max, %), absolute physical bounds (Abs. min/max), and the final calibrated percent adjustments

4.2.6 Performance metrics

Model performance was examined using three statistical metrics to assess goodness of fit: the Nash-Sutcliffe efficiency (NSE), percent bias (PBIAS), and Kling-Gupta efficiency (KGE) (Gupta et al., 2009; Nash & Sutcliffe, 1970). NSE quantifies the model's variance explanation relative to observed data (Nash & Sutcliffe, 1970). PBIAS measures systematic volume errors and the model's tendency to over- or under-estimate observations (Moriasi et al., 2015). KGE provides comprehensive assessment through comparison of means, variability, and correlation between observed and modeled streamflow (Gupta et al., 2009). These metrics with ranges and equations are illustrated in Table 4.4.

Metric	Equation	Unsatisfactory	Satisfactory	Good	Very Good
NSE	$1-\frac{\sum_{i=1}^{n}(Q_{obs,i}-Q_{sim,i})^2}{\sum_{i=1}^{n}(Q_{obs,i}-\bar{Q}_{obs})^2}$	≤ 0.50	0.50 – 0.65	0.65 – 0.75	≥ 0.75
PBIAS	$100\times\left[\frac{\sum_{i=1}^{n}(Q_{sim,i}-Q_{obs,i})}{\sum_{i=1}^{n}(Q_{obs,i})}\right]$	≥ ± 25 %	± 15 %– ± 25 %	± 10 % – 15 %	≤ ±10 %
KGE	$1-\sqrt{(r-1)^2+\left(\frac{\sigma_{sim}}{\sigma_{obs}}-1\right)^2+\left(\frac{\mu_{sim}}{\mu_{obs}}-1\right)^2}$	≤ 0.50	0.50 – 0.75	0.75 – 0.90	≥ 0.90

Note: $Q_{obs,i}$ and $Q_{sim,i}$ are observed and simulated streamflow at time i; $\bar{Q}_{obs}$ is mean observed streamflow; n is number of observations; r is Pearson correlation coefficient; σ and μ denote standard deviation and mean, respectively (subscripts: sim = simulated, obs = observed).

Table 4.4 Model performance metrics and their classification thresholds used in this study

4.2.7 CMIP6 GCMs future climate projections

Streamflow is predominantly governed by precipitation and temperature as key climate variables (C. Li & Fang, 2021; Wang et al., 2018). Daily outputs of maximum (T_{max}) and minimum (T_{min}) temperatures and precipitation data from five GCMs at approximately 1° resolution from CMIP6, comprising the historical simulations (1994–2014) and future projections (2015–2100) under two emission scenarios, were obtained from the Earth System Grid Federation website https://aims2.llnl.gov/search/cmip6/ (accessed at 08-02-2025) (Table 4.5; (Eyring et al., 2016)). The two selected scenarios from ScenarioMIP are SSP2-4.5 (+4.5 W m^{-2}; medium forcing middle-of-the-road pathway), and SSP5-8.5 (+8.5 W m^{-2}; high-end forcing pathway) (O'Neill et al., 2016). Temperature and precipitation data underwent bias-correction using observed meteorological stations data within each grid cell over the watershed using similar coordinates. The entire simulation period divided into the historical period (1994–2014) and three future periods as near-future (2015–2040), mid-future (2041–2070) and far-future (2071–2100). Bias-corrected GCM variables served as inputs to the already calibrated SWAT+ hydrological model to simulate historical and projected river runoff under both SSP scenarios. A two-year warm-up period (1994–1995) was incorporated to stabilize initial conditions. The model executed independently for each GCM, using its respective meteorological inputs under the designated scenarios. This procedure yielded future runoff projections for subsequent analysis.

ID	CMIP6 Model	Institute	Country	Spatial Resolution
1	BCC-CSM2-MR	Beijing Climate Center (BCC)	China	1.125° × 1.125°
2	CMCC-ESM2	Euro-Mediterranean Center on Climate Change (CMCC)	Italy	1.0° × 1.0°
3	MPI-ESM1-2-HR	Max Planck Institute for Meteorology (MPI)	Germany	0.9375° × 0.9375°
4	MRI-ESM2-0	Meteorological Research Institute (MRI)	Japan	1.125° × 1.125°
5	NorESM2-MM	Norwegian Climate Center (NCC)	Norway	0.9° × 1.25°

Table 4.5 Details of selected CMIP6 models used in this study

4.2.8 Bias correction of GCMs data

GCM outputs at coarse spatial resolution require bias correction due to scale mismatch and structural limitations in representing physical processes. Precipitation and temperature variables (maximum and minimum) from all five GCMs under both emission scenarios were bias-corrected against point-gauge observations using the Quantile Delta Mapping (QDM) method (Cannon et al., 2015). We selected QDM over alternative bias-correction methods (e.g., Linear Scaling and Empirical Quantile Mapping) for three main reasons: (1) QDM explicitly preserves relative changes in climate model quantiles while correcting systematic distributional biases; (2) unlike conventional quantile mapping, QDM avoids artificially distorting future model-projected trends; and (3) QDM has been widely used in climate-impact applications because it corrects historical distributional biases while preserving the modeled climate-change signal across quantiles, including extremes; however, method performance can vary by region, variable, and evaluation metric (Cannon et al., 2015; X. Li & Li, 2023; Tong et al., 2021; Tugrul et al., 2025). QDM operates through two steps: (1) identifying quantile relationships between observed and modeled data during the historical calibration period, and (2) applying these relationships to future projections while maintaining climate model projected relative changes (H. Li et al., 2010; Switanek et al., 2017). This approach employs variable-specific correction strategies: multiplicative correction for precipitation to account for its ratio-based nature, and additive correction for temperature to preserve absolute temperature differences. QDM was applied at the daily time step to precipitation, maximum temperature, and minimum temperature series used to force SWAT+. Transfer functions were fitted over the historical period (1994–2014) using corresponding observed daily gauge data and then applied to future projections. For precipitation, the mapping was applied to positive amounts while zero/near-zero values were retained to avoid generating spurious wet days; this corrects intensity distributions while maintaining occurrence characteristics.

here, $q = F_{m,p}\left(x_{m,p}\right)$ denotes the non-exceedance probability of a raw model value $x_{m,p}$ in projection period p. With this notation, the QDM transformations are:

For precipitation data, QDM employs a multiplicative bias correction approach to account for the inherently ratio-based nature of precipitation variability. The bias-corrected future precipitation data (P̂_p) is calculated as:

$$\widehat{P}_p = F_{o,c}^{-1}(q) \times \frac{x_{m,p}}{F_{m,c}^{-1}(q)} \tag{1}$$

For temperature data, an additive approach is used to preserve absolute differences:

$$\hat{T}_p = F_{o,c}^{-1}(q) + \left[x_{m,p} - F_{m,c}^{-1}(q)\right] \tag{2}$$

where F and F^{-1} represent the cumulative distribution functions and their inverses, with subscripts o, m, c, and p denoting observed, modeled, control (historical), and projection (future) periods, respectively.

To validate QDM performance, we compared observed, raw GCM, and bias-corrected precipitation and temperature for the historical period (1994–2014) across all five GCMs and meteorological stations (Figure. 4.4).

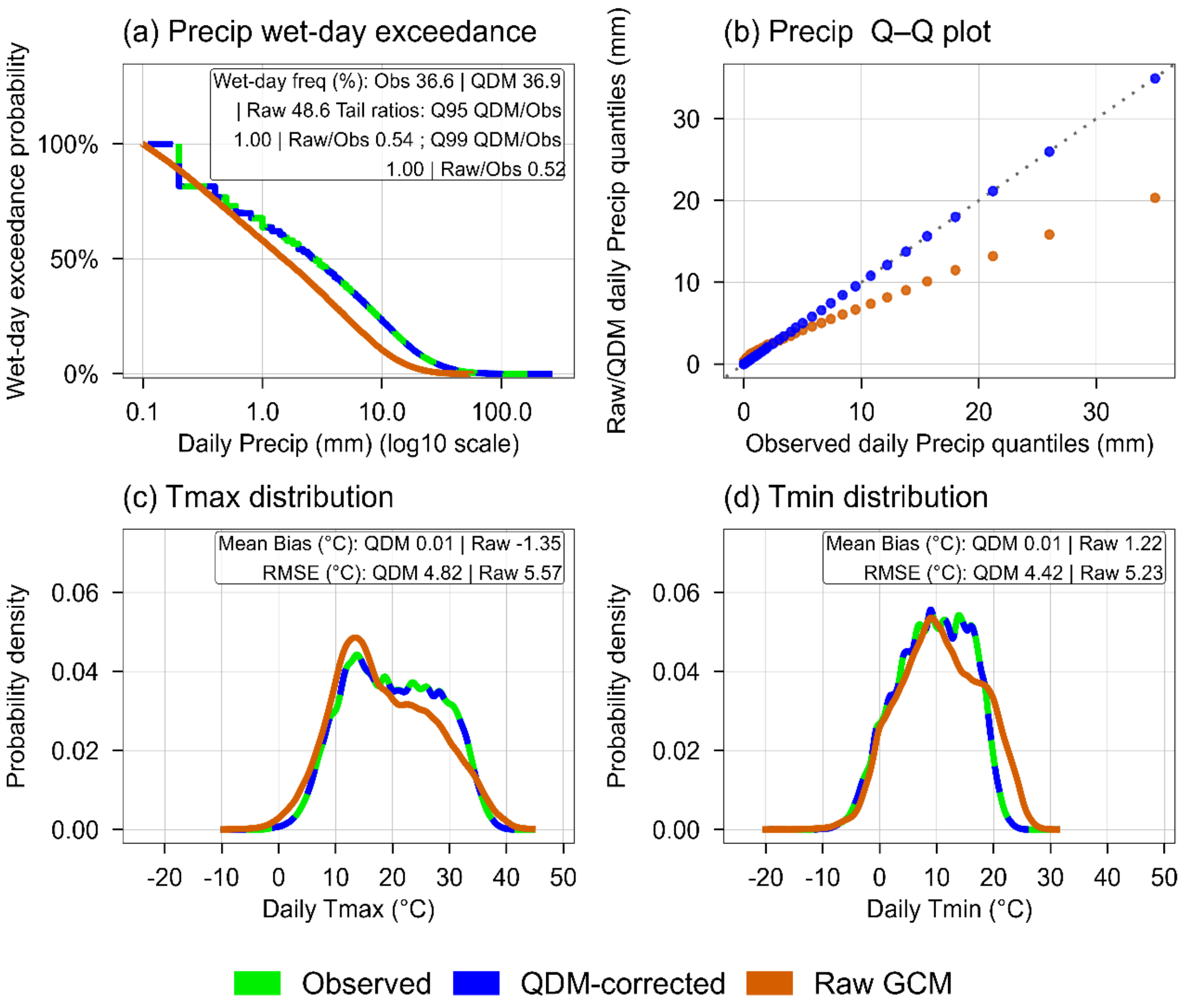

Figure 4.4 Evaluation of QDM bias correction (1994–2014). (a) wet-day precipitation exceedance with wet-day frequency and upper-tail ratios (Q95–Q99), (b) precipitation Q–Q comparison, and probability density distributions for (c) daily Tmax (d) daily Tmin

4.2.9 Drought predictions using Standardized drought indices

4.2.10 Standardized precipitation and runoff indices

Meteorological and hydrological drought conditions were assessed using SPI and SRI calculated following the methodology established by (McKee et al., 1993). Monthly data were aggregated to 12-month timescales to capture long-term meteorological and hydrological drought conditions. The 12-month timescale is particularly effective for assessing impacts on water resources, groundwater levels, and reservoir storage (Mishra & Singh, 2010; Tariq et al., 2024). Whereas, shorter accumulation periods (e.g., SPI-3, SPI-6) are often used to characterize seasonal meteorological and agricultural drought processes, 12-month index integrates cumulative water-balance deficits most relevant to the long-term climate-change impacts (Barker et al., 2016), assessed in this study. Calculations performed using SPEI package (v. 1.8.1) in R (Beguería et al., 2014). Fitting gamma probability density functions to the precipitation and runoff time series expressed as:

$$g(x) = \frac{1}{\beta^{\alpha}\Gamma(\alpha)} x^{\alpha-1} e^{-\frac{x}{\beta}} \quad (3)$$

where α and β represent the shape and scale parameters, x denotes the precipitation/runoff amount, and $\Gamma(\alpha)$ is the gamma function. The parameters are estimated using maximum likelihood estimation described by (Thom, 1966). While the gamma distribution is widely adopted for SPI/SRI, drought index values particularly in the tails can be sensitive to distributional choice and parameter estimation (Stagge et al., 2015).

To accommodate zero values in the time series, which commonly occur in precipitation and runoff data, the cumulative probability was calculated using the modified formulation:

$$H(x) = q + (1 - q)G(x) \quad (4)$$

where q represents the probability of zero precipitation/runoff occurrence and $G(x)$ denotes incomplete gamma function. The cumulative probabilities were subsequently transformed to standardized normal distributions using the equiprobability transformation, resulting in SPI and SRI values with a mean of 0 and a standard deviation of 1 (Edwards, 1997; Svoboda et al., 2012).

For the Arno River basin, zero monthly discharge at the outlet is not expected under typical historical conditions due to sustained baseflow, and the observed record indicates persistent non-zero flow. If occasional zero or near-zero simulated monthly values occur under extreme conditions, they represent very low-flow months and/or numerical truncation during aggregation; Eq. (4) ensures such rare cases do not introduce artefacts in standardization. To evaluate the credibility of drought projections, SRI-12 was computed from observed monthly discharge at the S. Giovanni alla Vena valle station for the overlapping period (2007–2014) and compared against SRI-12 derived from SWAT+ simulated discharge using the same gamma standardization procedure (Figure. 4.5).

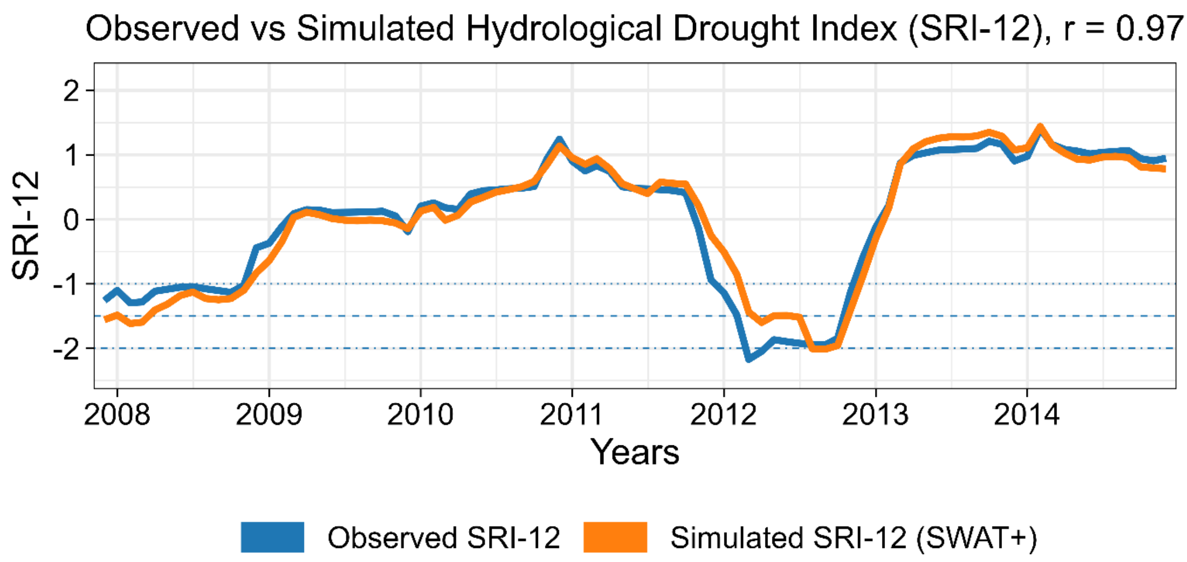

Figure 4.5 Observed vs SWAT+ simulated hydrological drought conditions expressed by the (SRI-12) at the S. Giovanni alla Vena valle outlet station (2007–2014)

4.2.11 Correlation analysis between SPI/SRI

Relationships between meteorological and hydrological drought indices were quantified using Pearson's correlation coefficient, which is appropriate given that the standardized indices are approximately normally distributed (Yisehak & Zenebe, 2021). Pearson's correlation coefficient quantifies the degree of linear dependence between two continuous variables and is expressed as:

$$r_{xy} = \frac{n\sum x_i y_i - \sum x_i \sum y_i}{\sqrt{(n\sum x_i^2 - (\sum x_i)^2)(n\sum y_i^2 - (\sum y_i)^2)}} \tag{5}$$

where r_{xy} denotes the Pearson correlation coefficient between x and y; n represents the number of observations; and x_i *and* y_i represent the values of x *and* y, respectively, for the i^{th} observation.

4.2.12 Drought event identification and characterization

Drought events were identified using run-sum methodology with standardized criteria: (1) SPI/SRI values ≤ -1.0, and (2) minimum duration ≥ 3 consecutive months (Table 4.6) (Yevjevich, 1967). The -1.0 threshold corresponds to moderate drought onset as originally defined by (McKee et al., 1993) and is widely adopted in drought literature, enabling comparison with published studies. Because event counts and severities depend on the chosen threshold and minimum duration, we emphasize relative differences across scenarios and periods rather than absolute event totals; alternative reasonable thresholds would change event counts but are unlikely to alter the direction of projected drought intensification. While, the 3-month minimum duration ensures identification of significant drought episodes while filtering short-term fluctuations. Three primary aggregate characteristics were calculated to provide comprehensive drought characterization:

Total Drought Duration (TDD) $$TDD = \sum_{i=1}^{n} D_i \tag{6}$$

where D_i represents the duration (in months) of each individual drought event i, and n is the total number of drought events.

Total Drought Severity (TDS) $$TDS = \sum_{i=1}^{n} |S_i| \tag{7}$$

where S_i represents the cumulative severity of each individual drought event i, calculated as the absolute sum of drought index values below the threshold (-1.0) during the event duration.

Drought Frequency (DF) $$DF = n \tag{8}$$

where n is the total number of drought events identified during the analysis period.

Drought category	SPI / SRI ranges
Extreme wet	Index ≥ +2.0
Severe wet	+1.5 ≤ Index < +2.0
Moderate wet	+1.0 ≤ Index < +1.5
Near normal/mild wet	0 ≤ Index < +1.0
Near normal/mild drought	−1.0 ≤ Index < 0
Moderate drought	−1.5 ≤ Index < −1.0
Severe drought	−2.0 ≤ Index < −1.5
Extreme drought	Index ≤ −2.0

Table 4.6 Summary of drought category and their scales for SPI/SRI values

4.3 Results

4.3.1 SWAT+ parameter sensitivity, calibration, and validation

Calibration was performed using nine hydrologically relevant parameters (Table 4.2), representing key runoff, soil-water, and groundwater processes. The selected parameter set is consistent with prior SWAT/SWAT+ applications in Mediterranean basins, which commonly identify curve number, soil properties, and baseflow-related parameters as influential controls on streamflow variability (Tariq et al., 2024; Leone et al., 2023; Pulighe et al., 2021).

The monthly simulation demonstrated robust performance during both calibration and validation. During calibration, NSE = 0.74, PBIAS = 7.74%, and KGE = 0.72 were achieved, indicating good agreement between simulated and observed discharge. Validation performance further improved (NSE = 0.93, PBIAS = 10.32%, KGE = 0.85), indicating very good model skill (Figure. 4.6). These values are broadly consistent with commonly used monthly-streamflow performance guidelines (D. N. Moriasi et al., 2007). The model captures both high-flow peaks and low-flow conditions and reproduces the seasonal cycle across the evaluation record, which includes contrasting wet (2010, 2011, 2013, and 2014) and dry (2007, 2008, and 2012) hydrological years, supporting its suitability for basin-scale drought assessment in climate impact applications.

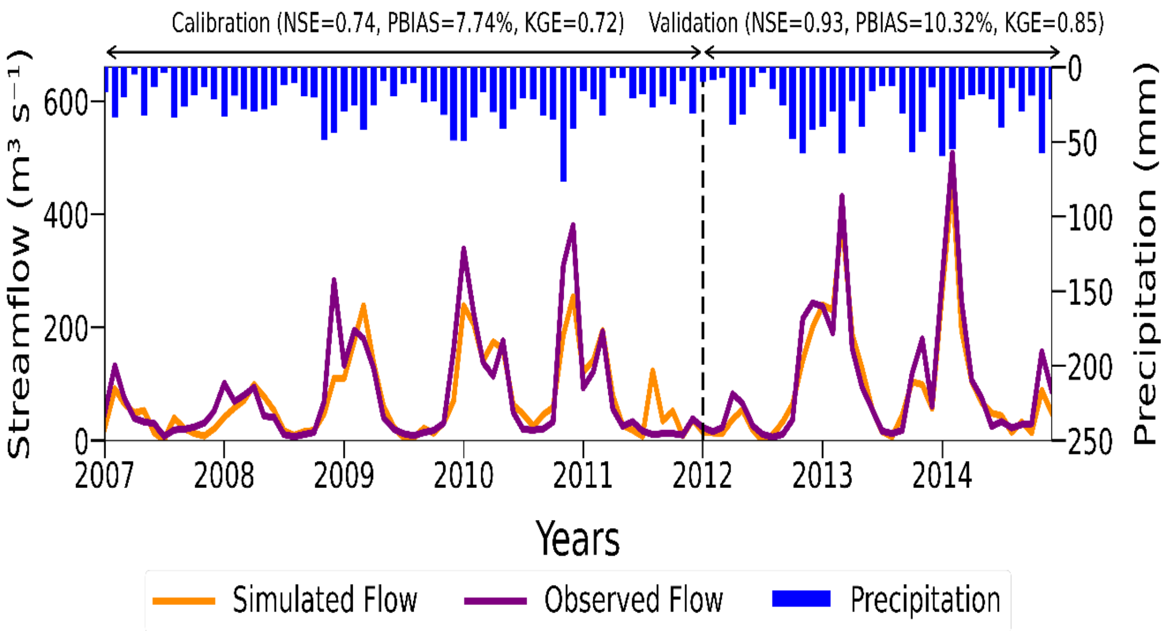

Figure 4.6 SWAT+ model calibration (2007–2011) and validation (2012–2014) performance for monthly streamflow at the S. Giovanni alla Vena valle gauging station

4.3.2 QDM bias correction

QDM bias correction was evaluated for precipitation and temperature during the historical period (Figure. 4.4). For precipitation, QDM corrected the wet-day frequency overestimation (raw: 48.6% vs. observed: 36.6%) to 36.9% and restored extreme quantiles to observed levels (Q95 and Q99 ratios = 1.00). For temperature, mean bias was reduced from −1.35°C/+1.22°C (Tmax/Tmin) to 0.01°C, with RMSE reductions of 13–15%. The Q–Q plot indicates correction across the full precipitation distribution, supporting the use of QDM-corrected climate inputs for subsequent drought projections.

4.3.3 Multi-model ensemble projected changes

Annual basin-mean precipitation, temperature, and river runoff were summarized using the multi-model ensemble median across the five bias-corrected CMIP6 GCMs for SSP2-4.5 and SSP5-8.5, with inter-model ranges (minimum–maximum) shown to represent between-model spread (Figure. 4.7). Linear trends were quantified using ordinary least squares regression, and statistical significance was evaluated using a two-sided t-test on the regression slope at the 95% confidence level.

Precipitation exhibits an overall declining tendency under both scenarios (Figure. 4.7a). Under SSP2-4.5, the ensemble median decreases at −0.51 mm yr^{-1}, whereas under SSP5-8.5 a stronger decline of −1.77 mm yr^{-1} is projected and is statistically significant ($p < 0.05$). The historical baseline period (1994–2014) shows pronounced interannual variability around a mean annual precipitation of 929 mm, and the model ranges indicate that substantial year-to-year variability persists under both scenarios, implying that drying trends can coexist with occasional wet extremes.

Temperature shows a clear and robust warming signal (Figure. 4.7b). The historical baseline mean annual temperature is approximately 14.7°C, and the ensemble median increases at 0.03°C yr^{-1} under SSP2-4.5 and 0.05°C yr^{-1} under SSP5-8.5; both trends are statistically significant ($p < 0.05$). This corresponds to late-century warming on the order of ~3°C (SSP2-4.5) and ~5°C (SSP5-8.5) relative to the baseline period.

River runoff broadly follows the precipitation signal, with decreasing trends under both scenarios (Figure. 4.7c). The ensemble median decreases by −0.07 m^3 s^{-1} yr^{-1} under SSP2-4.5 and by −0.19 m^3 s^{-1} yr^{-1} under SSP5-8.5 the latter statistically significant at $p < 0.05$. Historical runoff variability is substantial around a baseline mean of 69.4 m^3 s^{-1}, reflecting alternating low-flow and high-flow years. The inter-model ranges indicate that runoff projections retain large variability, consistent with compounded uncertainties from precipitation changes and temperature-driven evapotranspiration responses.

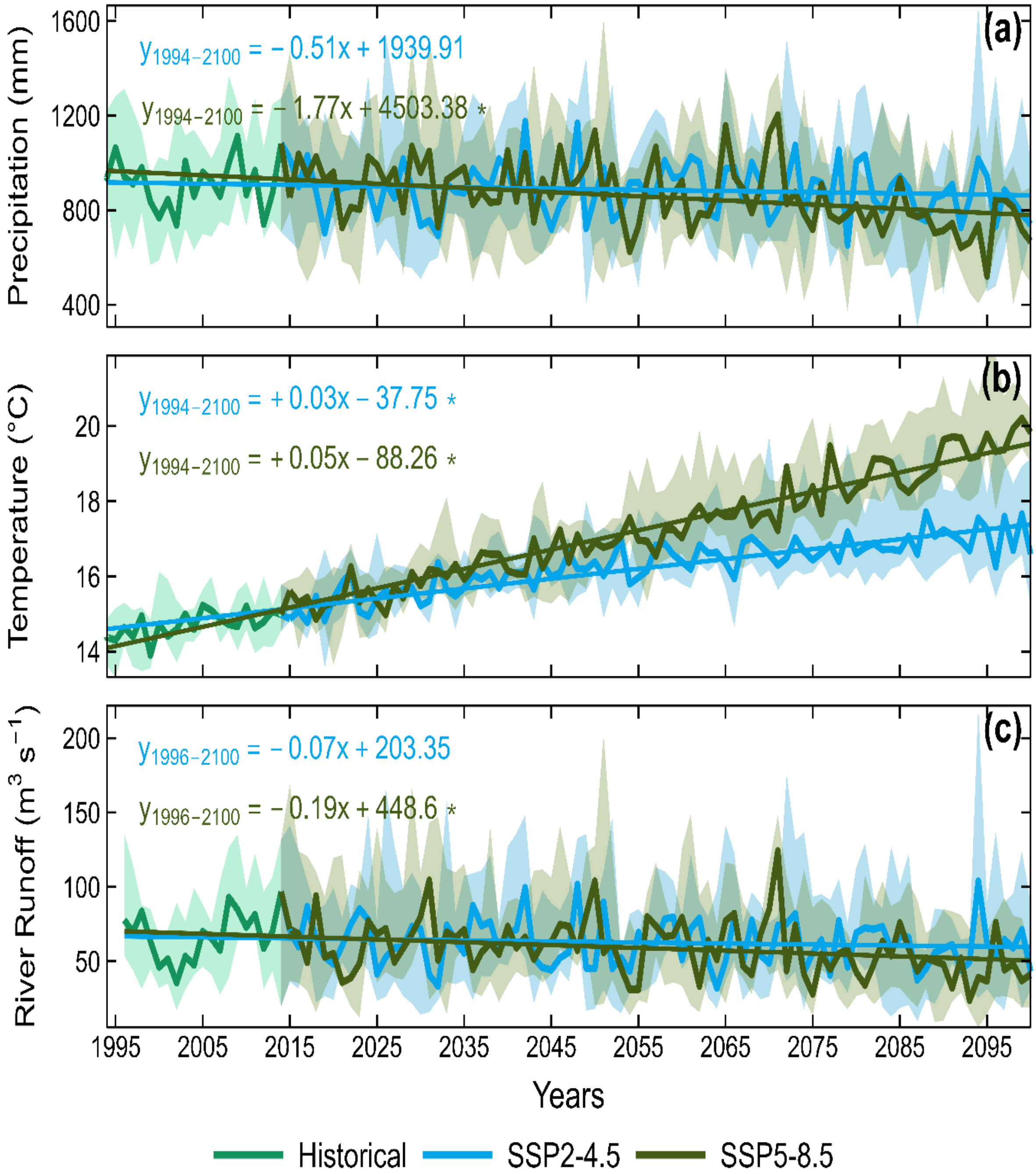

Figure 4.7 Multi-model ensemble projections of historical and future time series of SSP2-4.5 and SSP5-8.5. Solid lines are the multi-model median across five GCMs, and shaded areas showing the minimum and maximum values an (*) denotes significant slopes ($p < 0.05$)

4.3.4 Projected annual percentage changes relative to the historical baseline

Projected changes were evaluated across five GCMs under SSP2-4.5 and SSP5-8.5 relative to the historical baseline (1994–2014 for precipitation and temperature; 1996–2014 for river runoff) for three time windows: near-future (2015–2040), mid-future (2041–2070), and far-future (2071–2100).

Precipitation exhibits substantial inter-model spread, particularly under SSP2-4.5, with weaker consensus on the direction of change (Figure. 4.8a–b). Under SSP2-4.5, the ensemble-median change is small in the near-future (−38 mm yr^{-1}; −4.0%), with a wide range spanning −111 to +91 mm yr^{-1} (−11.9% to +9.8%) and only 3 of 5 models indicating decreases. By the mid-future (2041–2070), the median remains modest (−30 mm yr^{-1}; −3.2%), while agreement strengthens (4 of 5 models decreasing). In the far-future, 4 of 5 models converge on drying, with a median change of −27 mm yr^{-1} (−2.9%) but a broad range (−184 to +3 mm yr^{-1}; −19.7% to +0.3%). Under SSP5-8.5, the drying signal strengthens and becomes more consistent. Near-future (2015–2040) changes remain mixed (median −1 mm yr^{-1}; range −63 to +37 mm yr^{-1}), but by the far-future (2071–2100) all five GCMs agree on decreasing precipitation, with a median reduction of −140 mm yr^{-1} (−15.1%). Among individual GCMs, MPI-ESM1-2-HR consistently projects the strongest precipitation reductions in both scenarios (−19.7% under SSP2-4.5; −20.0% under SSP5-8.5), while BCC-CSM2-MR projects the most moderate response, including a slight increase (+0.3%) under SSP2-4.5 far-future (2071–2100). These inter-model differences likely reflect variations in atmospheric circulation patterns, convective parameterizations, and land–atmosphere feedbacks.

For temperature, all five GCMs project unequivocal warming across all time windows and both scenarios, exhibiting the lowest inter-model uncertainty. (Figure. 4.8c–d) illustrates temperature as percentage change relative to the historical baseline mean annual temperature (≈14.7°C, 1994–2014); warming is summarized as percent change together with the equivalent absolute ΔT (°C). Under SSP2-4.5, temperature increases from 5.0–7.3% in the near-future (2015–2040) (+0.74 to +1.07°C) to 9.5–18.1% in the mid-future (2041–2070) (+1.40 to +2.67°C), reaching 12.9–26.5% in the far-future (2071–2100) (+1.90 to +3.91°C). Under SSP5-8.5, warming intensifies from 5.4–9.1% in the near-future (2015–2040) (+0.80 to +1.34°C) to 12.6–22.7% in the mid-future (2041–2070) (+1.86 to +3.34°C) and 25.6–36.3% in the far-future (2071–2100) (+3.77 to +5.35°C). The normalized inter-model spread remains low in the near-future (2015–2040) (≈2.3–3.7% of baseline mean temperature) and increases by the far-future (2071–2100) (≈10.7–13.7%) as the absolute warming signal grows. Among the models, CMCC-ESM2 consistently defines the upper bound of warming (up to 36.3%, ≈+5.35°C under SSP5-8.5 far-future), whereas MPI-ESM1-2-HR tends to lie toward the lower end of warming despite projecting comparatively stronger precipitation and runoff declines, reflecting structural differences in climate sensitivity and hydroclimatic response.

River runoff changes show the widest inter-model divergence and the weakest agreement, reflecting the combined influence of precipitation variability and warming-driven evapotranspiration (Figure. 4.8e–f). Under SSP2-4.5, near-future runoff changes span −17 to +17 $m^3 s^{-1}$ (−24% to +25.1%), with a median reduction of −7 $m^3 s^{-1}$ (−10%) and only 3 of 5 models indicating decreases. The normalized spread reaches 49% of the historical baseline—more than double that of precipitation reflecting compounded uncertainties from precipitation variability, evapotranspiration responses, and nonlinear catchment processes. By the far-future (2071–2100) under SSP2-4.5, the ensemble-median change is close to neutral (−0.4 $m^3 s^{-1}$; −0.6%), but the range remains very large (−24 to +4 $m^3 s^{-1}$; −34.9% to +6%), indicating persistent uncertainty with only moderate agreement (3 of 5 models decreasing). Under SSP5-8.5, agreement strengthens with time. By the far-future (2071–2100), all five models converge on runoff decreases, with a median reduction of −17 $m^3 s^{-1}$ (−24%) and a comparatively narrower normalized spread of 14% (range −22 to −13 $m^3 s^{-1}$; −32% to −18.4%). MPI-ESM1-2-HR projects the most severe reductions (−34.9% under SSP2-4.5; −32% under SSP5-8.5), consistent with its strong precipitation declines, while MRI-ESM2-0 projects increases under SSP2-4.5 far-future (2071–2100) (+6%), reflecting its relatively moderate precipitation projections. The amplification of inter-model spread from precipitation to runoff in near-future (2015–2040) periods suggests that hydrological model nonlinearities compound climate input uncertainty.

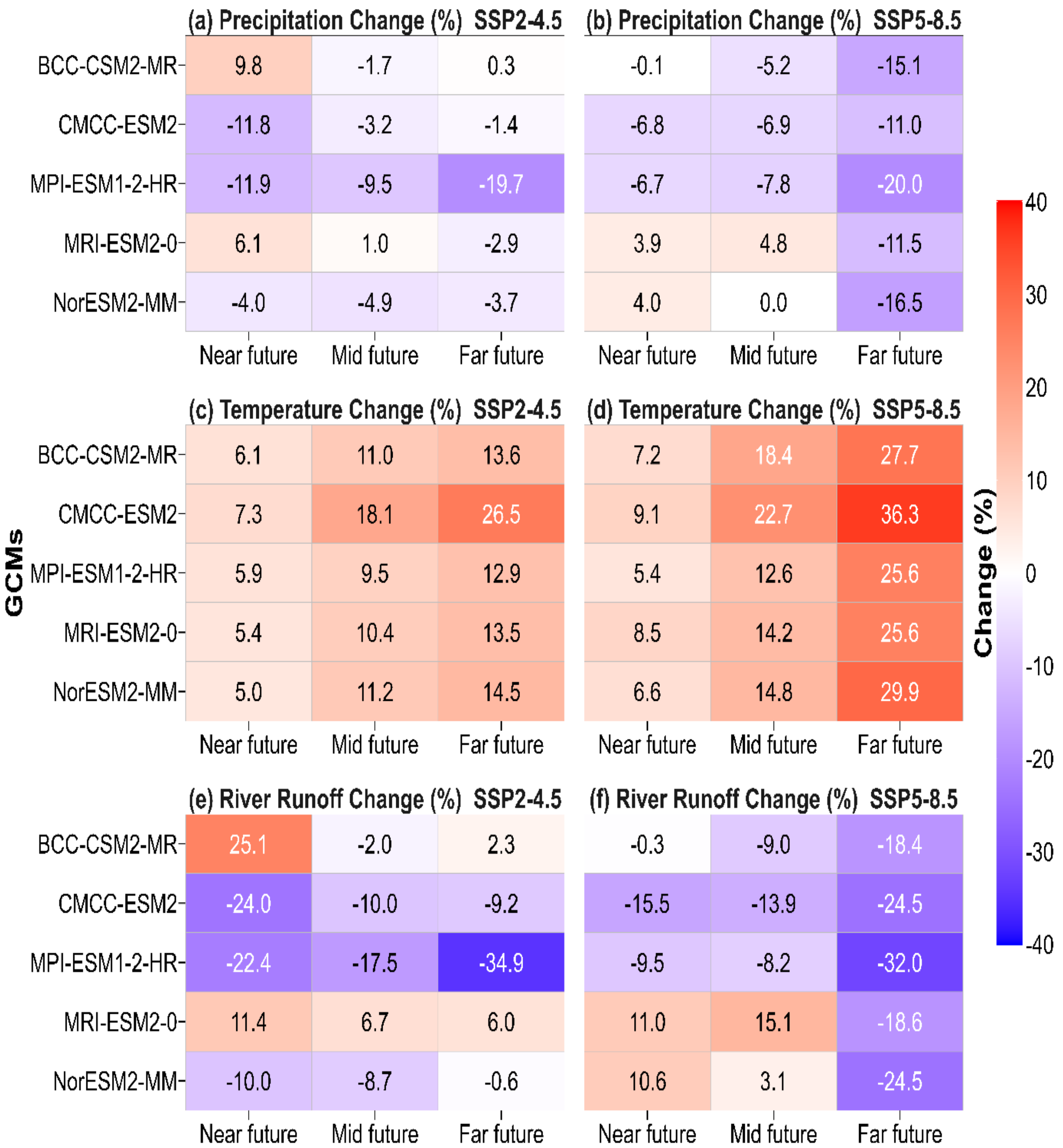

Figure 4.8 Annual Percentage changes from historical baselines for (a-b) precipitation, (c-d) temperature, and (e-f) river runoff across five GCMs under SSP2-4.5 (left) and SSP5-8.5 (right) scenarios for three future periods

4.3.5 Future drought projections and characterization

The SPI and SRI indices were calculated at the 12-month timescale for all GCMs across both scenarios and all temporal windows; the resulting time series reveal coherent drought patterns (Figures. 4.9 and 4.10). Pearson correlations (r) between the two indices remain consistently high across all GCMs, scenarios, and time windows (r = 0.80–0.95). All correlations are statistically significant at the 95% confidence level, indicating persistent concurrence of meteorological and hydrological droughts in both historical and future projections. During the historical period, correlation coefficients ranged from 0.80 to 0.93, with NorESM2-MM demonstrating the highest correlation (r = 0.93) and MRI-ESM2-0 showing the lowest (r = 0.80). Under SSP2-4.5, correlations spanned 0.84–0.95 across all future periods, while SSP5-8.5 exhibited slightly higher minimum thresholds ranging from 0.86–0.94. The multi-model consensus, with all GCMs maintaining correlations above 0.80 throughout all time windows and scenarios, indicates strong coupling between meteorological and hydrological drought indices.

Drought attributes, including duration (D), severity (S), and frequency (DF) were identified using the run-sum method. Drought events were defined by criteria (duration ≥ 3 months and SPI/SRI ≤ -1.0). Total drought duration (TDD), total drought severity (TDS), and drought frequency (DF) were subsequently estimated for all GCMs, scenarios, and time windows.

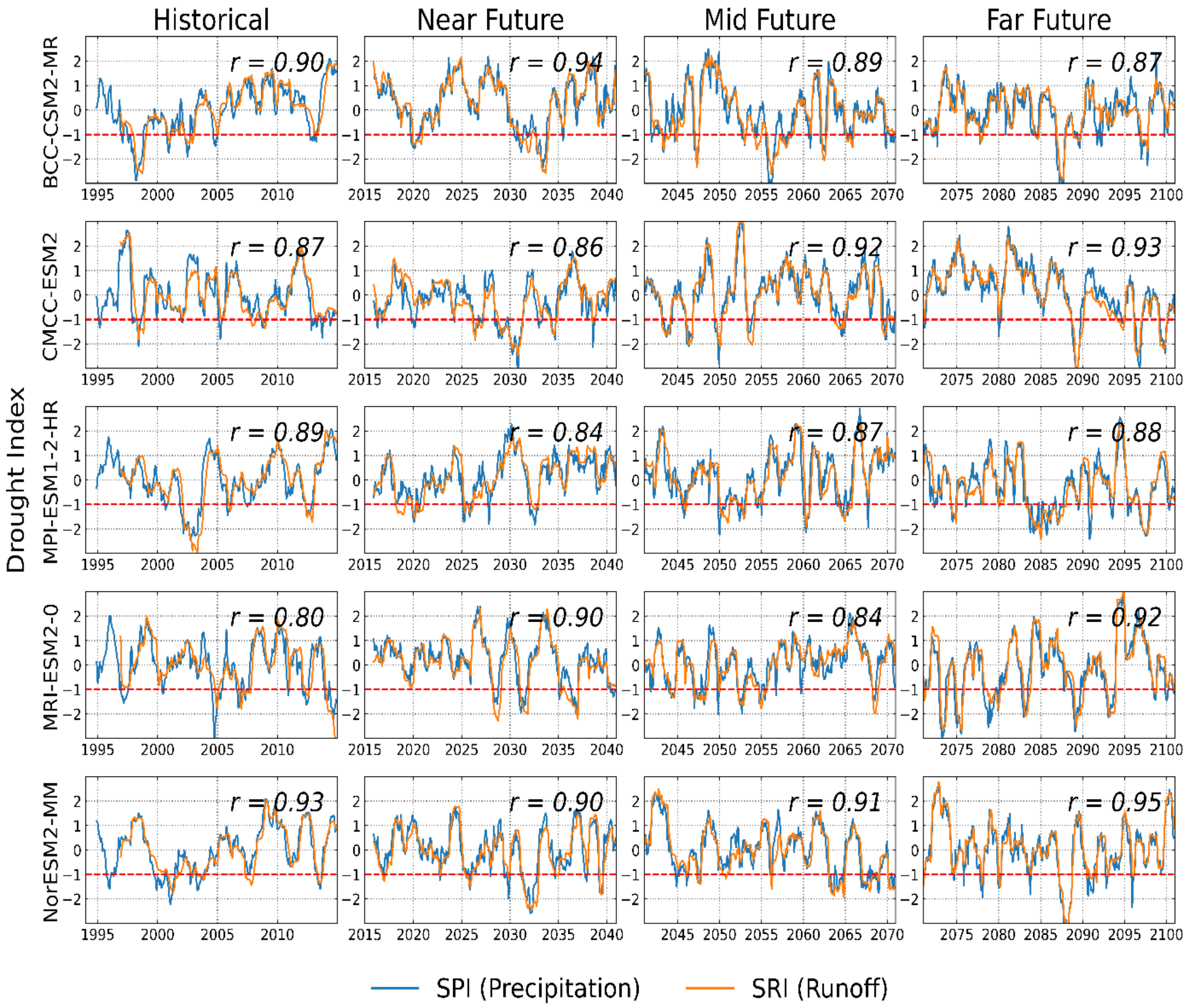

Figure 4.9 Drought indices (SPI) and (SRI) representation of five GCMs under SSP2–4.5 for historical baseline (1994 precipitation and 1996 river runoff–2014), near-future (2015–2040), mid-future (2041–2070) and far-future (2071–2100)

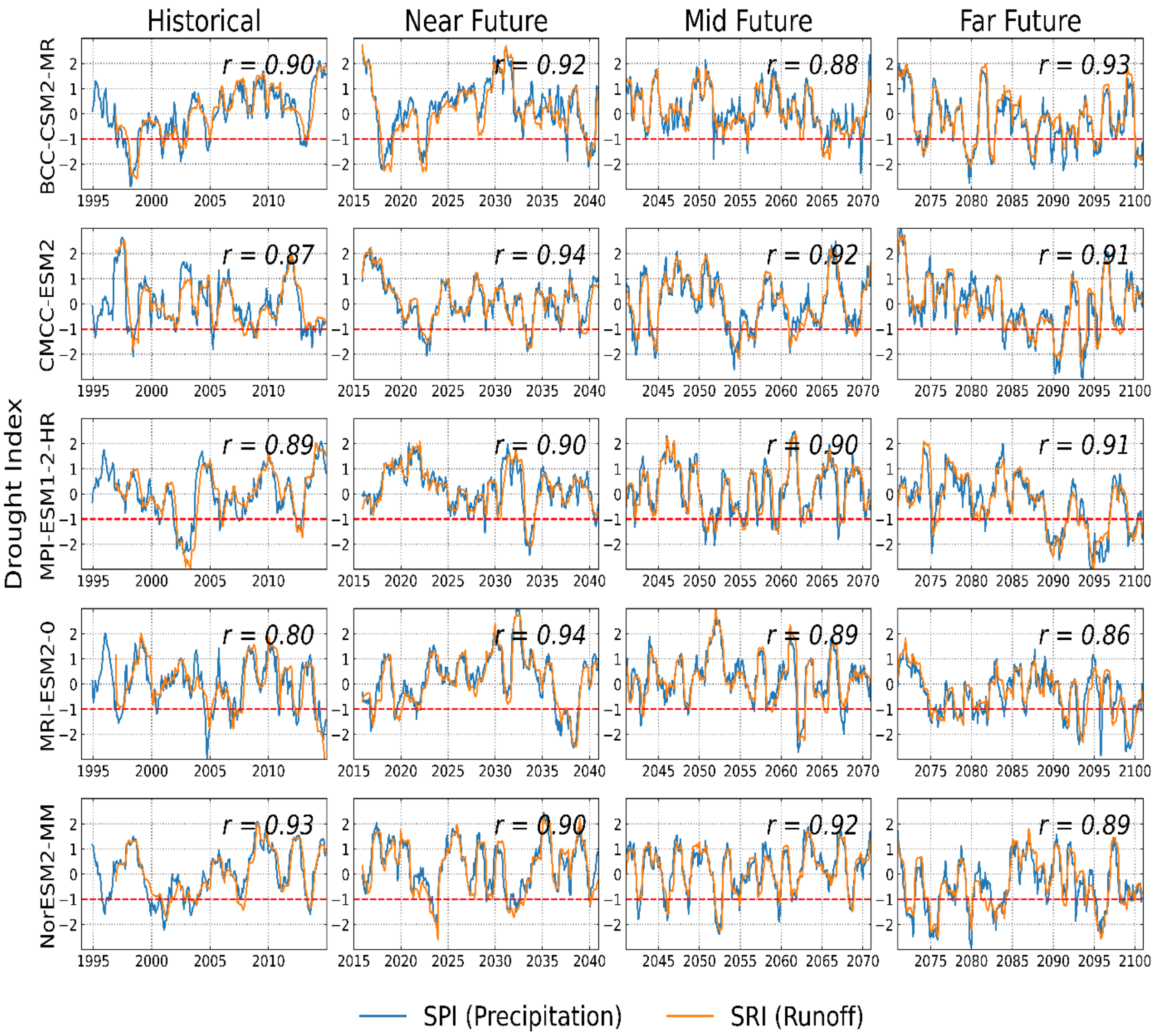

Figure 4.10 Drought indices (SPI) and (SRI) representation of five GCMs under SSP5–8.5 for historical baseline (1994 precipitation and 1996 river runoff –2014), near-future (2015–2040), mid-future (2041–2070) and far-future (2071–2100)

4.3.6 Meteorological drought characteristics (SPI-12)

Historical baseline TDD for SPI-12 ranged from 11 months CMCC-ESM2 to 41 months MRI-ESM2-0 and NorESM2-MM, reflecting substantial inter-model variability in simulating historical drought conditions (Figure. 4.11-a). Under SSP2-4.5, drought duration exhibited heterogeneous responses across GCMs and time windows. CMCC-ESM2 projected a pronounced near-future (2015–2040) intensification, with TDD increasing from 11 months historical to 60 months in near-future (2015–2040), and then stabilizing at 49 months at far-future (2071–2100). MRI-ESM2-0 simulated the highest far-future (2071-2100), TDD of 94 months. The SSP5-8.5 scenario amplified drought durations, with MRI-ESM2-0 projecting the maximum TDD of 99 months in far-future (2071-2100), followed by MPI-ESM1-2-HR 93 months and NorESM2-MM 90 months (Figure. 4.11-b). Notably, BCC-CSM2-MR demonstrated pronounced temporal variability, with TDD declining to 14 months during the mid-future (2041–2070) before increasing sharply to 81 months in far-future (2071–2100), suggesting complex non-linear temporal responses to intensified radiative forcing.

TDS across the GCMs intensified more markedly than duration metrics. Historical baseline drought severity values ranged from 15 CMCC-ESM2 to 61 MRI-ESM2-0 (Figure. 4.11-c). Under SSP2-4.5, MRI-ESM2-0 projected the highest far-future (2071–2100), severity of 166, compared to its historical baseline of 61. MPI-ESM1-2-HR demonstrated consistent severity amplification, with TDS increasing from 56 in the historical baseline to 128 far-future (2071–2100). The SSP5-8.5 scenario produced the most extreme drought severity projections, with MPI-ESM1-2-HR reaching a peak TDS 172 in the far-future (2071–2100), followed by MRI-ESM2-0 150 and NorESM2-MM 153 (Figure. 4.11-d).

DF patterns revealed complex temporal dynamics distinct from duration and severity trends. Historical DF ranged from 7 events CMCC-ESM2 to 20 events in MRI-ESM2-0 and NorESM2-MM. Under SSP2-4.5, MPI-ESM1-2-HR projected the highest far-future (2071–2100), frequency of 38 events, while several GCMs exhibited stable or declining frequencies despite concurrent increases in drought duration and severity, indicating a consolidation of drought events into longer and more intense episodes (Figure. 4.11-e). Under SSP5-8.5, BCC-CSM2-MR projected the maximum frequency of 39 events in far-future (2071–2100), with MPI-ESM1-2-HR maintaining elevated frequency of 37 events, collectively signifying a marked intensification of meteorological drought episodes under high-emission scenarios (Figure. 4.11-f).

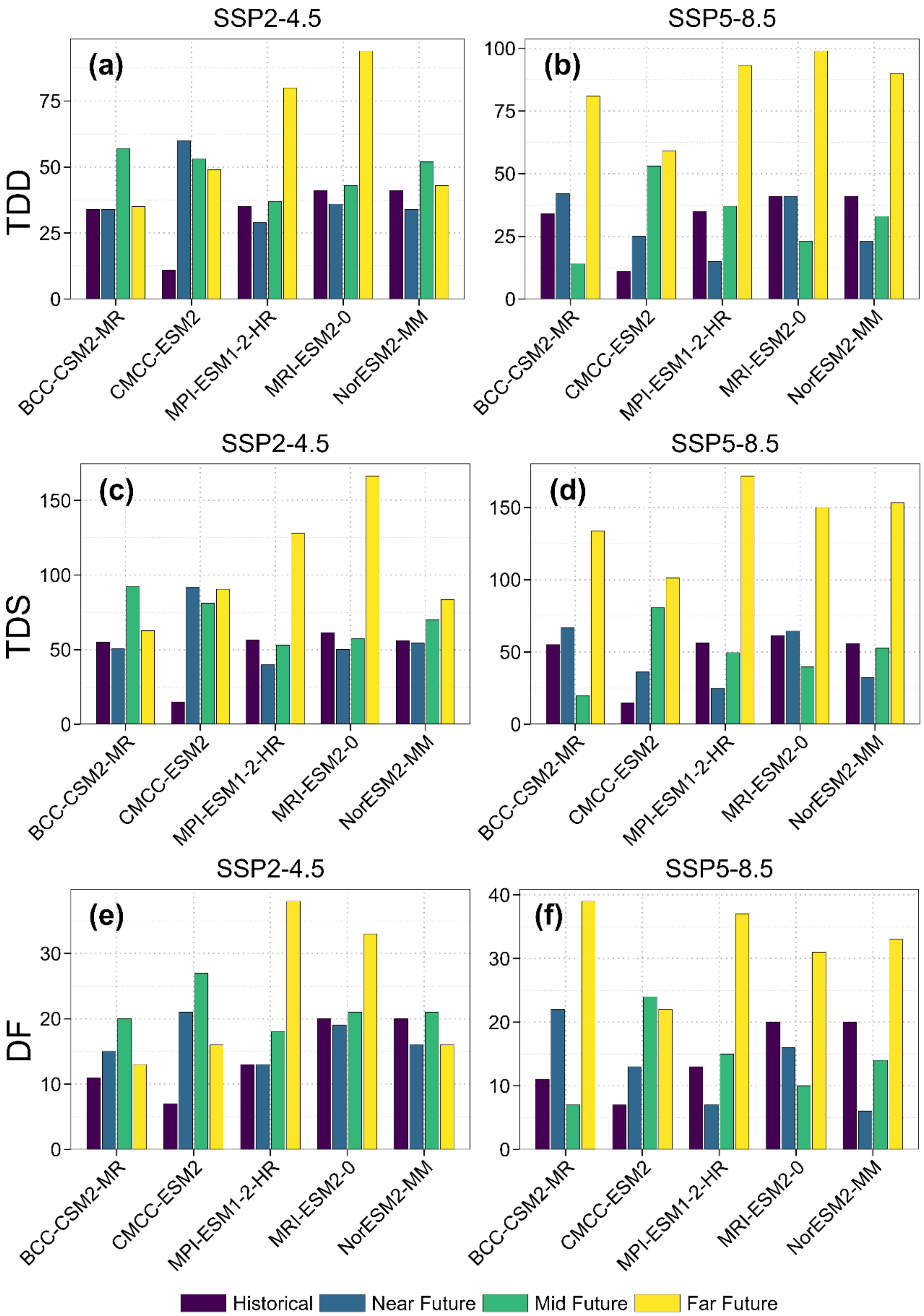

Figure 4.11 Total drought duration (TDD) (a–b), total drought severity (TDS) (c–d), and drought frequency (DF) (e–f) of Standardized Precipitation Index (SPI) of all GCMs, scenarios, and time windows

4.3.7 Hydrological drought characteristics SRI-12

To verify that SWAT+ reproduces observed hydrological drought characteristics, we compared SRI-12 computed from observed monthly discharge with SRI-12 derived from SWAT+ simulated discharge for 2007–2014 (Figure. 4.5). The two SRI-12 series show very strong agreement (r = 0.97), and the model captures the timing and persistence of major drought episodes, including the pronounced low-flow drought around 2012, supporting the use of SWAT+ simulated discharge for future drought projections.

Hydrological droughts SRI-12 revealed both similarities and important differences compared to meteorological droughts, reflecting the complex propagation of precipitation deficits through the hydrological systems and the moderating influence of catchment storage processes. Historical baseline TDD values for hydrological droughts ranged from 16 months CMCC-ESM2 to 32 months in MPI-ESM1-2-HR, MRI-ESM2-0, and NorESM2-MM each, systematically lower than corresponding SPI-12 baselines confirming the buffering capacity of hydrological systems. Under SSP2-4.5, BCC-CSM2-MR exhibited extreme temporal variability with TDD reaching 82 months in the mid-future (2041–2070), while MRI-ESM2-0 demonstrated consistent increases, reaching 86 months in the far-future (2071–2100), (Figure. 4.12-a). SSP5-8.5 scenario produced the most extreme hydrological drought projections, with MPI-ESM1-2-HR projected 106 months and NorESM2-MM projected 105 months TDD in the far-future (2071–2100), compared to their respective historical baselines of 32 months each (Figure. 4.12-b).

Hydrological TDS demonstrated amplified responses compared to meteorological droughts. Historical baseline TDS spanned from 20.9 CMCC-ESM2 to 62 MPI-ESM1-2-HR. Under SSP2-4.5, MRI-ESM2-0 projected the highest far-future (2071–2100), TDS of 147 while BCC-CSM2-MR exhibited extreme mid-future (2041–2070), severity of 121 (Figure. 4.12-c). SSP5-8.5 scenario produced extreme severity levels, with MPI-ESM1-2-HR simulating the maximum TDS of 177 the highest value across all drought indices and scenarios analyzed followed by NorESM2-MM projected a far-future (2071–2100), TDS of 163 compared to its historical baseline of 40, underscoring the potential for severe hydrological drought intensification (Figure. 4.12-d).

Hydrological DF patterns were systematically lower than their meteorological counterparts, confirming the temporal smoothing effect of catchment storage processes. Historical baseline events ranged from 6 BCC-CSM2-MR, CMCC-ESM2, NorESM2-MM each to 11 MPI-

ESM1-2-HR. Under SSP2-4.5, MRI-ESM2-0 recorded the highest far-future (2071–2100), frequency of 31 events, while BCC-CSM2-MR and CMCC-ESM2 exhibited a notable mid-future (2041–2070), peaks of 26 and 24 events, respectively (Figure. 4.12-e). Under SSP5-8.5, NorESM2-MM projected highest frequency of 26 events in the far-future (2071–2100), with MPI-ESM1-2-HR and MRI-ESM2-0 maintaining elevated frequencies of 20 and 19 events, respectively (Figure. 4.12-f). Across the five GCMs ensemble, consistent increases in hydrological drought duration and severity are projected under SSP5-8.5, indicating robust intensification of drought stress despite inter-model variability.

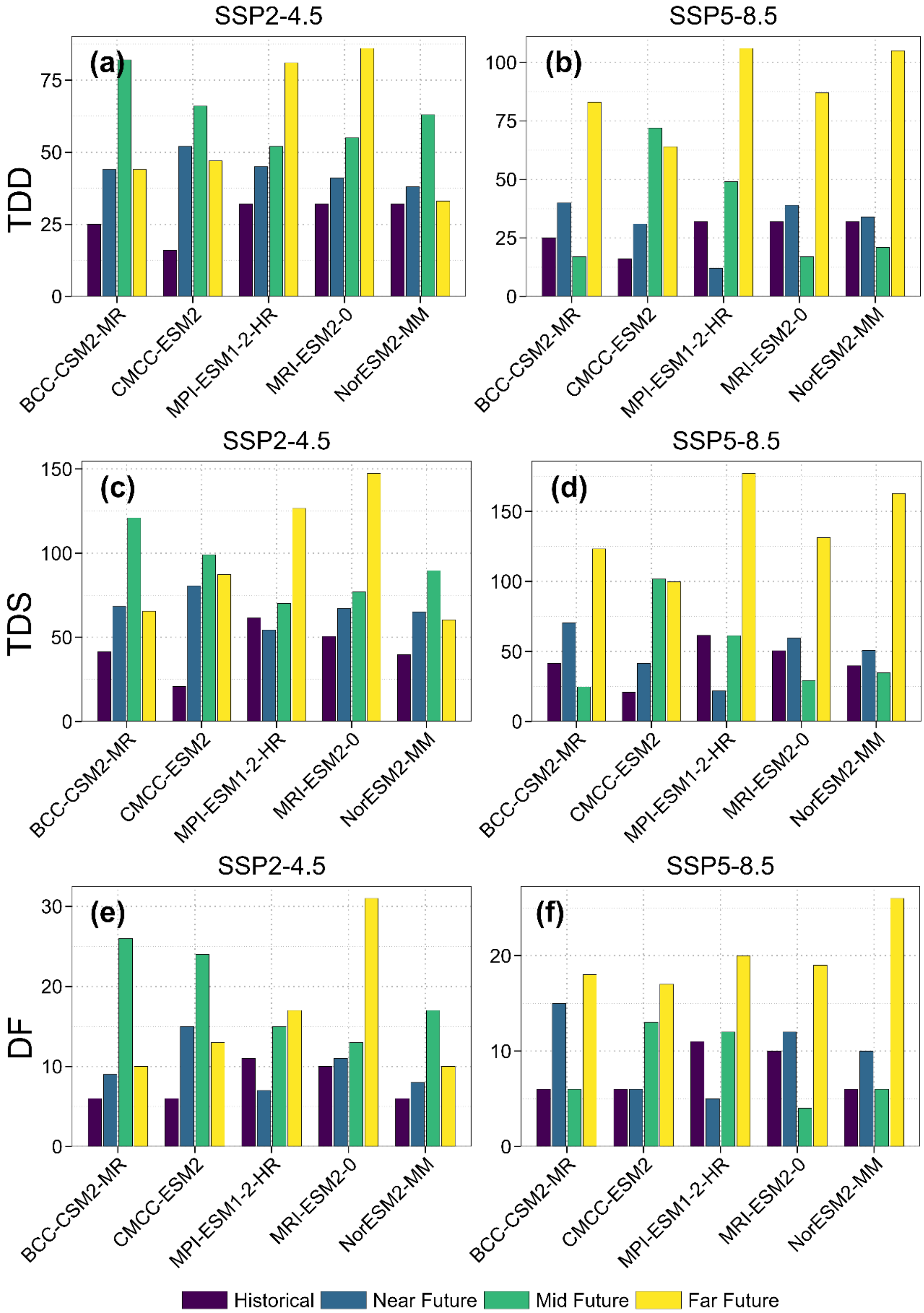

Figure 4.12 Total drought duration (TDD) (a–b), total drought severity (TDS) (c–d), and drought frequency (DF) (e–f) of Standardized Runoff Index (SRI) of all GCMs, scenarios, and time windows

4.4 Discussion

4.4.1 SWAT+ performance and QDM bias correction

The SWAT+ model demonstrated robust performance in simulating the hydrological processes of the Arno River basin, achieving very good model performance according to established criteria (D. N. Moriasi et al., 2007). The NSE values of 0.74 for calibration and 0.93 for validation align well with previous SWAT applications in Mediterranean watersheds, where reported similar performance metrics (NSE = 0.80 for calibration, NSE = 0.77 for validation) in the Segura River Basin, Spain (Senent-Aparicio et al., 2017). While the Segura Basin differs from the Arno River basin in elevation profile and snowmelt contributions, both basins share Mediterranean climate characteristics and demonstrate SWAT's consistent performance across diverse Mediterranean watersheds.

The sensitivity of parameters such as cn2, bd, and awc reflects the strong influence of land-use and soil properties on runoff generation in the Arno River basin, where agricultural and urban areas enhance surface runoff while alluvial soils in the floodplain modulate infiltration and soil water storage. Similarly, the importance of alpha and lat_ttime highlights the role of shallow aquifers and groundwater–stream interactions in sustaining baseflows Table 4.2. Notably, the snowmelt_lag parameter was also sensitive, underscoring the significance of snowmelt contributions from the Apennine headwaters. In SWAT+, snow accumulation and melt are simulated using a temperature index (degree-day) approach, where snowmelt_lag governs the temporal release of meltwater. This parameter's sensitivity confirms the contribution of snow processes to the basin's hydrological regime, particularly given the mountainous headwaters extending to 1,625m elevation in the Tuscan Apennines. These identified sensitive parameters are largely consistent with those reported in other Mediterranean basin studies, reflecting hydrological processes characteristic of the region such as rapid runoff generation in agricultural and urban areas, soil-water storage regulation in alluvial plains, baseflow support from shallow aquifers, and snowmelt-driven spring discharges from the Apennine headwaters. Such processes align with Mediterranean hydroclimatic regimes, where water availability is shaped by strong seasonality, high evapotranspiration demand, and recurrent drought stress (Fiseha et al., 2013; Leone et al., 2023; Pulighe et al., 2021; Senent-Aparicio et al., 2017; Tariq et al., 2024). While, the superior validation performance compared to calibration suggests good model transferability and robust parameterization, providing confidence in subsequent drought projections.

QDM was selected as the bias-correction approach because it is designed to correct historical distributional biases while preserving the modeled climate-change signal across quantiles (Cannon et al., 2015). The QDM validation (Figure. 4.4) illustrates effective bias correction across all climate variables. We note that a formal inter-method comparison (e.g., QDM vs. linear scaling or empirical quantile mapping) was beyond the scope of this study; therefore, results should be interpreted as conditional on the selected bias-correction method.

4.4.2 Climate projections and hydrological shifts

The projected climate trends for the Arno River basin align with broader Mediterranean assessments and demonstrate both consistency with previous studies and notable intensification under CMIP6 scenarios. The Mediterranean region has been identified as a climate change hotspot, with CMIP6 projections indicating amplified warming of approximately 1.6 times the global mean and robust summer drying signals (Cos et al., 2022; Lionello & Scarascia, 2018). The ensemble baseline climatology (historical period) provides the reference for the Arno River basin: mean annual precipitation of 929 mm, mean annual temperature of 14.7°C, and mean annual runoff of 69.4 $m^3 s^{-1}$. Relative to this baseline, projections indicate a strong warming signal across all models and scenarios, whereas precipitation and runoff exhibit larger inter-model spread and scenario dependence a pattern consistent with Mediterranean-wide assessments showing higher model agreement for temperature than precipitation (Tarín-Carrasco et al., 2024; Zittis et al., 2021).

The projected drought intensification reflects a systematic linking to climatic drivers and hydrological response. Rising temperatures directly increase atmospheric evaporative demand through higher vapor pressure deficit, amplifying actual evapotranspiration when soil moisture is available. In the Arno River basin, the projected warming of +3 to +5°C by century's end would increase potential evapotranspiration by an estimated 10–20%, consistent with Penman-Monteith sensitivity analyses for Mediterranean climates demonstrating that maximum temperature and relative humidity exert dominant controls on reference evapotranspiration (Vicente-Serrano, Azorin-Molina, et al., 2014). This enhanced evaporative loss, combined with declining precipitation, creates a compounding water deficit that propagates from meteorological to hydrological drought through pooling, lagging, and attenuation processes modulated by catchment storage (Huang et al., 2017; Van Loon, 2015). The seasonal dimension is critical: Mediterranean precipitation reductions typically concentrate in summer months when evaporative demand peaks, intensifying seasonal water stress through a double amplification of reduced supply and increased demand (IPCC, 2022b). In addition, warming in the Apennine headwaters may reduce snow accumulation and shift melt timing toward earlier in the year, weakening spring contributions to streamflow and increasing the likelihood of prolonged summer low-flow conditions a pattern documented across Mediterranean mountain regions where snow cover duration has decreased significantly in recent decades (Carrer et al., 2023; Fayad et al., 2017).

Our projected far-future runoff reductions align quantitatively with recent CMIP6-based Mediterranean assessments. The ensemble median runoff decline of 24% under SSP5-8.5 far-future (2071–2100), corresponding to −17 m^3 s^{-1}, falls within the range reported by (Abdelwahab et al., 2025), who projected mean annual flow reductions of −7% to −67% in the Carapelle basin (Apulia, Italy) depending on GCM selection. Similarly, hydrological modeling studies in southern Italian catchments have projected substantial streamflow reductions under high-emission scenarios, with reported declines up to −19% in the Crati River basin (Calabria) under RCP4.5 (Senatore et al., 2022). Our SPI–SRI correlation coefficients ($r = 0.80–0.95$) are consistent with (Tariq et al., 2024), who reported $r = 0.63–0.93$ for the Aterno-Pescara watershed using a comparable SWAT+ and CMIP6 framework, confirming robust drought propagation behavior across central Italian catchments. The baseline drought behavior is also consistent with regional evidence of increasing drought vulnerability across the Mediterranean, northern Italy, and Tuscany in recent decades (Baronetti et al., 2022; D'Oria et al., 2017; Spinoni et al., 2014).

4.4.3 Future drought propagation and intensification

Future drought analysis reveals distinctive propagation and intensification characteristics under climate change. The persistence of high correlations between meteorological and hydrological drought indices across both SSP scenarios indicates that drought propagation relationships remain broadly stable under intensified climate forcing. This stability suggests that meteorological drought indicators will remain informative for hydrological drought monitoring, supporting their use in early-warning contexts, although catchment storage, river regulation, and land-use change can modulate drought propagation (Muthuvel & Qin, 2025; Wu et al., 2022; Zhou et al., 2023).

The projected increases in TDD reaching up to 99 months for meteorological drought (SPI-12) and 106 months for hydrological drought (SRI-12) under SSP5-8.5, compared to historical baselines of 41 and 32 months, respectively indicate substantial drought intensification, accompanied by amplification in TDS. These magnitudes exceed values reported in earlier CMIP5-based studies; (Spinoni et al., 2020), using 103 CORDEX simulations, identified the Mediterranean as a global drought hotspot with projected increases in drought frequency and severity. This intensification potentially reflects methodological advances in CMIP6, including higher spatial resolution, updated aerosol forcing, improved land-surface schemes, and revised equilibrium climate sensitivity estimates (Cook et al., 2020; Eyring et al., 2016). Importantly, the temporal dynamics indicate a consolidation of drought conditions into fewer but longer and more intense episodes. In some models, this appears as declining event frequency despite increasing duration and severity, suggesting a structural shift in drought behavior with important implications for water resources management.

Differences between hydrological and meteorological drought characteristics highlight the buffering role of catchment storage processes while also revealing their limitations. Under SSP5-8.5 far-future (2071–2100), hydrological drought severity reaches TDS values up to 177 exceeding the maximum meteorological TDS of 172 suggesting that storage capacity may become insufficient to mitigate extreme drought stress in the late 21st century. This counterintuitive amplification reflects the enhanced evapotranspiration losses under warming conditions (Cammalleri et al., 2020). These results imply that natural resilience mechanisms in the basin could be exceeded under high-emission scenarios, underscoring the need for adaptive water management strategies.

Confidence in the projected intensification is strengthened by the coherence of the multi-model signal under SSP5-8.5 in the far-future (2071–2100), period. All five GCMs indicate increasing drought duration and severity, and the metrics intensify systematically with forcing magnitude (SSP5-8.5 > SSP2-4.5) and time horizon far-future (2071–2100) > mid-future (2041–2070). This consistent scaling across scenarios and periods is indicative of a forced climate response as a primary driver of the projected changes, rather than an outcome arising purely from model-specific behavior, while acknowledging that absolute extremes may still be influenced by structural model uncertainty and index-related assumptions.

4.4.4 Implications for water resources management

These drought intensification findings have direct implications for the Arno River basin. In agriculture, prolonged meteorological and hydrological droughts will intensify irrigation demand during already water-stressed summers, heightening risks of yield losses and economic instability in the Tuscan agricultural sector (Iglesias et al., 2007; Spinoni et al., 2018). In the upstream Arno River basin, SWAT simulations indicate that precipitation is partitioned into approximately 46% evapotranspiration and 25% runoff indicating that climate-driven increases in evaporative demand will directly reduce water availability for agricultural use (Pacetti et al., 2021).

For urban supply systems, the Bilancino reservoir on the Sieve River (84 million m³ total capacity) provides critical water supply regulation and maintains minimum environmental flows in the Arno during low-flow periods (Marchettini et al., 2009b); the projected multi-year droughts under SSP5-8.5 may reduce reservoir reliability and intensify competition among the approximately 2.2 million inhabitants dependent on basin water resources. Ecologically, sustained low-flow conditions threaten riparian vegetation and aquatic biodiversity, undermining resilience to climate extremes (Dudgeon et al., 2006; Gouveia et al., 2017). Recent assessments of Tuscan rivers demonstrate poor correlation between hydrological variables and EU Water Framework Directive ecological indicators, suggesting that climate-driven flow reductions may compound water quality challenges beyond simple quantity deficits (Arrighi et al., 2021). The projected streamflow reductions of 18–32% under SSP5-8.5 far-future (2071–2100) scenarios would severely compromise environmental flow maintenance during critical summer periods.

The shift toward fewer but significantly longer drought episodes requires fundamental changes in water management paradigms. Traditional approaches designed for frequent but shorter droughts may prove inadequate for the multi-year drought conditions projected under high-emission scenarios. Integrated strategies should combine nature-based solutions such as wetland and riparian forest restoration to enhance infiltration and groundwater recharge (Nesshöver et al., 2017), with infrastructure management through adaptive reservoir operations and flexible rule curves using seasonal climate forecasts can improve capacity to store winter flows for extended dry periods (Tilocca, 2024). The strong correlations between meteorological and hydrological drought indices provide opportunities for early warning systems with 3-6 month lead times, enabling proactive demand management and emergency preparedness. However, the projected amplification in drought severity requires institutional frameworks aligned with the European Union Water Framework Directive, including robust monitoring networks, stakeholder coordination, and adaptive allocation mechanisms with clear responsibilities and measurable targets (Garrote et al., 2016). Despite uncertainty in near-term projections, the consistent model convergence toward severe late-century impacts provides strong scientific justification for immediate implementation of adaptive measures. The integration of drought projections into basin-scale allocation strategies, agricultural planning, and ecosystem conservation policies becomes essential for building long-term resilience in the Arno River basin.

4.4.5 Uncertainty analysis and limitations

SWAT+ calibration and validation relied on a single downstream gauging station, which limits evaluation of sub-basin spatial performance. Accordingly, results are interpreted at the basin scale and emphasize relative changes and ensemble-consistent trends rather than absolute local-scale projections. Future work should consider multi-site calibration and spatial validation using additional discharge records where available. Future climate projections from CMIP6 models contain considerable uncertainty, particularly for Mediterranean precipitation where model agreement is generally lower than for temperature trends (Zittis et al., 2021). The inter-model variability in precipitation projections showing both increases and decreases in near-future before converging toward late-century drying reflects uncertainty documented in CMIP6 Mediterranean assessments (Cos et al., 2022). The assumption of static LULC, adopted to isolate climate-driven impacts, is also a limitation. In reality, future land-use trajectories in the Arno River basin (e.g., urban expansion, agricultural change, or upland vegetation shifts) could alter the partitioning of precipitation into runoff, infiltration, evapotranspiration, and groundwater recharge. Increased imperviousness typically enhances quick runoff and reduces recharge and baseflow, potentially intensifying hydrological drought relative to a static-LULC setup. Conversely, agricultural abandonment or reforestation can increase evapotranspiration and reduce water yield, also affecting low-flow regimes. However, comparative studies in Mediterranean and similar catchments suggest that climate forcing often exerts a larger influence on long-term streamflow change than land-use change (Serpa et al., 2015; Tamm et al., 2018). Consequently, our projections should be interpreted as climate-driven signals, while the magnitude of hydrological drought impacts may differ under plausible future LULC scenarios.

Additionally, drought classification in this study focuses on 12-month accumulation periods (SPI-12 and SRI-12) and may not capture shorter-term drought dynamics relevant for specific water-management applications. SPI/SRI values, particularly in the distribution tails, can be sensitive to the assumed probability distribution and parameter estimation used in standardization, introducing additional uncertainty in drought magnitude estimates. Moreover, calibration and validation were conducted at a monthly time scale, which is appropriate for

SPI-12 and SRI-12 assessment but smooths daily variability and may under-represent short-duration low-flow processes and drought onset and recovery dynamics. In interpreting extreme projected values (e.g., TDD up to 106 months; TDS up to 177), it is also important to recognize that Mediterranean drying signals exhibit substantial inter-model spread and scenario dependence across CMIP ensembles (Cos et al., 2022), and that parametric SPI/SRI standardization (often gamma-based) is sensitive to distributional assumptions and goodness-of-fit (Stagge et al., 2015). Together, these considerations support emphasizing ensemble-consistent tendencies and relative changes over time rather than over-interpreting absolute magnitudes of extreme drought metrics.

Future research should incorporate dynamic land-use scenarios when consistent projections become available to quantify combined climate–LULC effects, explore multi-timescale drought indices, evaluate daily-scale performance using low-flow-sensitive metrics, and couple SWAT+ with groundwater and managed-system representations (e.g., SWAT+MODFLOW) to account for reservoir operations and sectoral demands, while also assessing sensitivity to alternative bias-correction approaches and expanded climate-model ensembles.

4.5 Conclusions

This study quantified 21st-century climate-change impacts on streamflow and drought in the Arno River basin (Italy) using SWAT+ forced by QDM bias-corrected CMIP6 projections under SSP2-4.5 and SSP5-8.5. Relative to the historical baseline (1994–2014), all models indicate sustained warming across near, mid and far future (2015–2040), (2041–2070), (2071–2100), reaching 3°C under SSP2-4.5 and 5°C under SSP5-8.5 by late century. Annual precipitation exhibits an overall declining tendency in both scenarios, with projected trends of -0.51 mm yr^{-1} SSP2-4.5 and -1.77 mm yr^{-1} SSP5-8.5 and a clearer convergence toward drying in far-future (2071–2100), especially under SSP5-8.5. Streamflow decreases consistently with the precipitation signal, with trend reductions of -0.07 m^3 s^{-1} yr^{-1} SSP2-4.5 and -0.19 m^3 s^{-1} yr^{-1} SSP5-8.5. Under SSP5-8.5, far-future (2071-2100) projections converge toward substantial flow reductions (~18.4%–32.0% across models), implying potentially higher risk of persistent low-flow conditions.

Drought metrics based on SPI-12 and SRI-12 show marked intensification. Under SSP5-8.5, total drought duration reaches up to 99 months for meteorological drought (SPI-12) and 106 months for hydrological drought (SRI-12), compared with historical totals of 41 and 32 months, respectively. Strong SPI-12–SRI-12 correlations ($r = 0.80$–0.95) persist across scenarios and time windows, indicating coherent drought propagation and supporting the use of meteorological indicators for hydrological drought early warning, while acknowledging that catchment storage, regulation, and land-use change can modulate propagation. Across the ensemble, drought change commonly consolidates into fewer but longer and more severe episodes in several models, potentially stressing storage and management strategies designed around shorter, more frequent events.

Considering uncertainties (limited GCM ensemble size, basin-scale calibration, static land-use, and SPI/SRI standardization assumptions), the significant finding is the ensemble-consistent direction of change: warming-driven increases in evaporative demand, heightened likelihood of reduced streamflow, and greater risk of prolonged drought under higher forcing. These results support near-term adaptation aligned with longer drought episodes, including SPI/SRI-based early warning to enable staged response actions, demand-side measures, and adaptive reservoir operating rules that balance supply reliability with minimum environmental flows during critical low-flow periods. Overall, the projections provide actionable evidence for drought preparedness and climate adaptation planning in the Arno River basin.

Chapter 5 General conclusions and perspective

This PhD research focused on the hydroclimatic dynamics of the Arno River basin, Tuscany, Italy a culturally, economically, and ecologically significant Mediterranean catchment of 8,228 km² that supports approximately 2.2 million inhabitants, including the cities of Florence and Pisa. The Mediterranean region has been consistently identified as a climate change hotspot, where warming rates exceed the global mean by a factor of approximately 1.6 and where robust summer drying signals are projected to intensify throughout the twenty-first century. Yet, prior to this work, the Arno River basin lacked a comprehensive, integrated assessment that jointly examined observed hydroclimatic variability over recent decades and projected future changes in climate, streamflow, and drought under CMIP6 emission scenarios. This deficit represented a significant gap for water resources planning in a basin that has historically experienced both devastating floods and severe droughts. The analyses conducted during this PhD project sought to address this gap through two complementary research questions.

Question 1 – What are the characteristics, variability, trends, and co-variability of temperature, precipitation, and streamflow in the Arno River basin over the recent observational period (1994–2023)?

To address this question, Chapter 3 employed a comprehensive observational framework using data from 18 precipitation stations, 7 temperature stations, and the S. Giovanni alla Vena streamflow gauging station, analysed through non-parametric statistical methods including the Modified Mann-Kendall test, Sen's slope estimator, the Standardized Anomaly Index, coefficients of variation, and Spearman's rank correlation analysis. The climatological characterization revealed a pronounced Mediterranean regime: mean monthly temperature ranged from a basin-averaged minimum of 6.4 °C in January to 24.4 °C in August, while mean annual precipitation was approximately 895.8 mm, strongly concentrated in autumn (34.76%) and winter (30.09%), with summer contributing only 14.08%. The spatial distribution of precipitation exhibited a marked orographic gradient controlled by the Apennine Mountains, with annual totals ranging from approximately 720–830 mm in the central and southwestern lowlands to over 1,160 mm in the northeastern headwater areas along the Apennine ridge. Leave-one-out cross-validation of the IDW interpolation confirmed satisfactory spatial representation, with relative RMSE ranging from 10.9% in autumn to 14.1% in winter.

The variability analysis revealed that all hydroclimatic variables exhibited pronounced interannual fluctuations, though to markedly different degrees. Temperature showed moderate variability, with annual coefficients of variation of 3.9% (T_{max}), 4.5% (T_{avg}), and 6.6% (T_{min}), with winter displaying the highest seasonal variability (CV up to 40.2% for T_{min}). Precipitation was substantially more variable (annual CV = 18.2%, reaching 36.9% in winter and 36.0% in summer), while streamflow exhibited the highest variability of all three variables, with an annual CV of 33.4% and seasonal values reaching 65.8% in autumn and 50.3% in winter. The streamflow CV consistently exceeded the precipitation CV across all seasons, reflecting the nonlinear amplification of rainfall fluctuations through catchment storage, soil moisture, and runoff-generation processes. The Standardized Anomaly Index series illustrated the episodic character of Mediterranean hydroclimate, with sharp alternations between wet and dry years notably the contrast between the exceptionally wet 2010 (annual precipitation SAI = +2.55; streamflow SAI = +2.69) and the severely dry 2011 (precipitation SAI = −1.76) rather than a progressive directional shift.

Trend analysis detected a statistically significant warming trend of +0.052 °C yr^{-1} at the annual scale, corresponding to an increase of approximately 1.56 °C over three decades. Seasonally, autumn exhibited the strongest warming (+0.072 °C yr^{-1}), followed by summer (+0.064 °C yr^{-1}) and winter (+0.053 °C yr^{-1}), while spring warming remained non-significant. Positive temperature anomalies were concentrated from 2014 onward, with 2022 and 2023 recording the strongest warm anomalies (up to +1.94 °C for T_{max}, +1.54 °C for T_{avg}, and +1.37 °C for T_{min}), indicating a clear acceleration of warming in the most recent decade. In contrast, no statistically significant trends were detected in annual or seasonal precipitation (annual Sen's slope = +1.113 mm yr^{-1}, $\tau = 0.044$, $p = 0.735$) and streamflow (annual Sen's slope = −0.071 mm yr^{-1}, $\tau = -0.007$, $p = 0.957$), with all seasonal Mann-Kendall p-values well above conventional significance thresholds. Of the 30 years analysed for streamflow, 19 exhibited negative SAI values and 11 positive, indicating a predominance of below-average runoff conditions, but this asymmetry was not statistically significant.

Spearman's rank correlation analysis confirmed a predominantly precipitation-controlled streamflow regime. Precipitation and streamflow were strongly and positively correlated across all seasons, ranging from $\rho = 0.51$ in spring ($p < 0.01$) to $\rho = 0.93$ in autumn ($p < 0.001$), with the annual correlation reaching $\rho = 0.77$ ($p < 0.001$). Winter and spring together generated approximately 77% of annual runoff. A critical finding from Chapter 3 was the significant negative summer temperature-streamflow correlation ($\rho = -0.57$, $p < 0.001$), accompanied by a significant negative summer temperature–precipitation correlation ($\rho = -0.53$, $p < 0.01$). These results indicated that hotter summers tend to coincide with drier conditions and reduced runoff, identifying warming-driven evapotranspiration as an already active influence on warm-season hydrology-a finding that proved central to interpreting the future projections presented in Chapter 4.

Question 2 – How will the hydroclimatic regime, streamflow, and drought characteristics of the Arno River basin change under future climate scenarios, and what are the implications for drought propagation?

To address this question, Chapter 4 developed a modelling chain comprising the SWAT+ hydrological model, QDM bias correction applied to five CMIP6 GCMs (BCC-CSM2-MR, CMCC-ESM2, MPI-ESM1-2-HR, MRI-ESM2-0, and NorESM2-MM), and drought characterization through SPI-12 and SRI-12 indices under SSP2-4.5 and SSP5-8.5 scenarios. The SWAT+ model was calibrated (2007–2011) and validated (2012–2014) against observed monthly streamflow at the S. Giovanni alla Vena gauging station, achieving NSE values of 0.74 and 0.93, PBIAS of 7.74% and 10.32%, and KGE values of 0.72 and 0.85, respectively performance classified as good to very good according to established evaluation criteria. The model captured both high-flow peaks and low-flow conditions across contrasting wet and dry hydrological years, and the very strong agreement between observed and simulated SRI-12 during the overlapping period ($r = 0.97$) confirmed its suitability for drought assessment. The QDM bias correction effectively adjusted the distributional properties of GCM outputs, correcting wet-day frequency overestimation from 48.6% to 36.9% (observed: 36.6%) and restoring extreme quantiles (Q95 and Q99 ratios = 1.00) while preserving the projected climate change signal in the quantiles.

All five GCMs projected unequivocal warming across all time windows and both scenarios, with the highest inter-model agreement among the three analysed variables. The ensemble median warming rate was 0.03 °C yr^{-1} under SSP2-4.5 and 0.05 °C yr^{-1} under SSP5-8.5, values remarkably consistent with the observed rate of +0.052 °C yr^{-1} documented in Chapter 3. This consistency provided strong mutual validation between the observational record and the modelling framework. By the far-future (2071–2100), warming reached approximately 1.90–3.91 °C under SSP2-4.5 and 3.77–5.35 °C under SSP5-8.5 relative to the historical baseline (1994–2014), with CMCC-ESM2 consistently defining the upper bound of warming (up to +5.35 °C under SSP5-8.5) and MPI-ESM1-2-HR toward the lower end.

Annual precipitation exhibited declining tendencies under both scenarios (−0.51 mm yr^{-1} under SSP2-4.5; −1.77 mm yr^{-1} under SSP5-8.5, the latter statistically significant at $p < 0.05$). Critically, inter-model agreement on the direction of change strengthened progressively with time: in the near-future (2015–2040), only 3 of 5 models agreed on decreasing precipitation under SSP2-4.5, but by the mid-future (2041–2070) this increased to 4 of 5, and by the far-future (2071–2100) under SSP5-8.5, all five GCMs converged on decreasing precipitation, with a median reduction of approximately 140 mm yr^{-1} (−15.1%). This temporal evolution is consistent with the concept of signal emergence from climate noise, and importantly, it is coherent with the findings of Chapter 3, where the absence of a significant precipitation trend in the 1994–2023 record reflects the early phase of this emergence process when natural variability still dominates over the forced signal.

River runoff projections broadly followed the combined precipitation and temperature signals. The ensemble median decreased by −0.07 $m^3\ s^{-1}\ yr^{-1}$ under SSP2-4.5 and −0.19 $m^3\ s^{-1}\ yr^{-1}$ under SSP5-8.5 (the latter significant at $p < 0.05$). Under SSP5-8.5 far-future (2071–2100), all five GCMs converged on decreasing runoff, with reductions ranging from 18.4% to 32.0% across models and a median of 24%. The inter-model spread for runoff was substantially larger than for precipitation: the normalized spread reaching 49% of the historical baseline in the near-future under SSP2-4.5 reflecting the compounded uncertainties from precipitation variability, temperature-driven evapotranspiration responses, and nonlinear catchment processes. These projected declines are quantitatively consistent with recent CMIP6-based Mediterranean assessments, and the mechanism driving them was corroborated by the observational finding in Chapter 3: the significant negative summer temperature–streamflow correlation ($\rho = -0.57$) already demonstrated that rising temperatures reduce warm-season water availability through enhanced evapotranspiration, a process that the models project to intensify dramatically as warming reaches +3 to +5 °C by century's end.

Drought characterization using SPI-12 and SRI-12 revealed marked intensification under both scenarios. Historical baseline total drought duration (TDD) ranged from 11 to 41 months for meteorological drought (SPI-12) and from 16 to 32 months for hydrological drought (SRI-12). Under SSP5-8.5 far-future, TDD increased to up to 99 months (SPI-12) and 106 months (SRI-12), while total drought severity (TDS) amplified to 172 and 177, respectively. The fact that hydrological drought severity exceeded meteorological drought severity under the most extreme far-future projections represents a finding of particular significance: it indicates that the catchment's natural storage capacity, which historically buffered and attenuated meteorological drought signals, may become insufficient under enhanced evapotranspiration effectively transforming the hydrological system from a drought buffer into a drought amplifier. Pearson correlations between SPI-12 and SRI-12 remained consistently high across all models, scenarios, and time windows ($r = 0.80–0.95$), indicating that drought propagation relationships remain broadly stable under intensified climate forcing. This stability supports the operational use of meteorological indicators as reliable precursors for hydrological drought monitoring and early warning, even under future conditions substantially different from the present. The temporal dynamics further indicated a consolidation of drought conditions into fewer but longer and more intense episodes a qualitative regime shift with profound implications for water management.

Taken together, the findings from Chapters 3 and 4 indicate that the Arno River basin is currently in a transitional phase. Significant warming is underway and its hydrological fingerprint is already detectable through the summer temperature-streamflow coupling, but the full impact on water resources remains partially masked by the high natural variability that characterizes Mediterranean precipitation. The high degree of consistency between the two studies in warming rate magnitude, in the signal-to-noise behavior of precipitation, in the SWAT+ reproduction of the observed precipitation–streamflow relationships, and in the physical mechanism linking temperature to streamflow strengthens confidence in both the empirical baseline and the projection framework. As warming continues to intensify and the drying signal progressively emerges, the basin is projected to transition from a regime of episodic variability to one of structurally declining water availability and fundamentally altered drought behavior.

These findings have direct implications for water resources management and climate adaptation. The assumption that the historical variability envelope provides a reliable basis for water planning is no longer tenable for the Arno basin, as projected changes will shift water availability beyond the range of past experience (Milly et al., 2008). The Bilancino reservoir on the Sieve River (84 million m^3 capacity), which provides critical water supply regulation and maintains environmental flows during low-flow periods (Marchettini et al., 2009a), will face increasing pressure under the projected multi-year drought conditions, and current operating rules will likely require revision toward adaptive strategies incorporating seasonal climate forecasts (Giuliani et al., 2019). The strong precipitation–streamflow correlations documented in Chapter 3 and the persistent SPI–SRI correlations documented in Chapter 4 together provide an empirical and model-based foundation for drought early warning, with meteorological indicators offering advance notice of hydrological drought with lead times of several months. However, the projected amplification of hydrological drought relative to meteorological forcing under warming suggests that static warning thresholds calibrated to historical conditions may underestimate future drought severity, necessitating periodic recalibration. In the agricultural sector, prolonged summer droughts will intensify irrigation demand in a basin where approximately 46% of precipitation is already returned to the atmosphere through evapotranspiration (Pacetti et al., 2021), while ecologically, the projected streamflow reductions of 18.4–32.0% under SSP5-8.5 far-future threaten riparian ecosystems and environmental flow maintenance during critical summer periods.

While this research provides a comprehensive assessment, it also identifies areas requiring further investigation. Future studies should incorporate dynamic land-use change scenarios into the SWAT+ framework, as the static land-use assumption employed here cannot capture the potentially nonlinear interactions between urbanization, agricultural change, and climate forcing. Expanding the GCM ensemble beyond five members and incorporating higher-resolution regional climate models (e.g., EURO-CORDEX or convection-permitting simulations) would improve the characterization of precipitation uncertainty and the representation of extreme events. Multi-site calibration using additional gauging stations within the Arno system would enable sub-basin-scale impact assessment and identify spatial heterogeneity in drought vulnerability, with the Apennine headwaters warranting particular attention given their sensitivity to changes in snow processes (Carrer et al., 2023; Fayad et al., 2017). Coupling SWAT+ with groundwater models (e.g., SWAT+MODFLOW) and explicit representations of reservoir operations and abstraction regimes would bridge the gap between the naturalized projections presented here and the operational water availability experienced by users. Additionally, exploring drought indices at multiple accumulation periods alongside the Standardized Precipitation Evapotranspiration Index (SPEI) which explicitly accounts for temperature-driven evaporative demand (Beguería et al., 2014), would provide a more complete picture of drought dynamics, given that warming-driven evapotranspiration emerges from this thesis as an increasingly important control on hydrological drought.

The methodological framework developed in this thesis combining observational trend and variability analysis with process-based hydrological modelling and standardized drought characterization under multiple emission scenarios enabled a comprehensive quantification of the past, present, and projected future hydroclimatic conditions in the Arno River basin. The findings provide an actionable scientific evidence base for developing proactive, evidence-based adaptation strategies that account for both the inherent variability of the Mediterranean hydroclimate and the directional changes imposed by anthropogenic warming. This framework is readily transferable to other Mediterranean basins facing similar challenges, offering both a detailed case study and a methodological template for addressing the growing pressures on water resources in one of the world's most climate-vulnerable regions.

References

Abdelwahab, O. M. M., Ricci, G. F., Gentile, F., & De Girolamo, A. M. (2025). Modelling the impact of climate change on runoff and sediment yield in Mediterranean basins: The Carapelle case study (Apulia, Italy). *Frontiers in Water*, *7*. https://doi.org/10.3389/frwa.2025.1486644

Ahmed, A., Mahar, M., Egbedi, P., Mahar, A., Haider, M. A., Talpur, H. A., Chaiboontha, S., Shar, K. U., Abbasi, H., & Talpur, S. A. (2026). Climate-smart agriculture as disaster risk reduction: Effectiveness varies by hazard type in Pakistan. *Climate Smart Agriculture*, *3*(1), 100093. https://doi.org/10.1016/j.csag.2025.100093

Allen, R. G., Pereira, L. S., Raes, D., & Smith, M. (1998). FAO Irrigation and drainage paper No. 56. *Rome: Food and Agriculture Organization of the United Nations*, *56*(97), e156.

Aloui, S., Mazzoni, A., Elomri, A., Aouissi, J., Boufekane, A., & Zghibi, A. (2023). *A review of Soil and Water Assessment Tool (SWAT) studies of Mediterranean catchments: Applications, feasibility, and future directions*. https://doi.org/10.1016/J.JENVMAN.2022.116799

Arnold, J. G., Bieger, K., White, M. J., Srinivasan, R., Dunbar, J. A., & Allen, P. M. (2018). Use of Decision Tables to Simulate Management in SWAT+. *Water*, *10*(6), Article 6. https://doi.org/10.3390/w10060713

Arnold, J. G., Srinivasan, R., Muttiah, R. S., & Williams, J. R. (1998). Large Area Hydrologic Modeling and Assessment Part I: Model Development. *JAWRA Journal of the American Water Resources Association*, *34*(1), 73–89. https://doi.org/10.1111/j.1752-1688.1998.tb05961.x

Arrighi, C., Bonamini, I., Simoncini, C., Bartalesi, S., & Castelli, F. (2021). WFD Ecological Quality Indicators Are Poorly Correlated with Water Levels in River Catchments in Tuscany (Italy). *Hydrology*, *8*(4), 185. https://doi.org/10.3390/hydrology8040185

Aruffo, E., & Carlo, P. D. (2019). Homogenization of instrumental time series of air temperature in Central Italy (1930-2015). *Climate Research*, *77*, 193–204. https://doi.org/10.3354/cr01552

Asfaw, A., Simane, B., Hassen, A., & Bantider, A. (2018). Variability and time series trend analysis of rainfall and temperature in northcentral Ethiopia: A case study in Woleka sub-basin. *Weather and Climate Extremes*, *19*, 29–41. https://doi.org/10.1016/j.wace.2017.12.002

Baez-Villanueva, O. M., Zambrano-Bigiarini, M., Miralles, D. G., Beck, H. E., Siegmund, J. F., Alvarez-Garreton, C., Verbist, K., Garreaud, R., Boisier, J. P., & Galleguillos, M. (2024). On the timescale of drought indices for monitoring streamflow drought considering catchment hydrological regimes. *Hydrology and Earth System Sciences*, *28*(6), 1415–1439. https://doi.org/10.5194/hess-28-1415-2024

Barcikowska, M. J., Kapnick, S. B., Krishnamurty, L., Russo, S., Cherchi, A., & Folland, C. K. (2020). Changes in the future summer Mediterranean climate: Contribution of teleconnections and local factors. *Earth System Dynamics*, *11*(1), 161–181. https://doi.org/10.5194/esd-11-161-2020

Barker, L. J., Hannaford, J., Chiverton, A., & Svensson, C. (2016). From meteorological to hydrological drought using standardised indicators. *Hydrology and Earth System Sciences*, *20*(6), 2483–2505.

Baronetti, A., Dubreuil, V., Provenzale, A., & Fratianni, S. (2022). Future droughts in northern Italy: High-resolution projections using EURO-CORDEX and MED-CORDEX ensembles. *Climatic Change*, *172*(3), 22. https://doi.org/10.1007/s10584-022-03370-7

Bartolini, G., Grifoni, D., Magno, R., Torrigiani, T., & Gozzini, B. (2018). Changes in temporal distribution of precipitation in a Mediterranean area (Tuscany, Italy) 1955–2013. *International Journal of Climatology*, *38*(3), 1366–1374. https://doi.org/10.1002/joc.5251

Beguería, S., Vicente-Serrano, S. M., Reig, F., & Latorre, B. (2014). Standardized precipitation evapotranspiration index (SPEI) revisited: Parameter fitting, evapotranspiration models, tools, datasets and drought monitoring. *International Journal of Climatology*, *34*(10), 3001–3023. https://doi.org/10.1002/joc.3887

Bhatta, B., Shrestha, S., Shrestha, P. K., & Talchabhadel, R. (2019). Evaluation and application of a SWAT model to assess the climate change impact on the hydrology of the Himalayan River Basin. *CATENA*, *181*, 104082. https://doi.org/10.1016/j.catena.2019.104082

Bieger, K., Arnold, J. G., Rathjens, H., White, M. J., Bosch, D. D., Allen, P. M., Volk, M., & Srinivasan, R. (2017). Introduction to SWAT+, A Completely Restructured Version of the Soil and Water Assessment Tool. *JAWRA Journal of the American Water Resources Association*, *53*(1), 115–130. https://doi.org/10.1111/1752-1688.12482

Brunetti, M., Maugeri, M., Monti, F., & Nanni, T. (2006). Temperature and precipitation variability in Italy in the last two centuries from homogenised instrumental time series. *International Journal of Climatology*, *26*(3), 345–381. https://doi.org/10.1002/joc.1251

Burlando, P., & Rosso, R. (2002). Effects of transient climate change on basin hydrology. 2. Impacts on runoff variability in the Arno River, central Italy. *Hydrological Processes*, *16*(6), 1177–1199. https://doi.org/10.1002/hyp.1056

Caloiero, T., Caloiero, P., & Frustaci, F. (2018). Long-term precipitation trend analysis in Europe and in the Mediterranean basin. *Water and Environment Journal*, *32*(3), 433–445. https://doi.org/10.1111/wej.12346

Caloiero, T., Coscarelli, R., Gaudio, R., & Leonardo, G. P. (2019). Precipitation trend and concentration in the Sardinia region. *Theoretical and Applied Climatology*, *137*(1), 297–307. https://doi.org/10.1007/s00704-018-2595-1

Cammalleri, C., Naumann, G., Mentaschi, L., Bisselink, B., Gelati, E., De Roo, A., & Feyen, L. (2020). Diverging hydrological drought traits over Europe with global warming. *Hydrology and Earth System Sciences*, *24*(12), 5919–5935. https://doi.org/10.5194/hess-24-5919-2020

Campo, L., Caparrini, F., & Castelli, F. (2006). Use of multi-platform, multi-temporal remote-sensing data for calibration of a distributed hydrological model: An application in the Arno basin, Italy. *Hydrological Processes*, *20*(13), 2693–2712. https://doi.org/10.1002/hyp.6061

Cannon, A. J., Sobie, S. R., & Murdock, T. Q. (2015). Bias Correction of GCM Precipitation by Quantile Mapping: How Well Do Methods Preserve Changes in Quantiles and Extremes? *Journal of Climate*, *28*(17), 6938–6959. https://doi.org/10.1175/JCLI-D-14-00754.1

Caporali, E., Rinaldi, M., & Casagli, N. (2005). The Arno River Floods. *Giornale Di Geologia Applicata*, (1), 177–192. https://doi.org/10.1474/GGA.2005-01.0-18.0018

Carrer, M., Dibona, R., Prendin, A. L., & Brunetti, M. (2023). Recent waning snowpack in the Alps is unprecedented in the last six centuries. *Nature Climate Change*, *13*(2), 155–160. https://doi.org/10.1038/s41558-022-01575-3

Castelli, F., Menduni, G., & Mazzanti, B. (2009). A distributed package for sustainable water management: A case study in the Arno basin. *The Role of Hydrology in Water Resources Management (Proceedings of a Symposium Heldon the Island of Capri, Italy, IAHS Publication*, *327*, 52–61.

Chaouche, K., Neppel, L., Dieulin, C., Pujol, N., Ladouche, B., Martin, E., Salas, D., & Caballero, Y. (2010). Analyses of precipitation, temperature and evapotranspiration in a French Mediterranean region in the context of climate change. *Comptes Rendus. Géoscience*, *342*(3), 234–243. https://doi.org/10.1016/j.crte.2010.02.001

Cid, N., Bonada, N., Carlson, S. M., Grantham, T. E., Gasith, A., & Resh, V. H. (2017). High Variability Is a Defining Component of Mediterranean-Climate Rivers and Their Biota. *Water*, *9*(1), 52. https://doi.org/10.3390/w9010052

Cook, B., Mankin, J., Marvel, K., Williams, A. P., Smerdon, J., & Anchukaitis, K. (2020). Twenty-First Century Drought Projections in the CMIP6 Forcing Scenarios. *Earth's Future*. https://doi.org/10.1029/2019EF001461

Cos, J., Doblas-Reyes, F., Jury, M., Marcos, R., Bretonnière, P.-A., & Samsó, M. (2022). The Mediterranean climate change hotspot in the CMIP5 and CMIP6 projections. *Earth System Dynamics*, *13*(1), 321–340. https://doi.org/10.5194/esd-13-321-2022

Cosgrove, W. J., & Loucks, D. P. (2015). Water management: Current and future challenges and research directions. *Water Resources Research*, *51*(6), 4823–4839. https://doi.org/10.1002/2014WR016869

Cramer, W., Guiot, J., Fader, M., Garrabou, J., Gattuso, J.-P., Iglesias, A., Lange, M. A., Lionello, P., Llasat, M. C., Paz, S., Peñuelas, J., Snoussi, M., Toreti, A., Tsimplis, M. N., & Xoplaki, E. (2018). Climate change and interconnected risks to sustainable development in the Mediterranean. *Nature Climate Change*, *8*(11), 972–980. https://doi.org/10.1038/s41558-018-0299-2

D. N. Moriasi, J. G. Arnold, M. W. Van Liew, R. L. Bingner, R. D. Harmel, & T. L. Veith. (2007). Model Evaluation Guidelines for Systematic Quantification of Accuracy in Watershed Simulations. *Transactions of the ASABE*, *50*(3), 885–900. https://doi.org/10.13031/2013.23153

Dakhlaoui, H., Seibert, J., & Hakala, K. (2020). Sensitivity of discharge projections to potential evapotranspiration estimation in Northern Tunisia. *Regional Environmental Change*, *20*(2), 34. https://doi.org/10.1007/s10113-020-01615-8

Daly, C., Neilson, R. P., & Phillips, D. L. (1994). A Statistical-Topographic Model for Mapping Climatological Precipitation over Mountainous Terrain. *Journal of Applied Meteorology and Climatology*, *33*(2), 140–158. https://doi.org/10.1175/1520-0450(1994)033%253C0140:ASTMFM%253E2.0.CO;2

Diodato, N., Ljungqvist, F. C., & Bellocchi, G. (2021). Climate Patterns in the World's Longest History of Storm-Erosivity: The Arno River Basin, Italy, 1000–2019 CE. *Frontiers in Earth Science*, *9*. https://doi.org/10.3389/feart.2021.637973

D'Oria, M., Ferraresi, M., & Tanda, M. G. (2017). Historical trends and high-resolution future climate projections in northern Tuscany (Italy). *Journal of Hydrology*, *555*, 708–723. https://doi.org/10.1016/j.jhydrol.2017.10.054

D'Oria, M., Ferraresi, M., & Tanda, M. G. (2019). Quantifying the impacts of climate change on water resources in northern TUSCANY , ITALY , using high-resolution regional projections. *Hydrological Processes*, *33*(6), 978–993. https://doi.org/10.1002/hyp.13378

Dudgeon, D., Arthington, A. H., Gessner, M. O., Kawabata, Z.-I., Knowler, D. J., Lévêque, C., Naiman, R. J., Prieur-Richard, A.-H., Soto, D., Stiassny, M. L. J., & Sullivan, C. A. (2006). Freshwater biodiversity: Importance, threats, status and conservation challenges. *Biological Reviews*, *81*(2), 163–182. https://doi.org/10.1017/S1464793105006950

Edwards, D. C. (1997). *Characteristics of 20th Century Drought in the United States at Multiple Time Scales.* (No. AFIT97051). Article AFIT97051. https://apps.dtic.mil/sti/html/tr/ADA325595/

Eekhout, J. P. C., Nunes, J. P., Tramblay, Y., & De Vente, J. (2025). Severe Impacts on Water Resources Projected for the Mediterranean Basin. *WIREs Water*, *12*(2), e70012. https://doi.org/10.1002/wat2.70012

El Jeitany, J., Nussbaum, M., Pacetti, T., Schröder, B., & Caporali, E. (2024). Landscape metrics as predictors of water-related ecosystem services: Insights from hydrological modeling and data-based approaches applied on the Arno River Basin, Italy. *Science of The Total Environment*, *954*, 176567. https://doi.org/10.1016/j.scitotenv.2024.176567

El Jeitany, J., Pacetti, T., & Caporali, E. (2024a). Evaluating climate change effects on hydrological functionality and water-related ecosystem services. *Ecohydrology*, *17*(4), e2557. https://doi.org/10.1002/eco.2557

El Jeitany, J., Pacetti, T., & Caporali, E. (2024b). Evaluating climate change effects on hydrological functionality and water-related ecosystem services. *Ecohydrology*, *17*(4), e2557. https://doi.org/10.1002/eco.2557

Estrada, L., Garcia, X., Saló-Grau, J., Marcé, R., Munné, A., & Acuña, V. (2024). Spatio-temporal patterns and trends of streamflow in water-scarce Mediterranean basins. *Hydrology and Earth System Sciences*, *28*(24), 5353–5373. https://doi.org/10.5194/hess-28-5353-2024

Eyring, V., Bony, S., Meehl, G. A., Senior, C. A., Stevens, B., Stouffer, R. J., & Taylor, K. E. (2016). Overview of the Coupled Model Intercomparison Project Phase 6 (CMIP6) experimental design and organization. *Geoscientific Model Development*, *9*(5), 1937–1958. https://doi.org/10.5194/gmd-9-1937-2016

Fayad, A., Gascoin, S., Faour, G., López-Moreno, J. I., Drapeau, L., Page, M. L., & Escadafal, R. (2017). Snow hydrology in Mediterranean mountain regions: A review. *Journal of Hydrology, Investigation of Coastal Aquifers*, *551*, 374–396. https://doi.org/10.1016/j.jhydrol.2017.05.063

Fiseha, B. M., Setegn, S. G., Melesse, A. M., Volpi, E., & Fiori, A. (2013). Hydrological analysis of the Upper Tiber River Basin, Central Italy: A watershed modelling approach. *Hydrological Processes*, *27*(16), 2339–2351. https://doi.org/10.1002/hyp.9234

Gallart, F., Llorens, P., Latron, J., & Regüés, D. (2002). Hydrological processes and their seasonal controls in a small Mediterranean mountain catchment in the Pyrenees. *Hydrology and Earth System Sciences*, *6*(3), 527–537. https://doi.org/10.5194/hess-6-527-2002

García-Ruiz, J. M., López-Moreno, J. I., Vicente-Serrano, S. M., Lasanta–Martínez, T., & Beguería, S. (2011). Mediterranean water resources in a global change scenario. *Earth-Science Reviews*, *105*(3), 121–139. https://doi.org/10.1016/j.earscirev.2011.01.006

Garrote, L., Granados, A., & Iglesias, A. (2016). Strategies to reduce water stress in Euro-Mediterranean river basins. *Science of The Total Environment, Special Issue on Climate Change, Water and Security in the Mediterranean*, *543*, 997–1009. https://doi.org/10.1016/j.scitotenv.2015.04.106

Gebrechorkos, S. H., Sheffield, J., Vicente-Serrano, S. M., Funk, C., Miralles, D. G., Peng, J., Dyer, E., Talib, J., Beck, H. E., Singer, M. B., & Dadson, S. J. (2025). Warming accelerates global drought severity. *Nature*, *642*(8068), 628–635. https://doi.org/10.1038/s41586-025-09047-2

Ghinassi, M., Michielotto, A., Uguagliati, F., & Zattin, M. (2023). Mechanisms of microplastics trapping in river sediments: Insights from the Arno river (Tuscany, Italy). *Science of The Total Environment*, *866*, 161273. https://doi.org/10.1016/j.scitotenv.2022.161273

Giorgi, F. (2006). Climate change hot-spots. *Geophysical Research Letters*, *33*(8). https://doi.org/10.1029/2006GL025734

Giorgi, F., & Lionello, P. (2008). Climate change projections for the Mediterranean region. *Global and Planetary Change, Mediterranean Climate: Trends, Variability and Change*, *63*(2), 90–104. https://doi.org/10.1016/j.gloplacha.2007.09.005

Giuliani, M., Zaniolo, M., Castelletti, A., Davoli, G., & Block, P. (2019). Detecting the State of the Climate System via Artificial Intelligence to Improve Seasonal Forecasts and Inform Reservoir Operations. *Water Resources Research*, *55*(11), 9133–9147. https://doi.org/10.1029/2019WR025035

Gouveia, C. M., Trigo, R. M., Beguería, S., & Vicente-Serrano, S. M. (2017). Drought impacts on vegetation activity in the Mediterranean region: An assessment using remote sensing data and multi-scale drought indicators. *Global and Planetary Change, Climate Variability and Change in the Mediterranean Region*, *151*, 15–27. https://doi.org/10.1016/j.gloplacha.2016.06.011

Gupta, H. V., Kling, H., Yilmaz, K. K., & Martinez, G. F. (2009). Decomposition of the mean squared error and NSE performance criteria: Implications for improving hydrological modelling. *Journal of Hydrology*, *377*(1), 80–91. https://doi.org/10.1016/j.jhydrol.2009.08.003

Hamed, K. H., & Ramachandra Rao, A. (1998). A modified Mann-Kendall trend test for autocorrelated data. *Journal of Hydrology*, *204*(1), 182–196. https://doi.org/10.1016/S0022-1694(97)00125-X

Helsel, D. R., & Hirsch, R. M. (2002). Statistical methods in water resources. In *Techniques of Water-Resources Investigations* (Nos. 04-A3). U.S. Geological Survey. https://doi.org/10.3133/twri04A3

Hertig, E., & Tramblay, Y. (2017). Regional downscaling of Mediterranean droughts under past and future climatic conditions. *Global and Planetary Change, Climate Variability and Change in the Mediterranean Region*, *151*, 36–48. https://doi.org/10.1016/j.gloplacha.2016.10.015

Huang, S., Li, P., Huang, Q., Leng, G., Hou, B., & Ma, L. (2017). The propagation from meteorological to hydrological drought and its potential influence factors. *Journal of Hydrology*, *547*, 184–195. https://doi.org/10.1016/j.jhydrol.2017.01.041

Hurrell, J. W., & Van Loon, H. (1997). Decadal variations in climate associated with the north atlantic oscillation. *Climatic Change*, *36*(3), 301–326. https://doi.org/10.1023/A:1005314315270

Iglesias, A., Garrote, L., Flores, F., & Moneo, M. (2007). Challenges to Manage the Risk of Water Scarcity and Climate Change in the Mediterranean. *Water Resources Management*, *21*(5), 775–788. https://doi.org/10.1007/s11269-006-9111-6

IPCC. (2021). *Climate Change 2021 – The Physical Science Basis: Working Group I Contribution to the Sixth Assessment Report of the Intergovernmental Panel on Climate Change* (1st ed.). Cambridge University Press. https://doi.org/10.1017/9781009157896

IPCC. (2022a). *Climate Change 2022 – Impacts, Adaptation and Vulnerability: Working Group II Contribution to the Sixth Assessment Report of the Intergovernmental Panel on Climate Change* (1st ed.). Cambridge University Press. https://doi.org/10.1017/9781009325844

IPCC. (2022b). *Climate Change 2022 – Impacts, Adaptation and Vulnerability: Working Group II Contribution to the Sixth Assessment Report of the Intergovernmental Panel on Climate Change* (1st ed.). Cambridge University Press. https://doi.org/10.1017/9781009325844

IPCC. (2023). *Climate Change 2023: Synthesis Report. Contribution of Working Groups I, II and III to the Sixth Assessment Report of the Intergovernmental Panel on Climate Change [Core Writing Team, H. Lee and J. Romero (eds.)]. IPCC, Geneva, Switzerland.* https://doi.org/10.59327/IPCC/AR6-9789291691647

Keller, A. A., Garner, K., Rao, N., Knipping, E., & Thomas, J. (2023). Hydrological models for climate-based assessments at the watershed scale: A critical review of existing hydrologic and water quality models. *Science of The Total Environment*, *867*, 161209. https://doi.org/10.1016/j.scitotenv.2022.161209

Kendall, M. G. (1975). *Rank Correlation Methods* (4th ed.). Griffin.

Leone, M., Gentile, F., Porto, A. L., Ricci, G. F., & De Girolamo, A. M. (2023). Setting an ecological flow regime in a Mediterranean basin with limited data availability: The Locone River case study (S-E Italy). *Ecohydrology & Hydrobiology*, *23*(3), 346–360. https://doi.org/10.1016/j.ecohyd.2023.03.005

Li, C., & Fang, H. (2021). Assessment of climate change impacts on the streamflow for the Mun River in the Mekong Basin, Southeast Asia: Using SWAT model. *CATENA*, *201*, 105199. https://doi.org/10.1016/j.catena.2021.105199

Li, H., Sheffield, J., & Wood, E. F. (2010). Bias correction of monthly precipitation and temperature fields from Intergovernmental Panel on Climate Change AR4 models using equidistant quantile matching. *Journal of Geophysical Research: Atmospheres*, *115*(D10), 2009JD012882. https://doi.org/10.1029/2009JD012882

Li, X., & Li, Z. (2023). Evaluation of bias correction techniques for generating high-resolution daily temperature projections from CMIP6 models. *Climate Dynamics*, *61*(7), 3893–3910. https://doi.org/10.1007/s00382-023-06778-8

Lionello, P., Malanotte-Rizzoli, P., Boscolo, R., Alpert, P., Artale, V., Li, L., Luterbacher, J., May, W., Trigo, R., & Tsimplis, M. (2006). The Mediterranean climate: An overview of the main characteristics and issues. In *Developments in earth and environmental sciences* (Vol. 4, pp. 1–26). Elsevier. https://doi.org/10.1016/S1571-9197(06)80003-0

Lionello, P., & Scarascia, L. (2018). The relation between climate change in the Mediterranean region and global warming. *Regional Environmental Change*, *18*(5), 1481–1493. https://doi.org/10.1007/s10113-018-1290-1

Longobardi, A., & Villani, P. (2010). Trend analysis of annual and seasonal rainfall time series in the Mediterranean area. *International Journal of Climatology*, *30*(10), 1538–1546. https://doi.org/10.1002/joc.2001

López-Ballesteros, A., Srinivasan, R., & Senent-Aparicio, J. (2024). Introducing MapSWAT: An open source QGIS plugin integrated with google earth engine for efficiently generating ready-to-use SWAT+ input maps. *Environmental Modelling & Software*, *179*, 106108. https://doi.org/10.1016/j.envsoft.2024.106108

Lu, G. Y., & Wong, D. W. (2008). An adaptive inverse-distance weighting spatial interpolation technique. *Computers & Geosciences*, *34*(9), 1044–1055. https://doi.org/10.1016/j.cageo.2007.07.010

Lupon, A., Ledesma, J. L. J., & Bernal, S. (2018). Riparian evapotranspiration is essential to simulate streamflow dynamics and water budgets in a Mediterranean catchment. *Hydrology and Earth System Sciences*, *22*(7), 4033–4045. https://doi.org/10.5194/hess-22-4033-2018

Luppichini, M., Barsanti, M., Giannecchini, R., & Bini, M. (2021). Statistical relationships between large-scale circulation patterns and local-scale effects: NAO and rainfall regime in a key area of the Mediterranean basin. *Atmospheric Research*, *248*, 105270. https://doi.org/10.1016/j.atmosres.2020.105270

Mann, H. B. (1945). Nonparametric Tests Against Trend. *Econometrica*, *13*(3), 245–259. https://doi.org/10.2307/1907187

Marchettini, N., Patrizi, N., Pulselli, F. M., & Tiezzi, E. (2009a). *The role of a dam in a water management system in Italy: Physical and economic implications*. GBR. https://doi.org/10.2495/ECO090491

Marchettini, N., Patrizi, N., Pulselli, F., & Tiezzi, E. (2009b). The role of a dam in a water management system in Italy: Physical and economic implications. In *WIT Transactions on Ecology and the Environment* (Vol. 122, p. 545). https://doi.org/10.2495/ECO090491

Masseroni, D., Camici, S., Cislaghi, A., Vacchiano, G., Massari, C., & Brocca, L. (2021). The 63-year changes in annual streamflow volumes across Europe with a focus on the Mediterranean basin. *Hydrology and Earth System Sciences*, *25*(10), 5589–5601. https://doi.org/10.5194/hess-25-5589-2021

McKee, T. B., Doesken, N. J., & Kleist, J. (1993). The relationship of drought frequency and duration to time scales. *Proceedings of the 8th Conference on Applied Climatology*, (22). https://climate.colostate.edu/pdfs/relationshipofdroughtfrequency.pdf

Merheb, M., Moussa, R., Abdallah, C., Colin, F., Perrin, C., & Baghdadi, N. (2016). Hydrological response characteristics of Mediterranean catchments at different time scales: A meta-analysis. *Hydrological Sciences Journal*, *61*(14), 2520–2539. https://doi.org/10.1080/02626667.2016.1140174

Milly, P. C. D., Betancourt, J., Falkenmark, M., Hirsch, R. M., Kundzewicz, Z. W., Lettenmaier, D. P., & Stouffer, R. J. (2008). Stationarity Is Dead: Whither Water Management? *Science*, *319*(5863), 573–574. https://doi.org/10.1126/science.1151915

Mishra, A. K., & Singh, V. P. (2010). A review of drought concepts. *Journal of Hydrology*, *391*(1), 202–216. https://doi.org/10.1016/j.jhydrol.2010.07.012

Moriasi, D., Gitau, M., Pai, N., & Daggupati, P. (2015). Hydrologic and Water Quality Models: Performance Measures and Evaluation Criteria. *Transactions of the ASABE (American Society of Agricultural and Biological Engineers)*, *58*, 1763–1785. https://doi.org/10.13031/trans.58.10715

Muthuvel, D., & Qin, X. (2025). Probabilistic analysis of future drought propagation, persistence, and spatial concurrence in monsoon-dominant Asian regions under climate change. *Hydrology and Earth System Sciences*, *29*(14), 3203–3225. https://doi.org/10.5194/hess-29-3203-2025

Nakhaei, P., Kisi, O., Nakhaei, M., Fathollahi-Fard, A. M., & Gheibi, M. (2024). Assessment of climate change on river streamflow under different representative concentration pathways. *Journal of Environmental Management*, *366*, 121754. https://doi.org/10.1016/j.jenvman.2024.121754

Nash, J. E., & Sutcliffe, J. V. (1970). River flow forecasting through conceptual models part I — A discussion of principles. *Journal of Hydrology*, *10*(3), 282–290. https://doi.org/10.1016/0022-1694(70)90255-6

Nesshöver, C., Assmuth, T., Irvine, K. N., Rusch, G. M., Waylen, K. A., Delbaere, B., Haase, D., Jones-Walters, L., Keune, H., Kovacs, E., Krauze, K., Külvik, M., Rey, F., van Dijk, J., Vistad, O. I., Wilkinson, M. E., & Wittmer, H. (2017). The science, policy and practice of nature-based solutions: An interdisciplinary perspective. *Science of The Total Environment*, *579*, 1215–1227. https://doi.org/10.1016/j.scitotenv.2016.11.106

Noto, L. V., Cipolla, G., Pumo, D., & Francipane, A. (2023). Climate Change in the Mediterranean Basin (Part II): A Review of Challenges and Uncertainties in Climate Change Modeling and Impact Analyses. *Water Resources Management*, *37*(6), 2307–2323. https://doi.org/10.1007/s11269-023-03444-w

Odongo, R. A., De Moel, H., & Van Loon, A. F. (2023). Propagation from meteorological to hydrological drought in the Horn of Africa using both standardized and threshold-based indices. *Natural Hazards and Earth System Sciences*, *23*(6), 2365–2386. https://doi.org/10.5194/nhess-23-2365-2023

O'Neill, B. C., Tebaldi, C., van Vuuren, D. P., Eyring, V., Friedlingstein, P., Hurtt, G., Knutti, R., Kriegler, E., Lamarque, J.-F., Lowe, J., Meehl, G. A., Moss, R., Riahi, K., & Sanderson, B. M. (2016). The Scenario Model Intercomparison Project (ScenarioMIP) for CMIP6. *Geoscientific Model Development*, *9*(9), 3461–3482. https://doi.org/10.5194/gmd-9-3461-2016

Orke, Y. A., & Li, M.-H. (2021). Hydroclimatic Variability in the Bilate Watershed, Ethiopia. *Climate*, *9*(6), 98. https://doi.org/10.3390/cli9060098

Pacetti, T., Castelli, G., Schröder, B., Bresci, E., & Caporali, E. (2021). *Water Ecosystem Services Footprint of agricultural production in Central Italy*. https://doi.org/10.1016/J.SCITOTENV.2021.149095

Padulano, R., Gomez-Mogollon, L. A., Napolitano, L., & Rianna, G. (2025). Quantile-based bias-correction of extreme rainfall: Pros & cons of popular methods for climate signal preservation. *Journal of Hydrology*, *653*, 132814. https://doi.org/10.1016/j.jhydrol.2025.132814

Philandras, C. M., Nastos, P. T., Kapsomenakis, J., Douvis, K. C., Tselioudis, G., & Zerefos, C. S. (2011). Long term precipitation trends and variability within the Mediterranean region. *Natural Hazards and Earth System Sciences*, *11*(12), 3235–3250. https://doi.org/10.5194/nhess-11-3235-2011

Pulighe, G., Lupia, F., Chen, H., & Yin, H. (2021). Modeling Climate Change Impacts on Water Balance of a Mediterranean Watershed Using SWAT+. *Hydrology*, *8*(4), 157. https://doi.org/10.3390/hydrology8040157

Sen, P. K. (1968). Estimates of the Regression Coefficient Based on Kendall's Tau. *Journal of the American Statistical Association*, *63*(324), 1379–1389. https://doi.org/10.1080/01621459.1968.10480934

Senatore, A., Fuoco, D., Maiolo, M., Mendicino, G., Smiatek, G., & Kunstmann, H. (2022). Evaluating the uncertainty of climate model structure and bias correction on the hydrological impact of projected climate change in a Mediterranean catchment. *Journal of Hydrology: Regional Studies*, *42*, 101120. https://doi.org/10.1016/j.ejrh.2022.101120

Senent-Aparicio, J., Pérez-Sánchez, J., Carrillo-García, J., & Soto, J. (2017). Using SWAT and Fuzzy TOPSIS to Assess the Impact of Climate Change in the Headwaters of the Segura River Basin (SE Spain). *Water*, *9*(2), 149. https://doi.org/10.3390/w9020149

Serpa, D., Nunes, J. P., Santos, J., Sampaio, E., Jacinto, R., Veiga, S., Lima, J. C., Moreira, M., Corte-Real, J., Keizer, J. J., & Abrantes, N. (2015). Impacts of climate and land use changes on the hydrological and erosion processes of two contrasting Mediterranean catchments. *Science of The Total Environment*, *538*, 64–77. https://doi.org/10.1016/j.scitotenv.2015.08.033

Shepard, D. (1968). A two-dimensional interpolation function for irregularly-spaced data. *Proceedings of the 1968 23rd ACM National Conference On* -, 517–524. https://doi.org/10.1145/800186.810616

Shukla, S., & Wood, A. W. (2008). Use of a standardized runoff index for characterizing hydrologic drought. *Geophysical Research Letters*, *35*(2). https://doi.org/10.1029/2007GL032487

Silvestri, L., Saraceni, M., & Cerlini, P. (2022). *Links between precipitation, circulation weather types and orography in central Italy*. https://doi.org/10.13140/RG.2.2.34959.46240

Sobol', I. M. (1990). On sensitivity estimation for nonlinear mathematical models. *Matematicheskoe Modelirovanie*, *2*(1), 112–118.

Song, Y. H., & Chung, E.-S. (2025). Intercomparison of bias correction methods for precipitation of multiple GCMs across six continents. *Geoscientific Model Development*, *18*(20), 8017–8045. https://doi.org/10.5194/gmd-18-8017-2025

Spano, D., Mereu, V., Bacciu, V., Marras, S., Trabucco, A., Adinolfi, M., Barbato, G., Bosello, F., Breil, M., & Chiriacò, M. V. (2020). *Analisi del rischio: I cambiamenti climatici in Italia*. https://cittaclima.it/wp-content/uploads/2020/11/Presentazione_Spano-25.11.2020.pdf

Spearman, C. (1904). The Proof and Measurement of Association between Two Things. *The American Journal of Psychology*, *15*(1), 72–101. https://doi.org/10.2307/1412159

Spinoni, J., Barbosa, P., Bucchignani, E., Cassano, J., Cavazos, T., Christensen, J. H., Christensen, O. B., Coppola, E., Evans, J., Geyer, B., Giorgi, F., Hadjinicolaou, P., Jacob, D., Katzfey, J., Koenigk, T., Laprise, R., Lennard, C. J., Kurnaz, M. L., Li, D., … Dosio, A. (2020). Future Global Meteorological Drought Hot Spots: A Study Based on CORDEX Data. *Journal of Climate*, *33*(9), 3635–3661. https://doi.org/10.1175/JCLI-D-19-0084.1

Spinoni, J., Naumann, G., Carrao, H., Barbosa, P., & Vogt, J. (2014). World drought frequency, duration, and severity for 1951-2010: World drought climatologies for 1951-2010. *International Journal of Climatology*, *34*(8), 2792–2804. https://doi.org/10.1002/joc.3875

Spinoni, J., Vogt, J. V., Naumann, G., Barbosa, P., & Dosio, A. (2018). Will drought events become more frequent and severe in Europe? *International Journal of Climatology*, *38*(4), 1718–1736. https://doi.org/10.1002/joc.5291

Stagge, J. H., Tallaksen, L. M., Gudmundsson, L., Van Loon, A. F., & Stahl, K. (2015). Candidate Distributions for Climatological Drought Indices (SPI and SPEI). *International Journal of Climatology*, *35*(13), 4027–4040. https://doi.org/10.1002/joc.4267

Stahl, K., Hisdal, H., Hannaford, J., Tallaksen, L. M., van Lanen, H. a. J., Sauquet, E., Demuth, S., Fendekova, M., & Jódar, J. (2010). Streamflow trends in Europe: Evidence from a dataset of near-natural catchments. *Hydrology and Earth System Sciences*, *14*(12), 2367–2382. https://doi.org/10.5194/hess-14-2367-2010

Svoboda, M., Hayes, M., & Wood, D. (2012). *World Meteorological Organization: Standardized Precipitation Index User Guide, WMO-No. 1090*.

Switanek, M. B., Troch, P. A., Castro, C. L., Leuprecht, A., Chang, H.-I., Mukherjee, R., & Demaria, E. M. C. (2017). Scaled distribution mapping: A bias correction method that preserves raw climate model projected changes. *Hydrology and Earth System Sciences*, *21*(6), 2649–2666. https://doi.org/10.5194/hess-21-2649-2017

Talpur, H. A., Talpur, S. A., Mahar, A., Rosatelli, G., Baloch, M. Y. J., Ahmed, A., & Khan, A. H. A. (2024). Investigating drinking water quality, microbial pollution, and potential health risks in selected schools of Badin city, Pakistan. *HydroResearch*, *7*, 248–256. https://doi.org/10.1016/j.hydres.2024.04.004

Tamm, O., Maasikamäe, S., Padari, A., & Tamm, T. (2018). Modelling the effects of land use and climate change on the water resources in the eastern Baltic Sea region using the SWAT model. *CATENA*, *167*, 78–89. https://doi.org/10.1016/j.catena.2018.04.029

Tarín-Carrasco, P., Petrova, D., Chica-Castells, L., Lukovic, J., Rodó, X., & Cvijanovic, I. (2024). Assessment of Future Precipitation Changes in Mediterranean Climate Regions from CMIP6 ensemble. *EGUsphere*, 1–34. https://doi.org/10.5194/egusphere-2023-3057

Tariq, M., Rohith, A. N., Cibin, R., Aruffo, E., Abouzied, G. A. A., & Carlo, P. D. (2024). Understanding future hydrologic challenges: Modelling the impact of climate change on river runoff in central Italy. *Environmental Challenges*, *15*, 100899. https://doi.org/10.1016/j.envc.2024.100899

Tebaldi, C., Debeire, K., Eyring, V., Fischer, E., Fyfe, J., Friedlingstein, P., Knutti, R., Lowe, J., O'Neill, B., Sanderson, B., van Vuuren, D., Riahi, K., Meinshausen, M., Nicholls, Z., Tokarska, K. B., Hurtt, G., Kriegler, E., Lamarque, J.-F., Meehl, G., … Ziehn, T. (2021). Climate model projections from the Scenario Model Intercomparison Project (ScenarioMIP) of CMIP6. *Earth System Dynamics*, *12*(1), 253–293. https://doi.org/10.5194/esd-12-253-2021

Thom, H. C. S. (1966). *Some methods of climatological analysis* (Vol. 81). Secretariat of the World Meteorological Organization Geneva. https://library.wur.nl/WebQuery/titel/155524

Tilocca, Y. (2024). Adaptive management strategies for reservoirs in a changing climate. *Ukrainian Journal of Ecology*, *14*(1), 50–53. https://doi.org/10.15421/2024_537

Tong, Y., Gao, X., Han, Z., Xu, Y., Xu, Y., & Giorgi, F. (2021). Bias correction of temperature and precipitation over China for RCM simulations using the QM and QDM methods. *Climate Dynamics*, *57*(5–6), 1425–1443. https://doi.org/10.1007/s00382-020-05447-4

Tugrul, T., Oruc, S., & Gunes, B. (2025). Quantifying future rainfall extremes in Türkiye: A CMIP6 ensemble approach with statistical downscaling. *Acta Geophysica*, *73*(4), 3477–3494. https://doi.org/10.1007/s11600-025-01551-3

Ullah, I., Ma, X., Asfaw, T. G., Yin, J., Iyakaremye, V., Saleem, F., Xing, Y., Azam, K., & Syed, S. (2022). Projected Changes in Increased Drought Risks Over South Asia Under a Warmer Climate. *Earth's Future*, *10*(10), e2022EF002830. https://doi.org/10.1029/2022EF002830

Ullah, I., Zeng, X.-M., Syed, S., Wu, J., Yang, X., Syed, S., Wang, N., & Li, Y. (2025). A multivariate framework for assessing propagation thresholds from meteorological to hydrological drought across indus river Basins-South Asia. *Stochastic Environmental Research and Risk Assessment*, *39*(11), 5415–5433. https://doi.org/10.1007/s00477-025-03089-8

Van Loon, A. F. (2015). Hydrological drought explained. *WIREs Water*, *2*(4), 359–392. https://doi.org/10.1002/wat2.1085

Venturi, C., Campo, L., Caparrini, F., & Castelli, F. (2014). The assessment of the water consumption at regional scale: An application in Tuscany, Central Italy. *European Water*, *46*(46), 3–23.

Vicente-Serrano, S. M., Azorin-Molina, C., Sanchez-Lorenzo, A., Revuelto, J., Morán-Tejeda, E., López-Moreno, J. I., & Espejo, F. (2014). Sensitivity of reference evapotranspiration to changes in meteorological parameters in Spain (1961–2011). *Water Resources Research*, *50*(11), 8458–8480. https://doi.org/10.1002/2014WR015427

Vicente-Serrano, S. M., Lopez-Moreno, J.-I., Beguería, S., Lorenzo-Lacruz, J., Sanchez-Lorenzo, A., García-Ruiz, J. M., Azorin-Molina, C., Morán-Tejeda, E., Revuelto, J., Trigo, R., Coelho, F., & Espejo, F. (2014). Evidence of increasing drought severity caused by temperature rise in southern Europe. *Environmental Research Letters*, *9*(4), 044001. https://doi.org/10.1088/1748-9326/9/4/044001

Wang, Y., Bian, J., Zhao, Y., Tang, J., & Jia, Z. (2018). Assessment of future climate change impacts on nonpoint source pollution in snowmelt period for a cold area using SWAT. *Scientific Reports*, *8*(1), 2402. https://doi.org/10.1038/s41598-018-20818-y

Wang, Y., Yang, J., Chang, J., & Zhang, R. (2019). Assessing the drought mitigation ability of the reservoir in the downstream of the Yellow River. *Science of The Total Environment*, *646*, 1327–1335. https://doi.org/10.1016/j.scitotenv.2018.07.316

Wu, G., Chen, J., Shi, X., Kim, J.-S., Xia, J., & Zhang, L. (2022). Impacts of Global Climate Warming on Meteorological and Hydrological Droughts and Their Propagations. *Earth's Future*, *10*(3), e2021EF002542. https://doi.org/10.1029/2021EF002542

Xoplaki, E., González-Rouco, J. F., Luterbacher, J., & Wanner, H. (2004). Wet season Mediterranean precipitation variability: Influence of large-scale dynamics and trends. *Climate Dynamics*, *23*(1), 63–78. https://doi.org/10.1007/s00382-004-0422-0

Yevjevich, V. (1967). *An objective approach to definitions and investigations of continental hydrologic droughts* (Vol. 23). Colorado State University Fort Collins, CO, USA. https://api.mountainscholar.org/server/api/core/bitstreams/5f26da05-d712-49bc-acc0-397ec0f70fef/content

Yimer, E. A., Riakhi, F.-E., Bailey, R. T., Nossent, J., & van Griensven, A. (2023). The impact of extensive agricultural water drainage on the hydrology of the Kleine Nete watershed, Belgium. *Science of The Total Environment*, *885*, 163903. https://doi.org/10.1016/j.scitotenv.2023.163903

Yisehak, B., & Zenebe, A. (2021). Modeling multivariate standardized drought index based on the drought information from precipitation and runoff: A case study of Hare watershed of Southern Ethiopian Rift Valley Basin. *Modeling Earth Systems and Environment*, *7*(2), 1005–1017. https://doi.org/10.1007/s40808-020-00923-6

Yue, S., Pilon, P., Phinney, B., & Cavadias, G. (2002). The influence of autocorrelation on the ability to detect trend in hydrological series. *Hydrological Processes*, *16*(9), 1807–1829. https://doi.org/10.1002/hyp.1095

Yue, S., & Wang, C. (2004). The Mann-Kendall Test Modified by Effective Sample Size to Detect Trend in Serially Correlated Hydrological Series. *Water Resources Management*, *18*(3), 201–218. https://doi.org/10.1023/B:WARM.0000043140.61082.60

Zhou, Z., Ding, Y., Fu, Q., Wang, C., Wang, Y., Cai, H., Liu, S., Huang, S., & Shi, H. (2023). Insights from CMIP6 SSP scenarios for future characteristics of propagation from meteorological drought to hydrological drought in the Pearl River Basin. *Science of The Total Environment*, *899*, 165618. https://doi.org/10.1016/j.scitotenv.2023.165618

Zittis, G., Bruggeman, A., & Lelieveld, J. (2021). Revisiting future extreme precipitation trends in the Mediterranean. *Weather and Climate Extremes*, *34*, 100380. https://doi.org/10.1016/j.wace.2021.100380

Acknowledgements

I would like to express my deepest gratitude to my supervisor, Prof. Piero Di Carlo, whose mentorship, guidance, and unwavering support were instrumental in shaping the scientific foundations of this thesis. His expertise, patience, and encouragement have profoundly influenced my growth as a researcher throughout this journey.

I wish to sincerely acknowledge Prof. Gianluca Iezzi, who extended his support during difficult times of this PhD journey. His kindness and encouragement when it mattered most will not be forgotten.

I am also thankful to Prof. Nicola Sciarra, the PhD course coordinator, for his continued help and support throughout the doctoral programme.

I am also grateful to my colleagues and friends for their help, companionship, and support throughout this experience. Their presence made the challenges of this journey lighter and the successes more meaningful.

Vita

Hafeez Ahmed Talpur was born in Pakistan. He received his Bachelor's degree in Environmental Sciences from the University of Sindh, Jamshoro, Pakistan, in 2014, and his Master's degree in Environmental Sciences from the same institution in 2019. During his Master's programme, he also served as a teaching assistant at the University of Sindh. In February 2023, he enrolled in the doctoral programme in the 38th cycle of Geosciences at the Department of Engineering and Geology, Università degli Studi "G. d'Annunzio" Chieti-Pescara, Italy. He is currently a candidate for the degree of Doctor of Philosophy in Geosciences, with a concentration in Hydrology and Climate Change Impacts on Water Resources.